



Norwegian University of
Science and Technology

Spectroscopic Ellipsometry of InAs/(Al)GaAs Quantum Dots for Intermediate Band Solar Cells

Maja Bjerke Drøyli

Nanotechnology

Submission date: July 2017

Supervisor: Turid Worren Reenaas, IFY

Co-supervisor: Thomas Brakstad, IFY
Morten Kildemo, IFY

Norwegian University of Science and Technology
Department of Physics

Preface

This Master's Thesis was carried out as a part of the Master of Science degree in Nanotechnology at the Norwegian University of Science and Technology (NTNU) during the spring semester 2017 in Trondheim, Norway. The thesis was written at the Department of Physics.

I would first like to thank my supervisor Associate Professor Turid Worren Reenaas of the Department of Physics at the Norwegian University of Science and Technology. Through weekly meetings, and also by answering questions outside these meetings quickly and helpfully, she has given me great guidance throughout this thesis. She has helped me keep the right focus and make the right priorities in order to avoid the work load from becoming too big for a Master's Thesis.

Secondly, my co-supervisor Thomas Brakstad deserves a great thanks for teaching me how to use the ellipsometer and the software used for analyzing the measurements. He has answered my questions quickly and helpfully whether they regarded measurements, modeling or ellipsometry theory. A great thanks also goes to my other co-supervisor, Professor Morten Kildemo, for allowing me to work in his ellipsometry laboratory and for including me in very useful and interesting lectures in his optics class. I would also like to thank Dr. Mohana Rajpalke at the Department of Electronic Systems for growing samples for this thesis work.

Tore Helgedagsrud deserves a big thanks for putting down many hours of work helping me make the figures of the ellipsometry plots and reading parts of my thesis, correcting errors and suggesting improvements. Finally, I would like to thank my family for supporting me through my five years at NTNU, and for proofreading parts of my thesis.

Trondheim, 3. July 2017,

Maja Bjerke Drøyli

Abstract

As a step towards reducing the CO₂ emissions to the atmosphere, generating electricity from renewable energy resources instead of fossil fuels is a good contributor. Solar cells convert energy from sunlight directly into electricity, and they have long lifetimes and require little maintenance as they contain no mechanically moving parts. Even though efficiency has increased and prices have dropped significantly during the last decade, there are still many steps that can be made towards making solar cells even more attractive.

Intermediate band solar cells (IBSCs) have a theoretical potential of being 50 % more efficient than the theoretically most efficient single band-gap solar cells, which is what is used in today's commercial cells, without any major increase in cost. Many steps are yet to be taken to develop highly efficient IBSCs, and one way to increase the speed and reduce the costs of this development is to perform simulations of the cells, which can lead to a better understanding of how the cells work and which compositions provides the most efficient cells.

To simulate a solar cell, a good optical model is needed for that cell. Quantum dot (QD) IBSCs currently have no physically explainable, good optical models, and one way to create a model is by using spectroscopic ellipsometry (SE). In this thesis, InAs/(Al)GaAs QD-IBSCs are investigated using this technique. As a QD-IBSC has a relatively complex structure, different parts of this structure are studied separately to reduce the amount of unknowns in each measurement. This work looks into GaAs with varying doping, samples with two and ten layers of InAs QDs with GaAs and AlGaAs spacers, as well as full solar cell structures. Most emphasis is put into understanding the two-layer QD samples, as these are the simplest QD structures and therefore contain the least number of unknowns. Also, these samples have previously been measured using photoluminescence spectroscopy, atomic force microscopy, scanning electron microscopy and transmission electron microscopy, providing useful information for SE analysis.

Different models from literature are applied in the modeling of QDs and wetting layer. The QD samples are first modeled only using bulk GaAs, oxide and surface roughness, before a macroscopic model with bulk InAs values and an effective medium approximation (EMA) is applied, and at last an oscillator model of Lorentz oscillators is tried. This thesis finds that the simple model outperforms the more detailed models, indicating that the assumptions made in the detailed models are not correct. Applying the oscillator model gives some surprising results indicating a negative contribution to the pseudo-dielectric function (PDF) of the sample although the oscillators have positive amplitude. No explanation to this has been found, and it is not known if this is caused by a bug in the software used for analysis or if it has a physical explanation. However, when combining the two detailed models by making an EMA of InAs and an oscillator model, the oscillator model contributes as expected to the PDF, outperforming the simple model for some of the measurements.

Although the oscillator model showed some unexpected behaviour, it is still believed to be the model with most potential to make a good and physically explainable model for QDs.

Sammendrag

Et godt tiltak for å redusere CO₂-utslipp til atmosfæren er å erstatte bruken av fossile brennstoff med fornybare energikilder for å generere elektrisitet. Solceller konverterer energien fra sollys direkte til elektrisitet, og siden de ikke har noen mekaniske, bevegelige deler trenger de lite vedlikehold og har lang levetid. Det siste tiåret har effektiviteten økt og prisene falt drastisk for solceller, men det er fremdeles mye som kan gjøres for å gjøre solceller til en enda mer attraktiv energikilde.

Mellombåndsolceller har en teoretisk potensiell effektivitet som er 50 % høyere enn de teoretisk mest effektive solcellene med kun ett båndgap, som er dagens kommersielle solcelletype, uten at det vil være noen vesentlig prisforskjell mellom de to typene. Mye gjenstår før fungerende mellombåndsolceller er en realitet, og simuleringer av disse solcellene kan gi fortgang i utviklingen ved å bedre forståelsen av hvordan solcellene fungerer, og hvilke sammensetninger som gir de mest effektive solcellene.

For å simulere en solcelle trengs det en god optisk modell. Per dags dato finnes det ingen god, fysisk tolkbar, optisk modell for mellombåndsolceller med kvanteprikker (QDer), men en måte å lage optiske modeller er ved bruk av spektroskopisk ellipsometri (SE). I denne avhandlingen studeres InAs/(Al)GaAs mellombåndsolceller med QDer med denne teknikken. Ettersom en slik solcelle har en relativt kompleks struktur, er det gunstig å kunne studere mindre deler av den komplette strukturen separat for å redusere antallet ukjente parametre i hver SE-måling. I denne oppgaven studeres GaAs med varierende doping, prøver med to og ti lag med QDer med GaAs- eller AlGaAs-spacere mellom dem, samt to fulle solcellestrukturer; en med QDer og en referansecelle. Det fokuseres mest på prøvene med to QD-lag, ettersom dette er de enkleste QD-strukturene, og i tillegg er det tidligere blitt gjort målinger på disse prøvene med andre instrumenter, som bidrar med nyttig informasjon i analyseringen av SE-målingene

I denne avhandlingen anvendes ulike modeller fra litteraturen for å modellere QDene og "wetting"-laget. QDene modelleres først kun ved bruk av bulk-GaAs, oksid og overflateruhet, før en makroskopisk modell med bulk-verdier for InAs og effektivt medium-approximasjon (EMA) utprøves, og til slutt testes en modell med Lorentz-oscillatorer. Dette arbeidet finner at den enkleste modellen passer målingene bedre enn de to andre, hvilket indikerer feil i antakelsene som de mer detaljerte modellene er bygget på. Oscillatormodellen oppfører seg uventet, og ser ut til å gi et negativt bidrag til den pseudodielektriske funksjonen (PDF) selv om oscillatorene har positiv amplitude. Det har ikke lyktes å komme frem til en forklaring på denne oppførselen, og det er dermed ikke kjent om den skyldes en feil i programvaren som utfører modelleringen, eller om den kan forklares fysisk. Et interessant funn er at når oscillatormodellen kombineres med InAs i en EMA, oppfører den seg som forventet, og bidrar til å lage en modell som passer bedre enn den enkleste modellen for noen av prøvene.

Til tross for at oscillatormodellen oppfører seg uventet, forventes dette å være den av modellene presentert her som har størst potensiale til å lage en god og fysisk tolkbar modell for QDer.

Table of Contents

Preface	i
Abstract	iii
Sammendrag	v
Table of Contents	viii
List of Tables	ix
List of Figures	xii
Abbreviations	xiii
1 Introduction	1
2 Ellipsometry	5
2.1 Optical Constants	5
2.2 Polarization	6
2.3 Reflection	7
2.4 Mueller calculus	8
2.4.1 Stokes vectors	9
2.4.2 Mueller Matrices	10
2.5 Instrumental Setup	10
2.6 Data Analysis and Modeling	11
2.6.1 Physical Interpretation of Dielectric Function Features	11
2.6.2 Data fitting	12
2.6.3 B-splines	13
2.6.4 Oscillator models	13
2.6.5 Effective Medium Approximation	15
2.7 Drawbacks of Spectroscopic Ellipsometry	16

3	Background Theory	17
3.1	Indium Arsenide, Gallium Arsenide and InAs/GaAs Quantum Dots	17
4	Experimental Methods and Details	21
4.1	Setup	21
4.2	Samples	22
4.2.1	GaAs with Varying Doping	23
4.2.2	Two Layers of Quantum Dots	23
4.2.3	Ten layers of Quantum Dots with Varying Spacer Material	24
4.2.4	The Chalmers Samples	24
5	Results and Discussion	27
5.1	Simulations	27
5.2	GaAs with Varying Doping	30
5.2.1	Silicon-Doped GaAs	30
5.2.2	Beryllium-Doped GaAs	33
5.3	Samples with Two Quantum Dot Layers	34
5.3.1	Modeling of the Samples with Two QD Layers	35
5.4	Samples with Ten Quantum Dot Layers	46
5.4.1	Modeling the Samples with Ten QD Layers	48
5.5	GaAs substrates	54
5.6	Chalmers samples	56
6	Conclusions and Further Work	59
	Bibliography	63
	Appendix	67
A.1	Models of the two-layered QD samples	67
A.2	Models of the samples with ten QD layers	75
A.3	Models of the GaAs substrates	82
A.4	Models of the Chalmers samples	82

List of Tables

4.1	Details on optical elements in RC2-XI	21
4.2	Overview of GaAs samples with varying doping.	23
4.3	Details from growth and PL on 2QD samples	24
4.4	Nominal and measured layer thicknesses from MBE2471	26
5.1	Overview of different QD models	36
5.2	Fit parameters for simple models of 2QD samples	36
5.3	Details on Steimetz models for 9As541-2	41
5.4	Details on fit parameters of simple models on 10QD samples	48
5.5	Details on fit parameters for Steimetz model to 10QD samples	50
5.6	Details on fit parameters for Lee-Steimetz model on 10QD samples	53

List of Figures

2.1	Defining p- and s-directions	7
2.2	The behaviour of light reflected off or transmitted through a surface or interface	8
2.3	Reflection from a thin film sample	9
3.1	Band diagrams of GaAs and InAs	18
3.2	Close-up of band diagrams of GaAs and InAs	18
3.3	Illustration of the behaviour of a strained material	19
4.1	Overview image of the RCs ellipsometer	22
4.2	PL measurements of 2QD samples	24
4.3	Composition of 10QD samples	25
4.4	Composition of Chalmers samples	25
5.1	Simulations of different III-V semiconductors	28
5.2	Simulations of GaAs with varying surface roughness	29
5.3	Simulations of GaAs with varying oxide thickness	30
5.4	Measurements of GaAs with varying Si-doping	31
5.5	Measurements by Snyder <i>et al.</i> of GaAs with varying Si-doping	32
5.6	Simulations comparing undoped and Si-doped GaAs	32
5.7	Measurements of GaAs with varying Be-doping	33
5.8	Comparison of 2QD samples	34
5.9	Comparison of measurement with and without SFP	35
5.10	2QD sample measurements with simple models	37
5.11	Simulation comparing InAs oxide and GaAs oxide	38
5.12	SE measurements by Steimetz <i>et al.</i> of GaAs with varying amounts of InAs deposited	39
5.13	Different ways of modeling the oxide layer on top of QD samples by using EMAs	40
5.14	9As541-2 with simple model and Steimetz models	41
5.15	Difference in $\langle \varepsilon_2 \rangle$ between 9As503-2 and Steimetz models	42

5.16	Measurements and models by Lee <i>et al.</i> for 1 and 1.5 ML of deposited InAs on GaAs	43
5.17	9As503-2 with different models	44
5.18	Simple model-measurement difference for 2QD samples	45
5.19	Close-up on possible quantum effects in 9As541-2 below the band-gap . .	46
5.20	Comparison of 10QD samples	47
5.21	Oscillations of 9As157 fitted with ant without nominal Al-content	49
5.22	Comparison of different models for 9As159	51
5.23	Comparison of simple and Lee-Steimetz models for 9As157	53
5.24	Simple model-measurement difference for all QD samples	54
5.25	Measurements of single- and double-side polished n-type GaAs	55
5.26	Simulations of GaAs with and without backside reflections	56
5.27	Comparison Chalmers samples	57
5.28	Comparison of simple and semi-detailed model for MBE2471	58
5.29	Measurement MBE2471 together with best fitting model.	58

Abbreviations

AFM	=	Atomic force microscopy
AOI	=	Angle of incidence
AR5	=	Assessment report 5 from IPCC
CP	=	Critical point
DF	=	Dielectric function
EMA	=	Effective medium approximation
FWHM	=	Full width at half maximum
IB	=	Intermediate band
IBSC	=	Intermediate band solar cell
IPCC	=	Intergovernmental panel on climate change
KK	=	Kramers-Kronig
MBE	=	Molecular beam epitaxy
MEG	=	Multiple exciton generation
ML	=	Monolayer
MOVPE	=	Metal organic vapor phase epitaxy
MSE	=	Mean square error
NTNU	=	Norwegian University of Science and Technology
PL	=	Photoluminescence
QD	=	Quantum dot
SE	=	Spectroscopic ellipsometry
SEM	=	Scanning electron microscopy
SFP	=	Small focus probes
SR	=	Surface roughness
SRH	=	Shockley-Read-Hall
TEM	=	Transmission electron microscopy
UNL	=	University of Nebraska, Lincoln
VASE	=	Variable angle SE
WL	=	Wetting layer

Introduction

Over the last century, the earth has been facing rapidly increasing temperatures in both the sea and air over land. The fifth, and latest, assessment report (AR5) from the intergovernmental panel on climate change (IPCC) conclude that this trend must be seen as a result of the also rapidly increasing levels of several important greenhouse gases, such as carbon dioxide CO_2 , methane CH_4 and nitrous oxide N_2O . Many species of plants and animals are endangered as a direct result of this rapid temperature increase, and the predicted sea level rise as a result of melting terrestrial ice will affect millions of humans living in areas that risk being flooded if the temperatures keep on increasing. It is also found that climate change can lead to an increase in the frequency of extreme weather events.[1]

There are many ways to deal with climate changes and there exists no one solution that solves everything alone, but one way to reduce the CO_2 concentrations in the atmosphere is to replace fossil fuels as an energy source for electricity generation with renewable energy resources. There are many different renewable energy resources, and most of them are based on energy from the sun, either indirectly such as wind power, wave power, hydropower and bioenergy, or directly such as solar thermal energy and photovoltaics. An example of a non-solar renewable resource is tidal power.

Photovoltaics is a very interesting concept for electricity generation, as it is the only renewable energy technology that converts energy from sunlight directly into electricity. Photovoltaic cells contain no mechanically moving parts, giving them a very long lifetime almost without any maintenance requirements. Solar cells have become much more affordable through the recent years, but still limits can, and must, be pushed both in terms of price and efficiency to keep increasing their affordability. Most commercial cells today are made of Si and have a single band-gap, and are limited by the Shockley-Queisser limit [2], which is about 32 % for Si (for other a more ideal band-gap, the Shockley-Queisser limit is almost 33 %) [3]. To improve the efficiency beyond this, so-called *third generation* solar cells are needed. Many different approaches to overcome this efficiency limit have been suggested, with *multiple junction* cells currently holding the overall world record of most efficient solar cell with 34.5 % [4]. An issue with these multiple junction cells is that the multiple junctions make them very expensive and time consuming to make compared with single junction cells. One alternative solution might therefore be to introduce an extra en-

ergy band inside the band-gap of a single junction cell, to be able to exploit a larger range of the solar spectrum without the loss of energy of a low-band-gap solar cell. Such solar cells are called *intermediate band* solar cells, and their theoretical maximum efficiency is approximately 50 % larger than that of conventional cells [5]. Highly mismatched alloys and deep level impurities have been suggested as possible ways to make such intermediate bands, but quantum dots is the most studied alternative.

Quantum dot (QD) intermediate band solar cells (IBSCs) have been researched for about 10 years, and both optimal composition and growth conditions are yet to be found. The number of possible combinations is huge, so it is expected that many different cells must be made and tested before the optimal recipe is found. Therefore, it would be valuable to make simulations of cells of different compositions, to get an idea of what might lead to the most effective cells. However, to make good simulations, good optical models are required, and one way to find the optical model is through spectroscopic ellipsometry.

Spectroscopic ellipsometry (SE) measures the change in polarization of light after interfering with a sample, and from this it is possible to obtain knowledge on the dielectric function, refractive index and other important optical values for that sample. Some research has been made on QD-IBSCs using SE [6, 7, 8], but much more is needed to fully understand the properties of these structures. In this thesis, the goal of understanding how QD-IBSCs should be modeled optically has been approached by dividing the problem into smaller parts. An IBSC consists of many different layers, and to understand how each layer should be modeled is crucial to be able to model the whole structure. Most work will be put into modeling samples with QDs, as this is the least researched part of the IBSC. To this day, there is still no optical model for QDs that have been explained physically. Samples containing two and ten layers of QDs are investigated in this work, with both GaAs and AlGaAs spacers. In addition, GaAs samples with varying doping concentrations of silicon or beryllium are measured to see how this affects the optical properties of GaAs.

Different approaches for modeling InAs/GaAs QDs are found in literature, and this thesis will test models inspired by the works of Steimetz *et al.* (1996) [9] and Lee *et al.* (2001) [10]. Steimetz *et al.* takes a macroscopic approach to model QDs using the dielectric function of bulk InAs and an effective medium approximation. The approach of Lee *et al.* is to model an InAs wetting layer with a damped harmonic oscillator model consisting of two Lorentz oscillators.

This Master's Thesis is organized in 6 chapters:

Chapter 2 *Ellipsometry*. Introduces the basic theory behind ellipsometry measurements and modeling.

Chapter 3 *Background Theory*. Covers theory useful for the discussion and interpretation of the results.

Chapter 4 *Experimental Methods and Details*. Provides details on the instrumental setup, the library models and the samples investigated in this thesis.

Chapter 5 *Results and discussion.* Presents simulations, measurements and models, and discusses and interprets these.

Chapter 6 *Conclusions and Further Work.* Sums up the findings in Chapter 5 and suggests further investigations and measurements that will lead to a better understanding of the optical model of intermediate band solar cells.

Ellipsometry

In the following chapter theory on ellipsometry is reviewed, and spectroscopic ellipsometry, whose technique this work is based on, has been given special focus. The theory is largely based on *Handbook of Ellipsometry* edited by Tompkins and Irene (2005) [11], and *Chapter 2 A Short Course in Ellipsometry in Guide to Using WVASE32®* by J.A. Woollam Co., Inc [12].

Ellipsometry is a non-destructive technique that measures the change in polarization of electromagnetic waves transmitted through or reflected from a sample. Information such as optical constants, thickness, doping concentration, material depth profile, surface roughness and optical anisotropy and crystallinity can be extracted from the measured polarization change. The high sensitivity of this technique makes it valuable for measuring thin films, surfaces and microstructures.

2.1 Optical Constants

The refractive index, \tilde{n} , and the dielectric function, ε are among the most important constants for describing optical properties of a material. They are related as $\varepsilon = \tilde{n}^2$, and both of them are complex magnitudes $\varepsilon = \varepsilon_1 + i\varepsilon_2$ and $\tilde{n} = n + ik$. Given a polarization \vec{P} and an electric field \vec{E} , the dielectric function (DF) is defined as

$$\varepsilon = 1 + \frac{\vec{P}}{\varepsilon_0 \vec{E}}, \quad (2.1)$$

where ε_0 is the vacuum permittivity.

Although these optical properties are often spoken of as constants, they vary with wavelength. The DF considering these optical properties are related by the Kramers-Kronig (KK) relations, for which the real and imaginary counterparts are given respectively as

$$\varepsilon_1 - 1 = \frac{2}{\pi} \int_0^\infty \frac{\Omega \varepsilon_2(\Omega)}{\Omega^2 - \omega^2} d\Omega, \quad (2.2a)$$

$$\varepsilon_2 = \frac{\sigma_0}{\omega \varepsilon_0} - \frac{2\omega}{\pi} \int_0^\infty \frac{\varepsilon_1(\Omega) - 1}{\Omega^2 - \omega^2} d\Omega. \quad (2.2b)$$

2.2 Polarization

Recalling from Maxwell's equations, an electromagnetic wave consists of an electric field and a magnetic field, which are both normal to each other, and to the propagation direction. How the electric and magnetic fields behave describe the polarization of the light, and since they are orthogonal, only one of them is needed for this description.

The electric field of an electromagnetic wave can be expressed through the two Cartesian base vectors, $E_x(t)$ and $E_y(t)$, as functions of time:

$$E_x(t) = X \cos(-\omega t + \delta_x), \quad E_y(t) = Y \cos(-\omega t + \delta_y), \quad (2.3)$$

where ω is the angular frequency, δ_x and δ_y are absolute phases at $t = 0$ of the x- and y-components, respectively, and X and Y are their amplitudes.

The electric field vector, which is the sum of the components in x- and y-direction, will over time make an elliptic trajectory in the x-y plane ranging from $-Y$ and $-X$ to Y and X . From Equations 2.3, the equation of the ellipse can be obtained as [11, Eq. 1.89]

$$Y^2 E_x^2 + X^2 E_y^2 - 2XY E_x E_y \cos(\delta_x - \delta_y) = X^2 Y^2 \sin^2(\delta_x - \delta_y). \quad (2.4)$$

The amplitude of the electric field is denoted E_0 , and is given as $E_0 = \sqrt{X^2 + Y^2}$. Representing the amplitude of E_x relative to the amplitude of E_y as $\tan \psi_{xy}$ and the phase difference in x- and y-direction as Δ_{xy} , two measurable parameters are obtained:

$$\tan \psi_{xy} = X/Y, \quad \psi_{xy} \in (0, \pi/2), \quad (2.5a)$$

$$\Delta_{xy} = \delta_x - \delta_y, \quad \Delta \in (-\pi, \pi). \quad (2.5b)$$

Rewriting Equation 2.4 using E_0 , ψ_{xy} and Δ_{xy} gives

$$\frac{E_x^2}{E_0^2} + \tan^2 \psi_{xy} \frac{E_y^2}{E_0^2} - 2 \tan \psi_{xy} \frac{E_x E_y}{E_0^2} \cos \Delta_{xy} = \sin^2 \psi_{xy} \sin^2 \Delta_{xy}. \quad (2.6)$$

The two angles ψ_{xy} and Δ_{xy} can be represented by a complex number in a Cartesian coordinate system as

$$\rho_{xy} = \rho_r + i\rho_i = \frac{r_x}{r_y} = \frac{X \exp(i\delta_x)}{Y \exp(i\delta_y)} = \tan \psi_{xy} \exp(i\Delta_{xy}), \quad (2.7)$$

where ρ_{xy} is the ratio between the Fresnel reflection coefficients r_x and r_y in x- and y-directions, respectively. For $\Delta_{xy} = 0$, and hence also $\rho_i = 0$, the ratio between the x- and y-components of the electric field will be constant, and the polarization will consequently be linear. For $\rho_i < 0$ the polarization is right-handed and $\rho_i > 0$ gives left-handed polarization. For $\psi_{xy} = \pi/4$ and $\Delta_{xy} = \pm\pi/2$, leading to $\rho_{xy} = \pm i$ the polarization is circular.

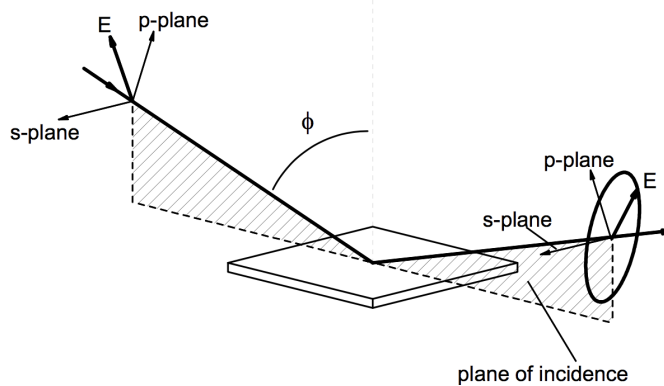


Figure 2.1: The p-direction, s-direction and the direction of propagation form a right-handed Cartesian coordinate system. Figure taken from [12].

2.3 Reflection

In ellipsometric measurements the common practice is to define one of the orthogonal basis vectors representing the electric field of the light as lying in the plane of incidence of the sample to be investigated, and the other one perpendicular to the plane of incidence. The direction of the vector lying in the plane of incidence is called the p-direction, and the direction of the other vector is called the s-direction. The p-direction, s-direction and direction of propagation define a right-handed Cartesian coordinate system, as shown in Figure 2.1. For many purposes it is convenient to define the p- and s-directions as the x- and y-directions discussed in Section 2.2.

The reflection of light incident on a surface of an isotropic medium, or interface between two isotropic media, is expressed using the Fresnel reflection coefficients [11, Eq. 3.15a,b],

$$r_p = \frac{N_1 \cos \phi_0 - N_0 \cos \phi_1}{N_1 \cos \phi_0 + N_0 \cos \phi_1}, \quad (2.8a)$$

$$r_s = \frac{N_0 \cos \phi_0 - N_1 \cos \phi_1}{N_0 \cos \phi_0 + N_1 \cos \phi_1}, \quad (2.8b)$$

where ϕ_0 and ϕ_1 are the angles of the incoming and transmitted light, respectively, as shown in Figure 2.2. N_0 and N_1 are the complex refractive indices of the medium the light is coming in from and reflected off or transmitted through, respectively. The corresponding transmission coefficients are given as

$$t_p = \frac{2N_0 \cos \phi_0}{N_1 \cos \phi_0 + N_0 \cos \phi_1}, \quad (2.9a)$$

$$t_s = \frac{2N_0 \cos \phi_0}{N_0 \cos \phi_0 + N_1 \cos \phi_1}. \quad (2.9b)$$

The angles of the light propagation, ϕ_0 and ϕ_1 , are related by Snell's law

$$N_0 \sin \phi_0 = N_1 \sin \phi_1. \quad (2.10)$$

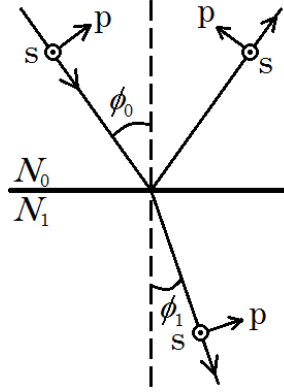


Figure 2.2: When light is incident on a surface or interface, the angle of the transmitted light ϕ_1 is related to the angle of the incident light ϕ_0 by Snell's law, given in Equation 2.10.

In samples with a thin film on a substrate, reflections from the film-substrate interface also contributes to the total reflection from the sample. This is illustrated in Figure 2.3, and for any isotropic media, the total amplitude of the reflection r_{tot} is [13, Eq. 3.67]

$$r_{tot} = r_{01} + t_{01}t_{10}r_{12}e^{i2\beta} + t_{01}t_{10}r_{10}r_{12}^2e^{i4\beta} + t_{01}t_{10}r_{10}^2r_{12}^3e^{i6\beta} + \dots \quad (2.11)$$

Here, r_{ij} is the reflection of a beam in medium i from the interface to medium j , and t_{ij} is the transmission of a beam from medium i to medium j . β is the film phase thickness, given by

$$\beta = \frac{2\pi}{\lambda}dN_1 \cos \phi_1, \quad (2.12)$$

where d is the film thickness and λ is the light wavelength in vacuum. From Equations 2.8 and 2.9, the following relations can be found:

$$r_{10} = -r_{01}, \quad t_{01}t_{10} = 1 - r_{01}^2. \quad (2.13)$$

Using these, and recognizing that Equation 2.11 is a geometric series, r_{tot} may be written as

$$r_{tot} = \frac{r_{01} + r_{12}e^{i2\beta}}{1 + r_{01}r_{12}e^{i2\beta}}. \quad (2.14)$$

Equations 2.11 and 2.14 are valid for p- and s-polarized light separately. For multiple isotropic layers, the calculations follow the same logic, taking into account reflections and transmissions between all layers.

2.4 Mueller calculus

Following [11, Ch. 1.4.4-1.4.5], the polarization of light travelling through different media is best described using vectors and matrices. Two different calculi, the Jones calculus and the Mueller calculus, are most commonly used for this purpose. As Mueller calculus is more convenient when dealing with both polarized and unpolarized light, it has been focused on this framework herein.

as there are no difference in intensities for the different polarizations. The degree of polarization, P , is given by

$$P = \frac{\sqrt{S_1^2 + S_2^2 + S_3^2}}{S_0}. \quad (2.19)$$

2.4.2 Mueller Matrices

To describe the change in light interacting with an optical system, a Mueller matrix is used. This 4×4 matrix, $\hat{\mathbf{M}}$, transforms the Stokes vector of the incoming light, \mathbf{S} , into a Stokes vector representing the light after transmission through or reflection from the optical system, \mathbf{S}' :

$$\mathbf{S}' = \begin{bmatrix} S'_0 \\ S'_1 \\ S'_2 \\ S'_3 \end{bmatrix} = \hat{\mathbf{M}}\mathbf{S} = \begin{bmatrix} M_{00} & M_{01} & M_{02} & M_{03} \\ M_{10} & M_{11} & M_{12} & M_{13} \\ M_{20} & M_{21} & M_{22} & M_{23} \\ M_{30} & M_{31} & M_{32} & M_{33} \end{bmatrix} \begin{bmatrix} S_0 \\ S_1 \\ S_2 \\ S_3 \end{bmatrix}. \quad (2.20)$$

For light passing through multiple polarizing elements, one Mueller matrix per element is multiplied with the Stokes vector of the incoming light as

$$\mathbf{S}_{out} = \hat{\mathbf{M}}_m \cdots \hat{\mathbf{M}}_2 \hat{\mathbf{M}}_1 \mathbf{S}_{in}, \quad (2.21)$$

where $\hat{\mathbf{M}}_i$ represents the i th optical element the light hits.

Light reflected off an isotropic surface can be described by

$$\hat{\mathbf{M}}_S = R_u \begin{bmatrix} 1 & -N & 0 & 0 \\ -N & 1 & 0 & 0 \\ 0 & 0 & C & S \\ 0 & 0 & -S & C \end{bmatrix}, \quad (2.22)$$

where $N = \cos 2\psi$, $C = \sin 2\psi \cos \Delta$ and $S = \sin 2\psi \sin \Delta$. R_u is given by

$$R_u = \frac{|r_x|^2 + |r_y|^2}{2}, \quad (2.23)$$

where $|r_x|^2$ and $|r_y|^2$ are the intensities of light polarized in x- and y-, or p- and s-directions, respectively.

2.5 Instrumental Setup

Ellipsometers consist of different components depending on the application of the instrument, but common for all of them is a light source and polarizer before the sample, and an analyzer and a detector after. The light source typically emits randomly polarized light, and the polarizer changes the light into a known polarization, e.g. linear or circular. The analyzer linearly polarizes the light, such that the detector can provide information of the intensity ratio between light with p- and s-polarization.

The angle of incidence (AOI) of the light upon the sample affects the ratio of p- and s-polarized light being reflected. For two transparent media, there is an angle where none

of the p-polarized light is reflected, called the *Brewster angle*. For samples that are not transparent, there is a corresponding angle where the amount of reflected p-polarized light is at its minimum, the *pseudo-Brewster angle*. At this angle, the reflectivity ratio ρ will be large, leading to higher sensitivity in the measurements. To further increase the measurement reliability, it is common to measure at different angles around the pseudo-Brewster angle. This is called *Variable Angle Spectroscopic Ellipsometry* (VASE).

Knowing the Mueller matrices of the different components of the instrument, the polarization change created by the sample, ρ , can be found. A simple model assuming that the sample has no surface overlayer gives the following relationship between the dielectric function ε , angle of incidence ϕ and reflectivity ratio ρ :

$$\varepsilon = \varepsilon_1 + i\varepsilon_2 = \sin^2 \phi \left(1 + \left[\frac{1 - \rho}{1 + \rho} \right]^2 \tan^2 \phi \right). \quad (2.24)$$

As all materials have a surface overlayer, the equation is never valid, but can be helpful in different ways. It is known as the pseudo-dielectric function, and is most often written $\langle \varepsilon \rangle$.

2.6 Data Analysis and Modeling

In this section theory on data analysis and some oscillator models are presented. For more details the reader is referred to [15].

In ellipsometry, measurements are only a minor part of the process of achieving useful information. The raw data from the measurements provide the ellipsometric angles ψ and Δ , but these do not directly provide any information of interest. To obtain optical constants or layer thicknesses, a model simulating the measured sample must be constructed, and its parameters must be adjusted to match the measured data as closely as possible. If the model has a physical interpretation, it can provide information on the optical constants. If a sample consist of multiple layers the model will (in most cases) also consist of the same layers, and therefore a good model can provide accurate information of each layer.

2.6.1 Physical Interpretation of Dielectric Function Features

When modeling the dielectric function (DF) of a measured sample, it is often important to be able to physically interpret the features of the function. As given in [16], the imaginary part of the DF is related to the energy-band structure of crystalline and microcrystalline materials as

$$\varepsilon_2(\omega) = \frac{4e^2}{\pi\mu^2\omega^2} \int_{BZ} |P_{cv}(\vec{k})| \delta \left[E_c(\vec{k}) - E_v(\vec{k}) - \hbar\omega \right] d\vec{k}, \quad (2.25)$$

where e is the electron charge, ω is the photon wavelength, μ is the combined density-of-states mass, $P_{cv}(\vec{k})$ is the momentum matrix element between the valence and conduction band states, and the integral is taken over the Brillouin Zone (BZ). The Dirac-Delta function $\delta(\vec{k})$, whose integral is unity, contributes only when the energy difference between conduction and valence band equals the photon energy. ε_1 can be found from ε_2

by using KK-relations. If instead integrating over a surface S of equal energy difference $E_c - E_v = \hbar\omega$ in \vec{k} -space, Equation 2.25 can be rewritten as

$$\varepsilon_2(\omega) = \frac{4e^2}{\pi\mu^2\omega^2} \int_S \frac{|P_{cv}(\vec{k})|^2}{|\Delta_k(E_c - E_v)|_{E_c - E_v = \hbar\omega}} dS. \quad (2.26)$$

If $|P_{cv}(\vec{k})|^2$ is varying slowly, the joint density of states J_{cv} can be defined as

$$J_{cv}(E_{cv}) = \int_S \frac{dS}{|\Delta_k(E_{cv})|_{E_{cv} = \hbar\omega}}, \quad (2.27)$$

where $E_{cv} = E_c - E_v$. Equation 2.26 can then be simplified into

$$\varepsilon_2(\omega) = \frac{4e^2}{\pi\mu^2\omega^2} |P_{cv}(\vec{k})|^2 J_{cv}(E_{cv}). \quad (2.28)$$

Looking at Equation 2.27, it is clear that J_{cv} contributes very strongly to ε_2 where $\Delta_k(E_{cv})$ is zero. This corresponds to where the conduction and valence bands are parallel, at maxima and minima ($\Delta_k(E_c(\vec{k})) = \Delta_k(E_v(\vec{k})) = 0$), or at saddle points where they are parallel but not flat ($\Delta_k(E_c(\vec{k})) = \Delta_k(E_v(\vec{k}))0$). These points are called *critical points* (CPs).

2.6.2 Data fitting

Building a model is usually based on some already known parameters of the sample. Thickness, optical properties, order and composition of the layers in the sample are examples of valuable information that eases the process of creating a good model, but ellipsometry can also be used as a way of determining e.g. thickness, if other parameters are known. The unknown parameters have to be optimized to fit the information from the measurements as good as possible, and these are called fit parameters. The general procedure when analyzing a measurement is to construct a model, fit the parameters, and then evaluating the results. If the results are not satisfactory, the model is adjusted and the process is repeated until the best result is found.

To find out how well a model fits the measurements, the error between model and measurement is found for all the different wavelengths measured. This is done by calculating the Mueller Matrix elements N, C and S (described in Section 2.4.2) from the optical model, and comparing these to the corresponding values derived from the measurements for each data point. The program used in this work uses the following equation for quantifying this error[15, Eq. 2-2]:

$$\text{MSE} = \sqrt{\frac{1}{3n - m} \sum_{i=1}^n \left[(N_{E_i} - N_{G_i})^2 + (C_{E_i} - C_{G_i})^2 + (S_{E_i} - S_{G_i})^2 \right]} \times 1000, \quad (2.29)$$

where n is the number of wavelengths, m is the number of fit parameters, and subscripts E_i and G_i represent measured and modelled data, respectively. MSE is an abbreviation for *mean square error*, however this is quite misleading in this case as the root is taken of the sum. For historical reasons, MSE will still be used in this thesis describing the

expression in Equation 2.29. It is natural to think that ψ and Δ might also be used to calculate the MSE, and the reasons why N , C and S are preferred are that these parameters are measured with approximately the same accuracy and precision on any sample using a rotating compensator ellipsometer, and that they are bounded between -1.0 and 1.0.

The lower the MSE, the better the model. What is considered an "acceptable" MSE depends on how complex the sample is. N , C and S derived from the measured data typically has an accuracy of 0.001, which means that the ideal MSE should be 1. For simple samples such as thin films, an MSE less than 2 is considered good, while for more complex samples with thick and/or multiple layers even an MSE of more than 10 might be acceptable. The software used in this thesis minimizes the MSE by adjusting the fit parameters using the Levenberg-Marquardt method, which is a standard, iterative, non-linear regression algorithm [15, p. 2-52].

Along with minimizing the MSE, there are also other important factors when finding the best model. One is that there should not be other, less complex models giving the same results. When searching for the best model, a strategy can be to add more layers or fit parameters to lower the MSE. However, this does not necessarily mean that the more complex model is more correct, and a general rule of thumb is that adding a new fit parameter can be justified if it decreases the MSE by more than 25 %. It is also important that the model has a physical interpretation. Examples of unphysical models are models with negative thickness, a negative absorption coefficient, or with the real part of the refractive index increasing towards longer wavelengths while the material is transparent (no absorption).

2.6.3 B-splines

B-spline curves are interpolation functions constructed from linear combinations of a set of basis functions defined by a parametric knot vector and a set of control points. An important advantage with B-splines is that they are in general non-interpolatory and thus effectively remove higher frequency noise from measured data [17]. The resolution is given by the number of control points and resolution order, and should be chosen such that all the essential features of the measured data are kept, but the noise eliminated. Another advantage of the B-splines function in CompleteEASE™ is that it can force the model into being KK-consistent, which provides more reliable results.

2.6.4 Oscillator models

Oscillators are often used to model the structures dielectric function, as they describe the contributions from the critical points discussed in Section 2.6.1. Calculated classically, the DF is assumed to be a collection of non-interacting oscillators,

$$\varepsilon(E) = \varepsilon_{\infty} + \sum_{i=1}^N \varepsilon_i, \quad (2.30)$$

where N is the number of CPs, ε_{∞} is a material constant and ε_i is the oscillator contribution from CP i .

Lorentz Oscillator

The Lorentz oscillator comes from a classical model assuming that an electron bound to an atom can be described as two objects with a spring between them. The electric field of a photon interacting with the electron will induce an oscillation in the electron, and the force from this field together with the spring force and a damping force makes out the total force on the electron. Due to the much larger mass of the atom nucleus compared to the electron, this can be assumed as a fixed object, and the equation describing the force on the electron is given by [18]

$$m_e \frac{d^2x}{dt^2} = -m_e \omega_0^2 x - m_e \Gamma \frac{dx}{dt} - e E_0 e^{i\omega t}. \quad (2.31)$$

Here m_e is the electron mass, x is the electron displacement from equilibrium position, ω_0 is the resonance angular frequency, Γ is the damping coefficient, e is the electron charge, E is the amplitude of the applied field, and ω is the frequency of the light. A possible particular solution to 2.31 is on the form $x(t) = x_0 e^{i\omega t}$, which gives the following expression for the displacement magnitude:

$$x_0 = -\frac{e}{m_e} \frac{E_0}{\omega_0^2 - \omega^2 + i\Gamma\omega}. \quad (2.32)$$

Charge displacement is directly related to polarization as

$$P = -eN x(t), \quad (2.33)$$

where N is the number of electrons per unit volume. Combining Equations 2.32 and 2.33 with Equation 2.1, gives the following expression for the dielectric function:

$$\varepsilon = \frac{e^2 N}{\varepsilon_0 m_e} \frac{1}{\omega_0^2 - \omega^2 + i\Gamma\omega}. \quad (2.34)$$

Rewriting this expression into a real and an imaginary part gives

$$\varepsilon_1 = 1 + \frac{e^2 N}{\varepsilon_0 m_e} \frac{\omega_0^2 - \omega^2}{(\omega_0^2 - \omega^2)^2 + \Gamma^2 \omega^2}, \quad \varepsilon_2 = \frac{e^2 N}{\varepsilon_0 m_e} \frac{\Gamma \omega}{(\omega_0^2 - \omega^2)^2 + \Gamma^2 \omega^2}. \quad (2.35)$$

Looking at ε_2 , it can be seen that it has a peak with maximum at the resonance frequency ω_0 and Γ corresponding to the full width at half maximum (FWHM). For large ω_0 compared to Γ , ε_2 becomes symmetric. It is possible to have a model consisting of multiple Lorentz oscillators, and the DF in terms of energy would then become [11, Eq. 3.35b]

$$\varepsilon(E) = 1 + \sum_j \frac{B_j}{E_{0,j}^2 - E^2 + i\Gamma_j E}, \quad (2.36)$$

where j is the number of oscillators, B_j is the oscillator strength and $E_{0,j}$ the peak position of oscillator j .

Tauc-Lorentz Oscillator

The Tauc-Lorentz oscillator was developed by Jellison and Modine in 1996 to model amorphous materials [19], but its properties makes it useful also for modeling crystalline semiconductors around and above the band-gap. The Tauc-Lorentz oscillator is the product of the Lorentz oscillator in Equation 2.35 and the Tauc joint density of states which, expressed through ε_2 , is given as [20]

$$\varepsilon_{2,T}(E) = \begin{cases} A_T(E - E_g)^2/E^2, & E > E_g \\ 0, & E \leq E_g \end{cases}, \quad (2.37)$$

where A_T is a proportionality constant. The product of Equations 2.37 and the ε_2 -part of 2.35 gives the Tauc-Lorentz oscillator [19]

$$\varepsilon_{2,TL}(E) = \begin{cases} \left[\frac{AE_0\Gamma(E - E_g)^2}{(E^2 - E_0^2) + \Gamma^2 E^2} \frac{1}{E} \right], & E > E_g \\ 0, & E \leq E_g \end{cases}, \quad (2.38)$$

where A is the strength of the oscillator.

Gaussian Oscillator

While the Lorentz oscillator is good for modeling one-mode systems, the Gaussian is often a better choice when there is a distribution of modes. The Gaussian oscillator is in the CompleteEASE™ manual given as

$$\varepsilon_G(E) = A \left[\left(\Gamma \left(\frac{E - E_0}{\sigma} \right) + \Gamma \left(\frac{E + E_0}{\sigma} \right) \right) + i \left(\exp \left(- \left(\frac{E - E_0}{\sigma} \right)^2 \right) + \exp \left(- \left(\frac{E + E_0}{\sigma} \right)^2 \right) \right) \right], \quad (2.39)$$

where A is the oscillator amplitude, equal to the ε_2 value at E_0 , and σ is defined as

$$\sigma = \frac{B_r}{2\sqrt{\ln(2)}}. \quad (2.40)$$

Γ is a convergence series to make the line shape of ε_1 KK consistent, and B_r is the broadening, which approximately corresponds to the FWHM in ε_2 .

2.6.5 Effective Medium Approximation

Some samples might contain a layer that consists of two or more materials, which makes them harder to model. If the materials of this layer are known, a solution can be to average between their optical functions. The effective medium approximation (EMA) is a set of theories on how to best perform this average, and different theories apply to different compositions. Common for the theories that will be discussed here is the following expression [11, ch. 3.4.5]:

$$\frac{\langle \varepsilon \rangle - \varepsilon_h}{\langle \varepsilon \rangle + \gamma \varepsilon_h} = \sum_j f_j \frac{\varepsilon_j - \varepsilon_h}{\varepsilon_j + \gamma \varepsilon_h}. \quad (2.41)$$

Here $\langle \varepsilon \rangle$ is the effective medium DF, ε_h is the DF of the host material, ε_j is the DF of the j th constituent, and f_j is the corresponding volume fraction. γ is a constant related to the shape of the inclusions, e.g. $\gamma = 2$ for spheres.

The earliest EMA theory is the *Lorentz-Lorentz*, where $\varepsilon_h = 1$, i.e. air. This model is not often used, as it assumes that the constituents are mixed on the atomic scale, which is rarely the case. The *Maxwell-Garnet* theory is often the best choice when the fraction of one of the materials is much larger than the other. Here, the dominant material is said to be the host, $\varepsilon_h = \varepsilon_1$. When there is no clear majority of any material, the *Bruggeman* theory is often the preferred alternative. This theory does not pick a host material, but instead defines $\varepsilon_h = \langle \varepsilon \rangle$. Bruggeman theory is often successfully used for modeling surface roughness by defining a layer consisting of 50 % void [11, ch. 3.4.5][15].

The program used in this work assumes $\gamma = 2$ for all models and theories, and does not allow more than three constituents.

2.7 Drawbacks of Spectroscopic Ellipsometry

Although spectroscopic ellipsometry is an important tool for gaining knowledge on optical properties and layer thicknesses of a sample in a quick and non-destructive way, it also has some drawbacks. The main problem using SE is that no information can be collected directly from the measured data. A model fitting the data must be constructed, and this model needs to have a physical interpretation to give valuable information on e.g. optical properties. Also, constructing a model often requires a lot of information about the sample - if there are too many unknown parameters, the results will be less reliable. For some measurements, the modeling will not be possible without first using other instruments, such as atomic force microscopy, scanning electron microscopy, tunneling electron microscopy or x-ray diffraction to determine some of the properties of the sample.

Background Theory

In this chapter, theory on some of the most important materials and systems of the samples investigated in this thesis is covered. The chapter is meant to provide information that might be useful in the discussion of the results, and is not seeking to be a complete guide to any of the subjects covered here. The reader is referred to the cited works in the chapter if seeking additional information.

3.1 Indium Arsenide, Gallium Arsenide and InAs/GaAs Quantum Dots

Two of the most important semiconductors in the structures investigated in this thesis are gallium arsenide, GaAs, and indium arsenide, InAs. They are both direct band-gap III-V semiconductors with zinc-blende crystal structure. GaAs has many different applications, and is often used in light-emitting diodes, field-effect transistors and integrated circuits. Its room temperature band-gap of 1.424 eV makes it a good material for use in photovoltaics as it absorbs a large range of the solar spectrum while still maintaining a high output voltage [21]. The band structures of GaAs and InAs are given in Figure 3.1(a) and (b), respectively. Close-ups of Figure 3.1 are found in Figure 3.2, and show occurrences of parallel bands. As discussed in Section 2.6.1, parallel bands correspond to critical points, where the joint density of states is very large. For the systems investigated in this work, the joint density of states is assumed to be linearly proportional with ε_2 .

The lattice constant of InAs is approximately 7 % larger than the lattice constant of GaAs. Because of this lattice mismatch, InAs is highly strained when grown on GaAs in layers up to about 1.7 ML thickness, illustrated by Figure 3.3 [23, ch. 4.1]. For layers thicker than this, the strain makes the InAs form in clusters. These clusters, or islands, are known as quantum dots, QDs, and the coherent InAs film below the clusters is called the wetting layer, WL. This type of growth is called Stranski-Krastanov (SK) growth mode, and occurs when the deposited atoms are more strongly bound to the substrate than to each other, until the deposited film reaches a certain thickness [23, ch. 4.1]. The size and

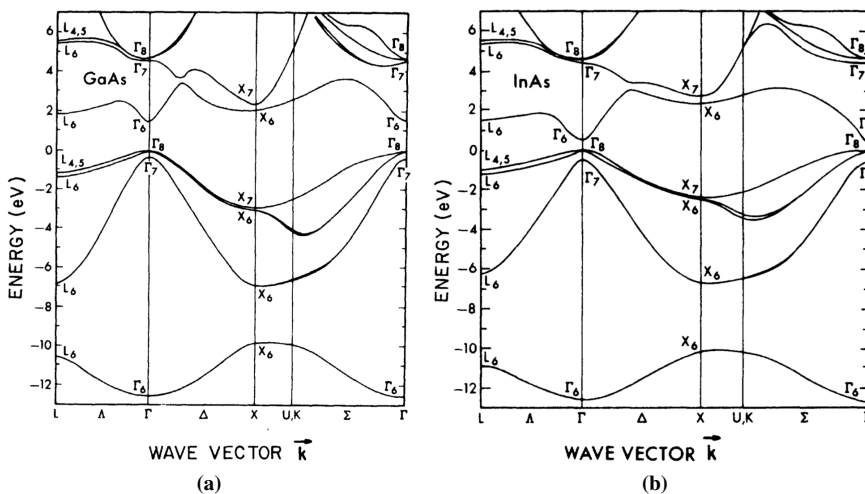


Figure 3.1: Band diagrams of (a) GaAs and (b) InAs over the whole Brillouin zone. Figures taken from [22].

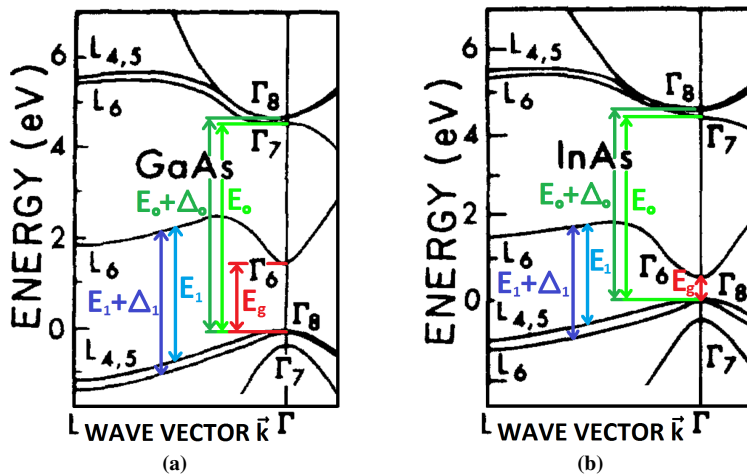


Figure 3.2: Close-ups of the band diagrams in figure 3.1 of (a) GaAs and (b) InAs. The arrows point to parallel bands, corresponding to critical points. Figures adapted from [22].

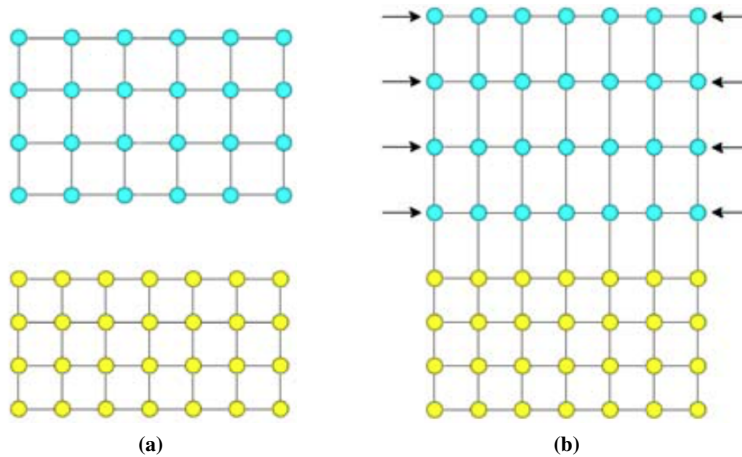


Figure 3.3: When a material is grown on a substrate of a different material with the same crystal structure but smaller lattice constant (a), the deposited material will try to fit the crystal structure of the substrate if it is more strongly bound to that than to itself (b). To fit the smaller crystal structure the deposited material decreases its unit cell footprint area, and to maintain the same unit cell volume, the height of the unit cells increases. Figures taken from [23, ch. 4.1].

composition of the QDs depend on the growth conditions, and they vary significantly with growth temperature.

Quantum dot (QD)-based IB solar cells consist of a p-i-n junction with quantum dots in the intrinsic region. The quantum dots are made from a low band-gap material embedded in a high band-gap material, confining carriers in all three dimensions. This leads to the density of states function taking the shape of delta functions. The energy level positions depend on confining potential, determined by the offset in band-gap between the QD and surrounding material, and the size of the QD. [23, Ch. 3.2]

The QD carrier confinement is very similar to a three dimensional particle in a box-problem, differing by the geometric shape of the QDs, which is closer to a sphere cap or cone than a box. The calculations for available states of such shapes will not be performed in this thesis as there are too many sources of uncertainty to produce any quantitative results, but the concept is worth considering qualitatively. The energies corresponding to allowed wavenumbers are inverse proportional to the square of the size of the box, which means that for a large box, many more energies are allowed in the box, and they are tightly spaced compared to a smaller box. Generally, this means that the smaller the box, the higher the quantum confinement [24, ch. 5.2]. In InAs/(Al)GaAs QDs the diameter is larger than the height, which means that electrons will be more confined in the growth direction than in the plane normal to it.

Chapter 4

Experimental Methods and Details

This chapter will describe the setup of the ellipsometer, and the different samples analyzed in this work. Nominal values of thickness and composition are presented along with other information of the samples from earlier investigations by different methods, but as making the samples has not been a part of this project, detailed description of how they are made are left out from this thesis.

4.1 Setup

The ellipsometer used in this work is a RC2 Model XI by J. A. Woollam Co., Inc. The RC2-XI is an ellipsometer with a compensator both in the source and receiver optics, which makes it able to measure all 16 Mueller Matrix elements. The wavelength range of the ellipsometer is 210-1690 nm, corresponding to approximately 0.7-5.9 eV, which is around and above the band-gap of GaAs and GaAs alloys with Al and In. Details about the components of the ellipsometer can be found in Table 4.1, accompanied by Figure 4.1. For very small samples and samples with non-uniform thickness, focus probes can be installed to decrease the beam spot size. [25]

Table 4.1: Details on optical elements in RC2-XI [25]. The components are listed in the same order as the light passes them.

Component	Details
Light source	150 W Xenon lamp
Source optics	Achromatic lens, fixed MgF ₂ Rochon polarizer, achromatic prism compensator continuously rotating at 10 Hz
Receiver optics	Through-hole quadrant (front alignment) detector, compensator continuously rotating at 6 Hz, fixed polarizer, two different detectors; Si CCD (193-1000 nm) and InGaAs photodiode array (1000-1700 nm)



Figure 4.1: Experimental setup of the RC2 ellipsometer with 1) light source, 2) source optics, 3) vertical sample mount, 4) receiver optics and 5) goniometer arm for variable angle measurements. Figure adapted from [26].

The program used for both measurements and analysis is CompleteEASE™ by J. A. Woollam Co., Inc., and with this program follows a library of already measured samples. Some of these are used in this work, and most of the models are measured by the University of Nebraska, Lincoln (UNL), who are known to make good and trustworthy models of a great variety of materials. All simulations and many of the models presented in this thesis will be based on models found in the CompleteEASE™ library. For the library models used in this work made by others than the UNL, it will be specified at the first use of the model.

4.2 Samples

To try to understand how to model complex solar cell structures, the problem was broken down into smaller pieces by measuring samples only containing layers similar to certain parts of the whole structure. GaAs substrates with a 2 μm thick layer of doping are measured to gain knowledge on how varying doping concentrations affect the ellipsometric data of GaAs. Thereafter, samples with two layers of quantum dots are measured, before proceeding to measure samples with ten QD layers and at last the full IBSC structures. To compare the UNL library GaAs with the substrates used for most of the samples, two undoped, pure GaAs substrates, one single-side and one double-side polished, are also measured. All measurements are performed at 55°-75° with 5° intervals and 20 seconds measurements on each angle. The samples are aligned at 65°, except for some of the

measurements using focus probes that are aligned at each angle. All samples have been grown using molecular beam epitaxy (MBE), and all QDs have been formed by Stranski-Krastanov epitaxial growth.

4.2.1 GaAs with Varying Doping

The GaAs substrates in these samples are nominally undoped and from the same producer but different wafers. Some of the samples are double-side polished, and all the samples were measured using small focus probes (SFP) due to their small sizes. On top of the substrates are $2\mu\text{m}$ of MBE grown GaAs with varying doping, Be is used as the p-type dopant and the n-type dopant is Si. An overview of the samples are found in Table 4.2.

Table 4.2: Overview of GaAs samples with varying doping.

Sample	Doping [cm^{-3}]	Double-side Polished
9As005	Be 1.3×10^{17}	Yes
9As004	Be 3.9×10^{18}	Yes
9As057	Be 1.0×10^{19}	No
9As006	Si 1.5×10^{17}	Yes
9As009	Si 5.6×10^{17}	Yes
9As048	Si 2.0×10^{18}	No

4.2.2 Two Layers of Quantum Dots

Two different samples with two InAs QD layers are investigated in this thesis. The samples, 9As541-2 and 9As503-2, are grown on n-type GaAs (001) substrates with a GaAs spacer between the two QD layers, and the uppermost QD layer is on top of the sample. The samples are grown by Sedsel Fretheim Thomassen in her PhD work at the Department of Physics using the MBE lab at Department of Electronic Systems, both at NTNU. The two samples are picked for this project because of their differences in PL spectra, measured by Maryam Gholami Mayani. The PL spectra of the two samples are shown in Figure 4.2, and by choosing samples with large differences in PL, the chance of observing differences in SE measurements is increased. The PL measurements were performed at low temperatures. The growth conditions of the two samples are nominally the same, except for the amount of InAs per QD layer, and the QD temperature. The nominal spacer thickness is 50 nm, but the spacer thickness of 9As541-2 has been measured to (41 ± 0.5) nm by Per Erik Vullum at the Department of Physics using TEM. Table 4.3 gives details on the two samples. The average QD size at the surface is measured using AFM/SEM. For 9As503-2 the mean height is 2.6 nm and mean diameter 16.1 nm, while the QDs of 9As541-2 are so small that they could not be measured properly using these instruments. The measured mean QD height of a sample in the same series with QDs grown at 395°C is 0.6 nm [23, paper II], so it is expected that sample 9As541-2 has QDs smaller than this. More details on the samples can be found in Dr. Thomassen's PhD thesis [23].

Sample 9As541-2 is so small that it had to be measured using focus probes, while 9As503-2 is measured both with and without SFP.

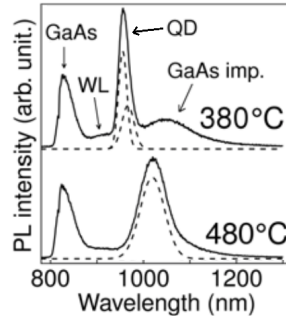


Figure 4.2: PL measurements of samples 9As541-2 (380°C) and 9As503-2 (480°C). Figure adapted from [23, paper II].

Table 4.3: Details from growth and PL on samples 9As503-2 and 9As541-2.

	9As541-2	9As503-2
Growth temperature [°C]	380	481
InAs deposited per QD layer [ML]	2.2	2.3
QD PL Peak position [nm]	958	1020

4.2.3 Ten layers of Quantum Dots with Varying Spacer Material

Samples with ten layers of QDs were grown using MBE by Dr. Mohana Rajpalke at the Department of Electronic Systems. The two samples discussed in this thesis, 9As157 and 9As159, differ nominally only by the QD spacer material, which is GaAs, and $\text{Al}_{0.25}\text{Ga}_{0.75}\text{As}$, respectively. The structure of the two samples with nominal values, is found in Figure 4.3. For both samples, the QD growth temperature was kept at 480°C, and a layer of $\text{Al}_{0.8}\text{Ga}_{0.2}\text{As}$ followed by a thick layer of GaAs is placed between the n-type substrate and the QD stack to improve the contrast and hence the details from the QDs. Other samples grown by Mohana Rajpalke under similar conditions in the same MBE have been inspected using TEM, which has confirmed that nominal and actual thicknesses agree.

4.2.4 The Chalmers Samples

The Chalmers samples are IB solar cell structures grown in 2012 by Mahdad Sadeghi at Chalmers University of Technology for the RCN project *Nanomaterials for 3rd Generation Solar Cells*. The bottom and top layers of these samples are the same for all samples, while the active layer varies. In this thesis, samples MBE2471 and MBE2472 are investigated. MBE2471 has a GaAs spacer and 50 layers of InAs QDs. MBE2472 is a reference cell without QDs, but with a 1 μm thick undoped GaAs absorption layer instead. MBE2471 has been measured in TEM by Espen Undheim, which provides actual layer thicknesses. Figure 4.4 shows the composition of the samples with nominal values. For MBE2471, actual thickness of the layers is found in Table 4.4.

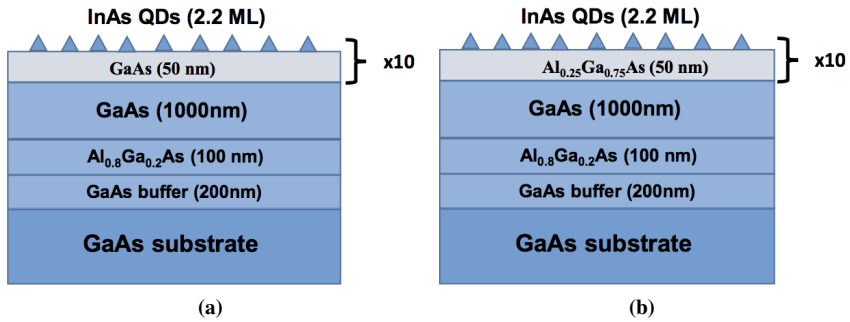
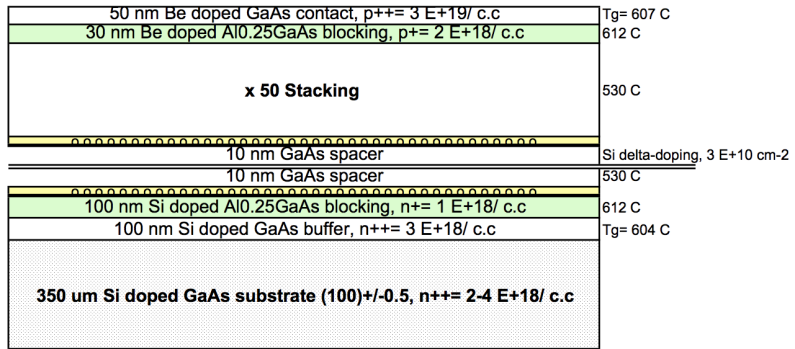
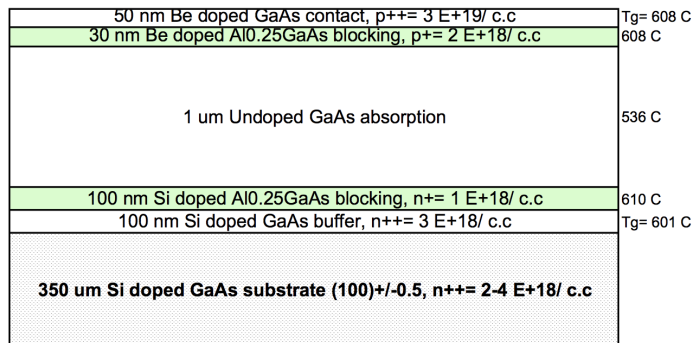


Figure 4.3: Samples (a) 9As157 and (b) 9As159 with 10 QD layers and GaAs and $\text{Al}_{0.25}\text{Ga}_{0.75}\text{As}$ spacers, respectively. Figures by Mohana Rajpalke.



(a)



(b)

Figure 4.4: Samples (a) MBE2471 and (b) MBE2472 are equal except for the QD layers in MBE2471 and the Si δ -doping in the middle of each spacer layer. Blocking layer is the same as emitter. Figures by Mahdad Sadeghi.

Table 4.4: Nominal and TEM-measured layer thicknesses from MBE2471. ¹⁾ found by dividing the total bright field measured thickness of the QD stack, 1084.1 nm, by the number of QD layers, 50. ²⁾ calculated from the superlattice reflections and believed to be more accurate than ¹⁾. Data taken from [27]

Layer	Nominal thickness [nm]	Measured thickness [nm]
Contact	50	48.4
P-emitter	30	29.8
Spacer ¹⁾	20	22.1
Spacer ²⁾	20	20.7
N-emitter	100	107.7
Buffer	100	104.3

Results and Discussion

In this chapter the findings from simulations, modeling and other data analysis performed in this work are presented. For the samples containing QDs, different models found in literature will be tested and adapted to the samples studied herein. To easily compare and physically interpret the results, SE plots are presented in terms of the imaginary part of the pseudo-dielectric function, $\langle \varepsilon_2 \rangle$, as a function of energy given in electron volts. To make the plots easy to read, some plots only show the data measured or simulated at 65° . When modeling the measurements in this thesis, the complexity of the samples and models lead to a huge number of parameters that can be fitted for each model. Therefore, parameters that could have been fitted in some cases are kept constant without any further discussion. In the work performed for this thesis, many more parameters have been varied and fitted to investigate how they affect the models addressed in this work. However, only the most important findings are presented herein. For all the models presented and discussed in this work, details on composition, thicknesses and other fit parameters are found in the appendix.

5.1 Simulations

A good way to understand how GaAs and other materials appear in SE measurements is to perform simulations varying different parameters. All GaAs samples exposed to air have oxide layers and surface roughness, but to what extent varies with e.g. exposure time and temperature, and how the surface has been treated. Therefore, simulations of different materials and compositions relevant for the work in this thesis will be presented in this section. Also, more simulations will be presented in later sections of the chapter where they are discussed together with measurements and models. In Figure 5.1, the bulk dielectric functions of different III-V semiconductors are found. The figure shows that for all the different materials, there are two clear peaks; the one at lowest energy is located at around 2.7 eV for InAs, 3.8 eV for $\text{Al}_{0.8}\text{GaAs}$, and somewhere in between for the other compositions. The other peak has its maximum somewhere between 4.4 eV and 4.8 eV. To ease the discussion of the changing PDFs, the peak at lower energy will be referred to

as *Peak 1*, and the other as *Peak 2*. From Figure 5.1, it is also clear that Peak 1 actually consists of two peaks, which will be called 1a and 1b, with 1a being the peak of lowest energy. For some of the materials, Peak 2 can also be divided into Peaks 2a and 2b, following the same pattern as for Peak 1 with *a* being the peak of lower energy.

A clear trend with decreasing In-content and increasing Al-content shifts Peak 1 towards higher energies and increases the strength of Peak 2. The band-gap is where $\langle \varepsilon_2 \rangle$ becomes non-zero, corresponding to the material beginning to absorb light, and the large variations in band-gap energy for the different materials are evident.

Comparing the simulations of InAs and GaAs in Figure 5.1 with their respective band structures in Figure 3.2, it can be seen that the energy differences at the critical points in Figure 3.2 corresponds with the peaks in Figure 5.1. Peaks 1a and 1b are located at approximate energies E_1 and $E_1 + \Delta_1$ for both InAs and GaAs. For InAs, E_0 and $E_0 + \Delta_0$ appear as one peak, while for GaAs, Peaks 2a and 2b are found at around E_0 and $E_0 + \Delta_0$, respectively. Also, shown in Figure 3.1, there are parallel bands around $\vec{k} = \Delta$ that can contribute to Peak 2 [22].

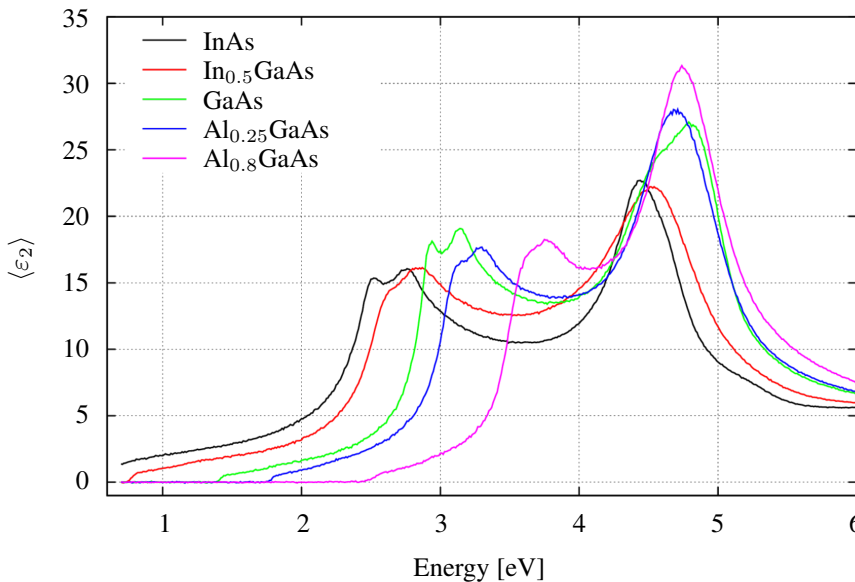
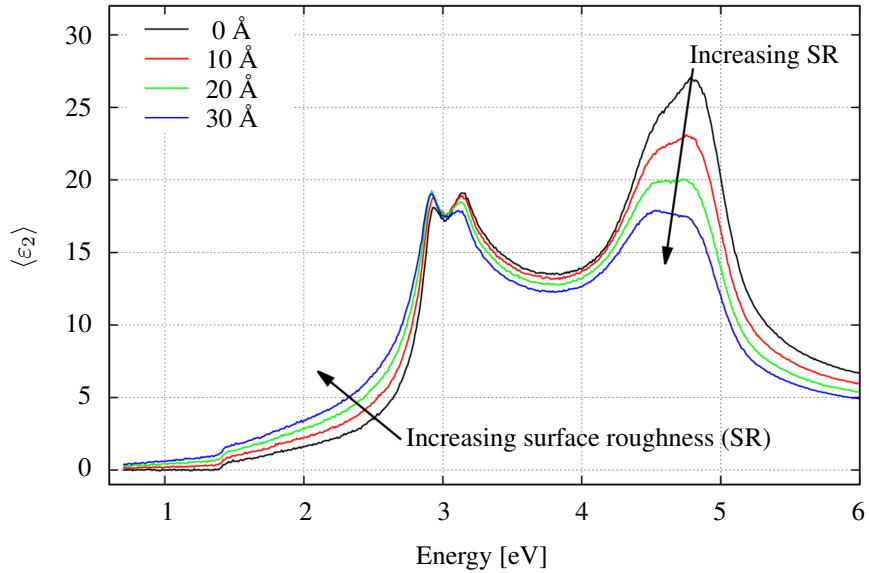
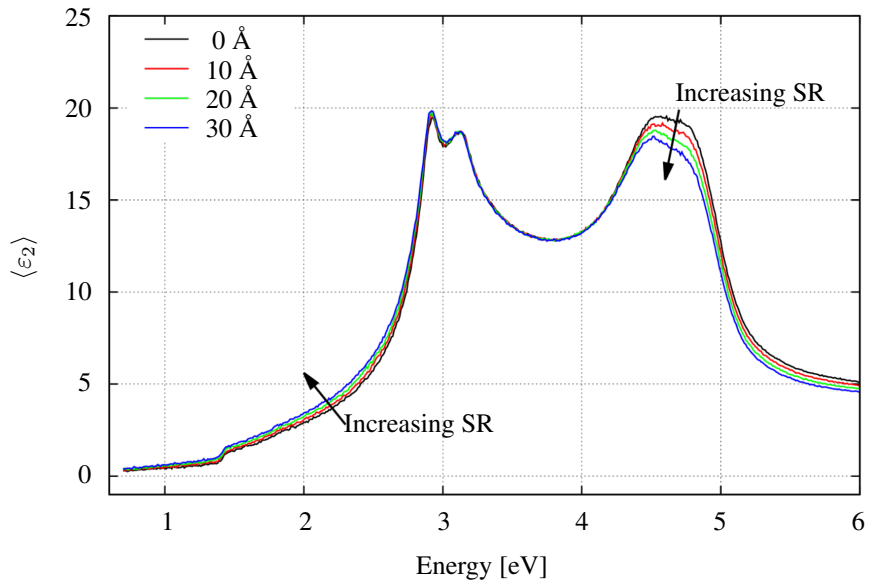


Figure 5.1: Simulations at 65° of different bulk III-V semiconductors without oxides or surface roughness.

Simulations of GaAs with oxide varying both oxide thickness and surface roughness are found in Figures 5.2 and 5.3. These plots show that the effects on $\langle \varepsilon_2 \rangle$ from surface roughness and GaAs oxide on a GaAs substrate are very similar. Both increasing surface roughness and increasing oxide thickness leads to a decrease of Peak 2 and an increase in $\langle \varepsilon_2 \rangle$ between the band-gap and Peak 1. Comparing Figures 5.2(a) and (b) it becomes clear that surface roughness affects $\langle \varepsilon_2 \rangle$ to a larger extent when no oxide is present. Looking closely at Peak 1 in Figures 5.2(a) and 5.3, a shift can be seen from Peak b being the most dominant one for low surface roughness/oxide thickness to Peak a having the highest amplitude for higher values of surface roughness/oxide thickness.



(a)



(b)

Figure 5.2: Simulations at 65° showing how $\langle \epsilon_2 \rangle$ of GaAs with (a) no oxide layer and (b) 20 Å of GaAs oxide varies with surface roughness. GaAs oxide model from [28].

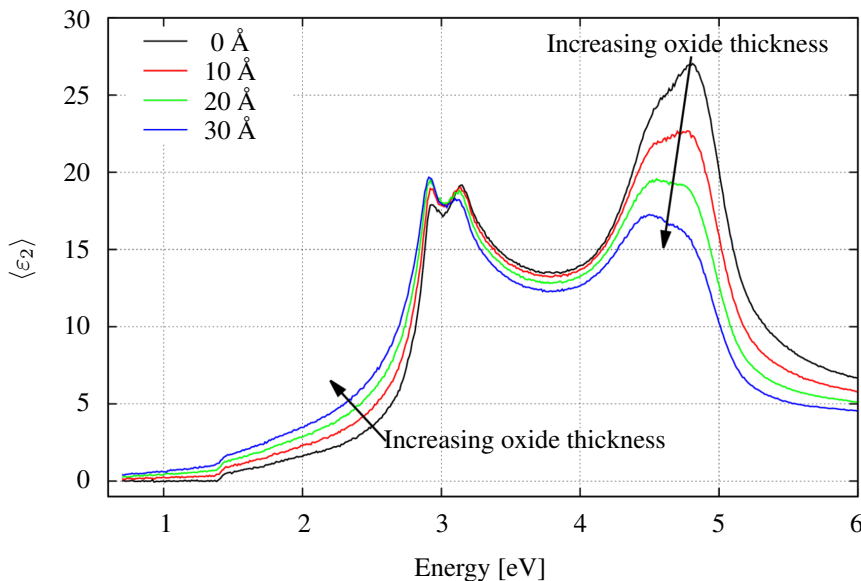


Figure 5.3: Simulations at 65° showing how the PDF of GaAs oxide on a GaAs substrate varies with varying oxide thickness. GaAs oxide data from [28].

5.2 GaAs with Varying Doping

Following the effects of surface roughness and oxide thickness on the PDF in the previous section, this section undertakes GaAs samples with varying doping in terms of the PDF.

5.2.1 Silicon-Doped GaAs

Three different Si-doped samples were measured using SFP, shown in Figure 5.4. For the Silicon doped samples, a clear trend with doping concentration is found. Figure 5.4 shows that for energies higher than around 3.2 eV, $\langle \epsilon_2 \rangle$ increases with doping, and the increase is especially high around Peak 2. Also, for 9As048, Peak 1a and b appear to be wider and more even in amplitude so that they look like one peak, and the same can be said for Peak 2. Below 2.8 eV, $\langle \epsilon_2 \rangle$ decreases with increasing doping.

The trends with decreasing doping concentration are very similar to the trends for increasing oxide thickness and/or surface roughness. It is therefore worth considering if the differences between the Si-doped samples might actually be due to varying oxide thicknesses and not because of the doping. This would support the findings of Snyder *et al.* (1992) [29], who report only minor differences between Si-doped GaAs samples ranging from $4.6 \times 10^{17} \text{ cm}^{-3}$ to $3.3 \times 10^{18} \text{ cm}^{-3}$. $\langle \epsilon_2 \rangle$ for various doping concentrations found by Snyder *et al.* is shown in Figure 5.5, and it is clear that the trends for Peak 2 are the opposite of what is found in the samples measured in this thesis. The findings of Snyder *et al.* are also supported by the simulation in Figure 5.6, which shows the same trends for heavily Si-doped GaAs compared to undoped GaAs. All three Figures 5.4, 5.5 and 5.6 agree that heavy doping smooths out Peak 1.

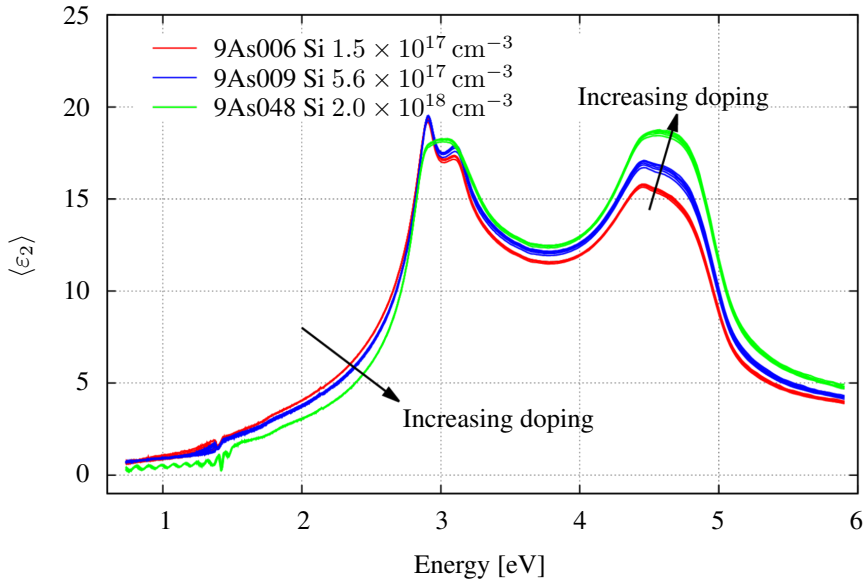


Figure 5.4: Measurements at 55-75° of undoped GaAs substrates with a 2 μm Si-doped GaAs layer of varying doping concentration show a trend of increasing $\langle \epsilon_2 \rangle$ values around Peak 2 and decreasing values below Peak 1.

Overall, the strength of Peak 2 is much weaker for the samples in this work compared to the findings in [29]. This might indicate that the samples in this thesis have thicker oxide layers than the samples measured therein, which is highly likely as the samples measured in this work were grown at least a year, and likely longer, before they were measured, and they have been stored in air at room temperature.

However, several articles report that GaAs oxide thickness stabilizes rather quickly [30, 31], and within over a year, the samples should have similar oxide thicknesses. Therefore, it is unlikely that difference in oxide thickness is the reason alone for the trends in Figure 5.4. Considering that all of the samples measured in this work are MBE grown, the surface roughness should be minimal, and as GaAs oxide certainly is present on the samples, the effect of varying surface roughness should not be strong enough to explain the differences in Figure 5.4.

One might also consider the possibility that the Si doping might affect the oxide thickness. Si is known to oxidize easily, and it could therefore be assumed that the most heavily doped samples will have a thicker oxide. This would however be the opposite trend of what is observed, as the samples with the lowest doping are most similar with those with thickest oxide. Also, considering the amount of Si relative to GaAs, the effect would probably be negligible. The samples in Figure 5.5 are chemomechanically etched crystals, and it is not known how the samples providing the data in Figure 5.6 were made. It might be possible that difference in processing can lead to difference in composition and hence ellipsometry measurements, but it is unlikely that this alone explains the opposing trends of samples that should be very similar. As a consequence, it is therefore impossible to draw any conclusions to what actually causes the trends found in Figure 5.4.

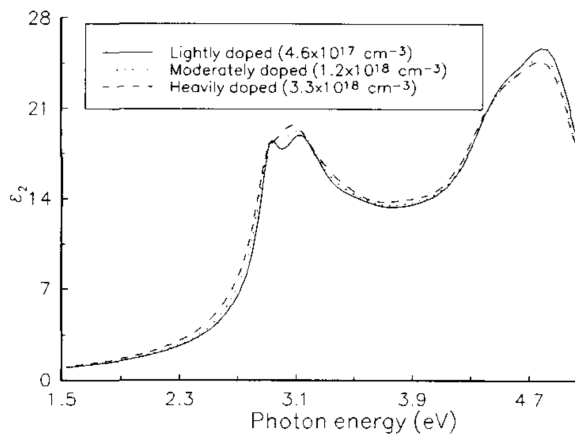


Figure 5.5: Measurements by Snyder *et al.* indicate that Peak 2 decreases and Peak 1 smooths out with increasing Si-doping concentrations. The poor quality of the figure is as it is in the original article. Taken from [29].

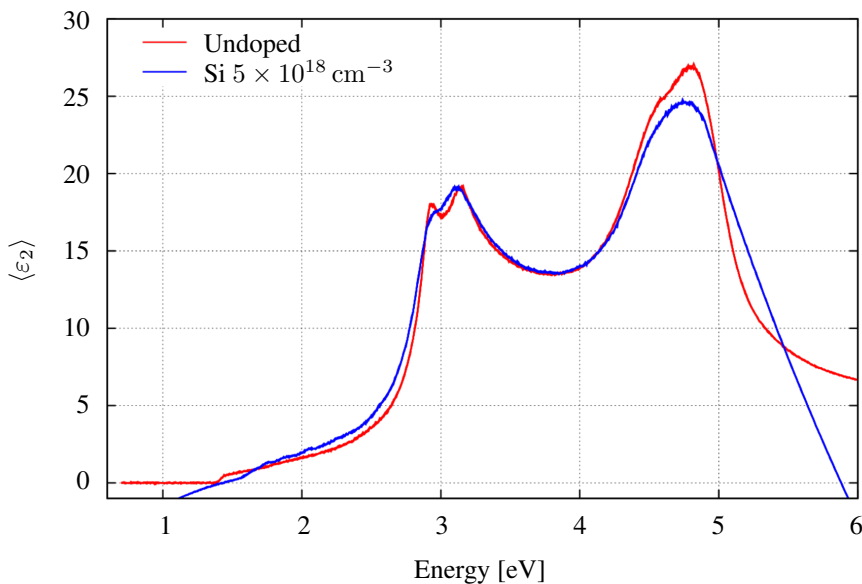


Figure 5.6: Simulation at 55-75° comparing library values of undoped and Si-doped GaAs. It appears that doping smooths out Peak 1 and decreases the strength of Peak 2. The measurement of doped GaAs should not be trusted above 5 eV. Doped GaAs measured by H. Yao.

5.2.2 Beryllium-Doped GaAs

As the Si-doped samples, Be-doped samples with three different doping concentration were measured, and plots of the imaginary part of the PDF are given in Figure 5.7. For the Beryllium doped samples, there are also significant differences between the different samples, but not any clear trends. From Figure 5.7 it is clear that the highest doped sample, 9As057, has the highest $\langle \varepsilon_2 \rangle$ value above 3.2 eV, and the lowest below 2.8 eV. However, sample 9As004, having the second highest doping, appears to be less similar to 9As057 than 9As005 despite 9As004 being closer in doping concentration.

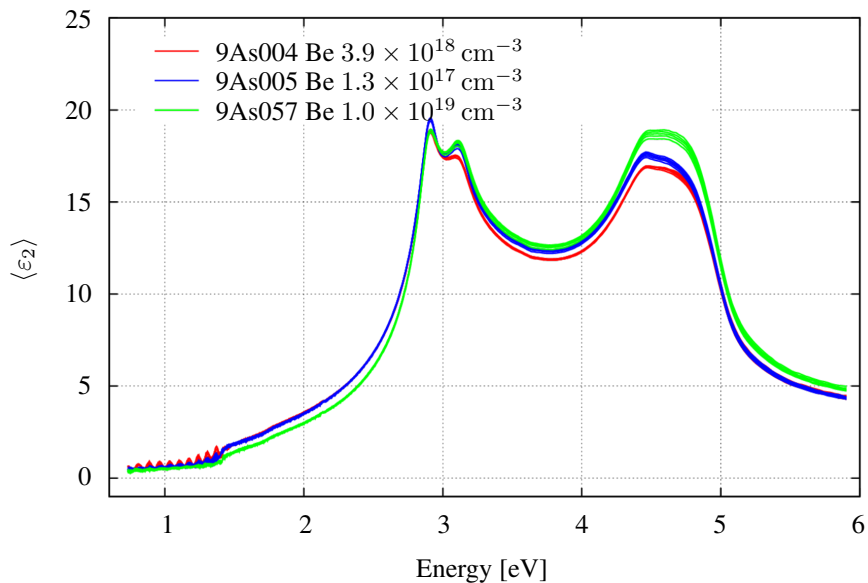


Figure 5.7: Measurements at 55-75° of undoped GaAs substrates with a 2 μm Be-doped GaAs layer of varying doping concentration show no clear trends in $\langle \varepsilon_2 \rangle$ with doping concentration.

The author has not succeeded in coming up with a physical explanation to this, but as these samples are old and have been handled by many different people, it is possible that some of the samples have switched boxes and thus mistakenly being assigned the wrong doping concentration. This might also be the case for the Si-doped samples discussed in Section 5.2.1. The easiest and most reliable way to confirm this is to make a Hall bar and perform Hall measurements on the samples. This is a time-consuming process, and has not been conducted in this work. Instead, not too much emphasis will be put into the measurements of the neither the Be-doped nor the Si-doped samples when modeling the more complex structures.

5.3 Samples with Two Quantum Dot Layers

To investigate how QDs affects SE measurements of full QD-IBSC structures, it can be beneficial to isolate the problem and eliminate other layers that increase the uncertainty when analyzing SE measurements. Therefore, samples consisting only of stacked InAs QD layers are investigated. Presented in this section are the simplest structures measured in this thesis, consisting only of two QD layers grown on a GaAs substrate with a GaAs spacer between them. These samples will hereby be referred to as the 2QD samples.

The 2QD samples have very similar nominal compositions, however, different growth conditions has led to different mean QD sizes for the two samples. Differences are also seen in SE measurements, and in Figure 5.8 measurements at 65° using SFP are plotted together. Focus probes often lead to higher uncertainty in the measurements [25], but even though the samples were only aligned at 65° , they do not appear very different when measured at different angles. Comparing sample 9As503-2 measured with and without focus probes in Figure 5.9 shows that there are differences, indicating that the use of focus probes leads to different, and (as long as there are no large local variations on the sample) probably less accurate results. However, the differences in Figure 5.9 are less prominent than the differences between the two different samples in Figure 5.8.

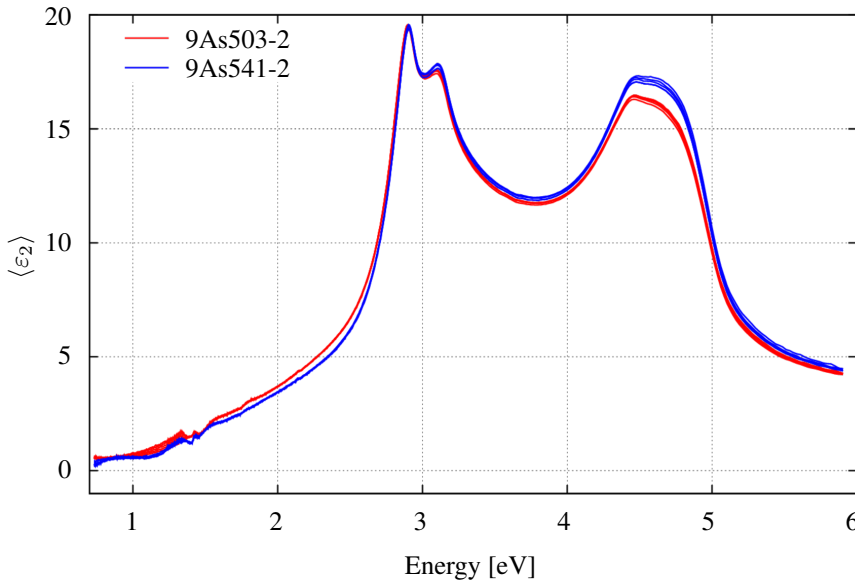


Figure 5.8: Comparison of SFP measurements of 9As503-2 and 9As541-2.

When comparing the two samples, one could argue that the no SFP measurement of sample 9As503-2 should be used to lower the uncertainty, however, comparing samples on equal conditions may also exclude discrepancies due to the different measuring method. For example, SFP focus the light before it hits the sample, which means that not all photons are parallel when incident on the sample surface. Because of this, measurements using focus probes does not go as deeply into the sample as the parallel light, meaning that

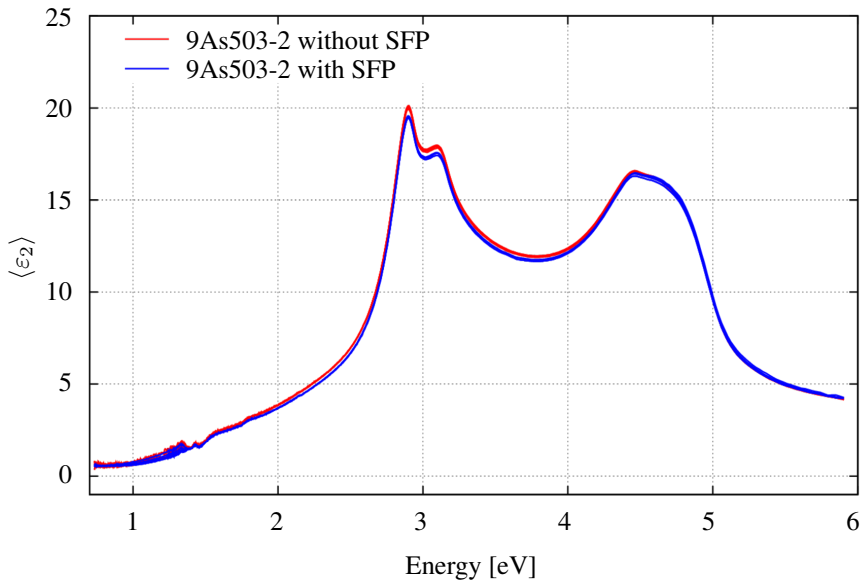


Figure 5.9: Comparison 9As503-2 measured with and without SFP.

regular measurements may contain more information of the layers deeper into the sample than SFP measurements, leading to different data without any of them actually being wrong. When modeling 9As503-2, the data measured without SFP is used.

The differences in $\langle \varepsilon_2 \rangle$ between 9As503-2 and 9As541-2 are largest around Peak 2, and at such high energies, the differences most likely come from differences at the, or very close to, the surface. This agrees with the known differences in the top layer QDs for the two samples.

5.3.1 Modeling of the Samples with Two QD Layers

For the 2QD samples, three different models are investigated in order to learn more about the effects of QDs in SE. First, a simple model assuming there are no QDs present is discussed, before looking into two models inspired by the works of Steimetz *et al.* [9] and Lee *et al.* [10]. A quick overview of the three models is found in Table 5.1. When fitting a model to the measurements, the fitting parameters are allowed to vary within what is considered reasonable for that parameter to make the best fit possible while still avoiding unphysical results.

All samples containing QDs are grown on n-type doped substrates with a doping concentration of $1 - 5 \times 10^{18} \text{ cm}^{-3}$. In the library, the only model with a similar concentration is the one given in Figure 5.6. The only reference found to who made this model is the name H. Yao, without a given affiliation, and the model is clearly not to be trusted above 5 eV and below the band-gap. The measured samples with varying doping could also be considered as possible models for the substrates, but there is a lot of uncertainty related to if these samples have the doping they are said to. Therefore, it is chosen to use the UNL

Table 5.1: Overview of the different approaches to model the QD samples in this thesis.

Model	Details
Simple	Does not try to model the QDs or WL. Fitted only using InAs oxide and surface roughness.
Steimetz	Models the WL as 1 ML of bulk, relaxed InAs. QDs modeled as Maxwell-Garnet EMA.
Lee	Models the QDs and WL with a damped harmonic oscillator model.

model for undoped GaAs. As discussed in Section 5.2, this will probably lead to deviations from the measurements, but as it is the most trustworthy model, it is considered to be the best option. Regardless of which model is chosen there might be deviations between the sample substrates, as the exact doping concentration is not known, but can vary from $1 - 5 \times 10^{18} \text{ cm}^{-3}$.

Finding a Simple Model

Three different possible simple models were made, and Figure 5.10 shows how they fit the measurements. The simplest, consisting only of a GaAs substrate and surface roughness, fits the samples quite well considering its simplicity, however, as there is no reason to believe that the samples do not have oxides on their surfaces, the model is definitely not correct. As the effects of surface roughness and oxide are very similar, it is probably compensating for the lack of an oxide in the model by increasing the surface roughness thickness, and this is supported by the thicknesses of the fitted models shown in Table 5.2. In this table, MSE, surface roughness and oxide layer thickness are given for all the simple models. Both from Figure 5.10 and Table 5.2, it is evident that for 9As503-2, the models with an oxide layer fit the measurements better. For 9As541-2, all models have approximately the same MSE, which is significantly higher than the MSE for all models of 9As503-2, but the surface roughness is very different in the SR only model compared to the two models with oxide layers. As the mean QD height is measured to be 26 \AA for 9As503-2 and below 6 \AA for 9As541-2, it is obvious that the models with oxide layers are more accurate than the models with no oxide layer.

Table 5.2: Fit parameters and MSE for three different simple models for the two 2QD samples.

Model	MSE	Surface roughness (SR) [\AA]	Oxide thickness [\AA]
<i>9As541-2</i>			
SR only	10.367	34.55	-
SR + GaAs oxide	10.361	6.90	28.36
SR + InAs oxide	10.267	0.95	30.63
<i>9As503-2</i>			
SR only	7.787	39.38	-
SR + GaAs oxide	5.371	20.86	29.68
SR + InAs oxide	5.267	18.41	31.41

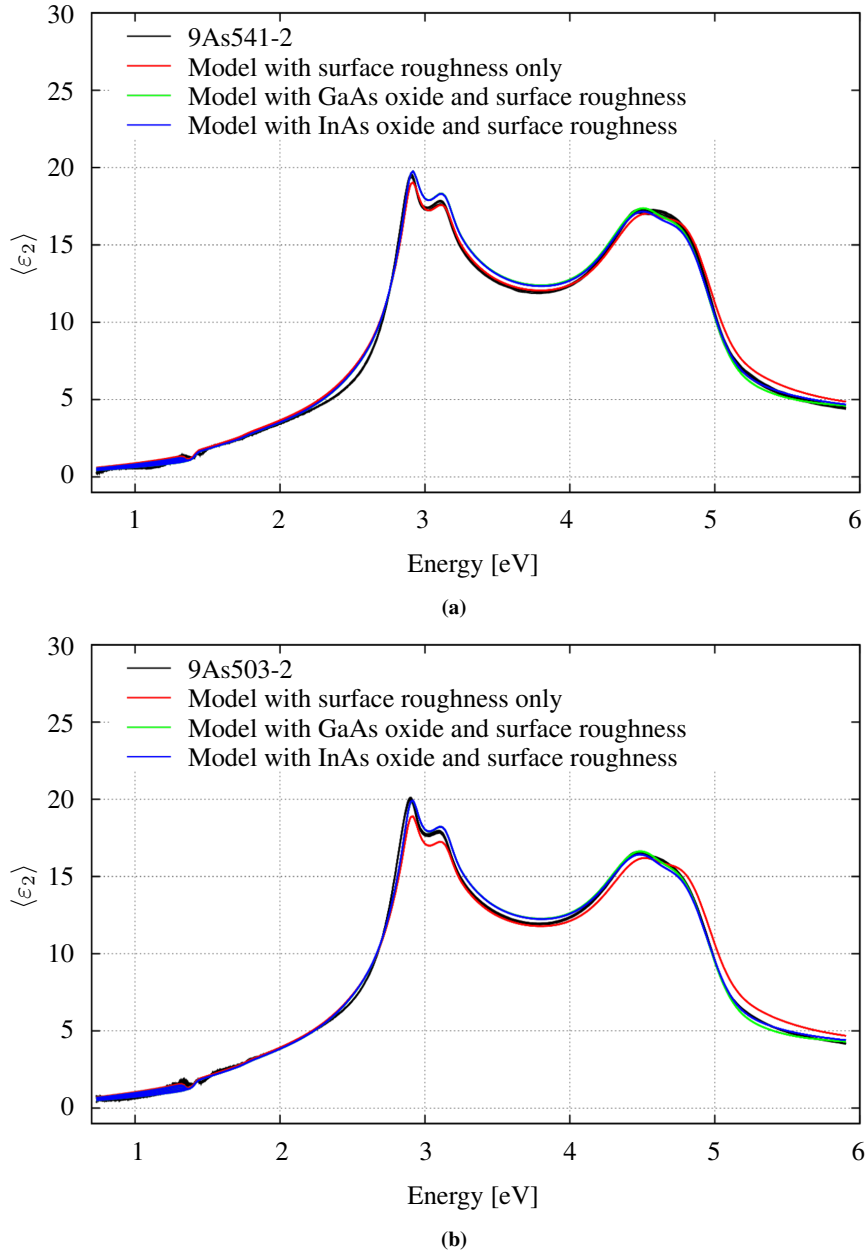


Figure 5.10: Measurement compared with different simple models for (a) 9As541-2 and (b) 9As503-2.

Figure 5.10 shows that whether the modelled oxide layer is GaAs oxide or InAs oxide, makes very little difference for the fit of the model. The two oxide models are different only above approximately 4.2 eV, which is explained by looking at their bulk dielectric functions found in Figure 5.11. Further, the values in Table 5.2 indicate that the models fit the measurements approximately equally good, with InAs oxide giving a slightly lower MSE.

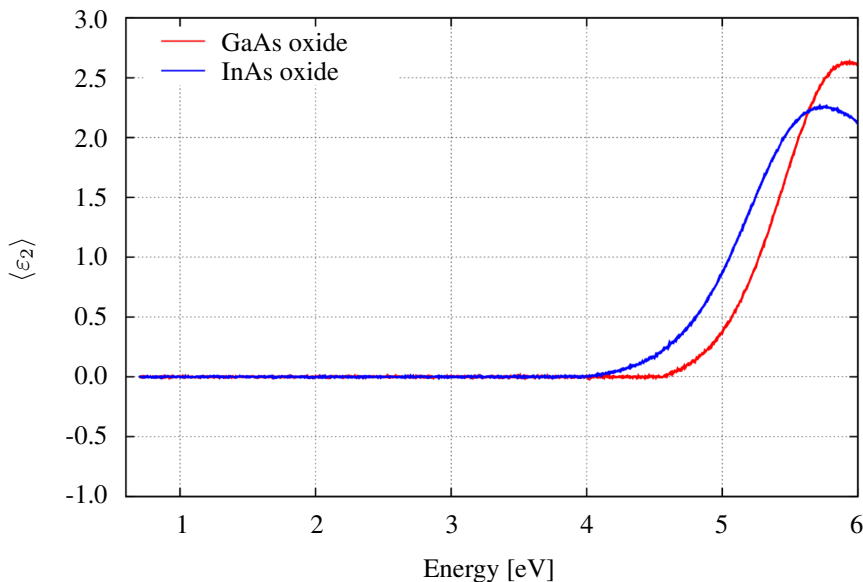


Figure 5.11: Simulation at 55-75° comparing bulk values of GaAs oxide and InAs oxide without surface roughness. InAs oxide starts to absorb light at around 4 eV, and has a higher absorption than GaAs oxide up to about 5.7 eV, where $\langle \epsilon_2 \rangle$ of GaAs oxide exceeds that of InAs oxide. Data from Zollner (1993)[28].

As there are InAs QDs on top of the samples it is expected that the oxide mainly will contain InAs, but as the oxide appears to be quite thick compared to both the QD height and the WL thickness, it is reasonable to believe that there will also be gallium present in the oxide. However, these models show that there are little difference as to which oxide is used, and findings by Hollinger *et al.* (1994) [32] indicate that InAs and GaAs oxidizes at approximately the same rate, which means that the model of choice is not very important for the result. As InAs oxide gives a slightly better model for both 2QD samples, and as it probably is the most correct with respect to composition, InAs oxide will be used as the top oxide for the rest of the modeling.

The Steimetz Model

A more complex, but still macroscopic model is used by Steimetz *et al.* (1996) to model InAs QDs grown on top of a GaAs substrate measured in situ [9]. As the 2QD samples measured in this work, the samples in [9] are also grown on GaAs (001), but the growth-

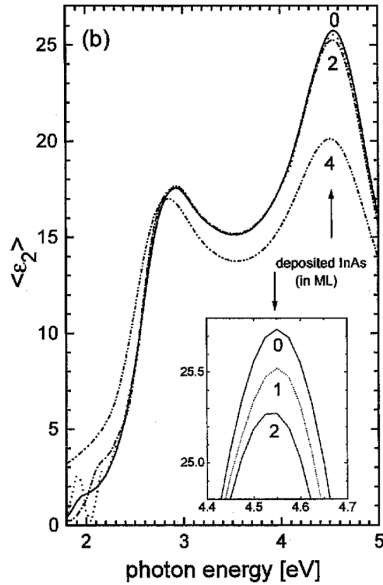


Figure 5.12: Ellipsometry spectra measured after the deposition of well defined amounts of InAs on GaAs (001). Figure taken from [9].

method is metalorganic vapour phase epitaxy (MOVPE) and not MBE. It is not known how large differences different growth methods might lead to. Steimetz *et al.* have done SE for varying amounts of InAs deposited, which are found in Figure 5.12. The trend with decreasing amplitude of Peak 2 and increasing $\langle \epsilon_2 \rangle$ below Peak 1 agrees with the findings in Figure 5.8, as 9As503-2 has 2.3 ML of InAs deposited and 9As541-2 has 2.2 ML.

The Steimetz model is based on two approximations. The first is that the WL is modelled as a single monolayer of bulk InAs. This is of course not correct, as the WL is strained, which gives InAs different properties and different ellipsometric spectra [33, 34]. Furthermore, the WL may actually be thicker than 1 ML, Pryor (1998) states that InAs/GaAs(001) wetting layer normally is 1-2 ML thick [35]. The QDs are modeled as clusters of bulk InAs using a Maxwell-Garnet EMA. The height of the EMA layer is set to be the same as the mean QD height, and Steimetz *et al.* calculate the InAs EMA fraction as the deposited InAs thickness minus 1 ML for the WL divided by the QD height.

For this thesis, a different approach to calculating the InAs volume fraction has proven to give better fitting models. By assuming that the QDs have the approximate shape of a sphere cap, the mean QD volume can be calculated from the mean height and diameter [36, p. 69]. Combining this with the measured QD density gives a QD volume fraction of 6 % for 9As503-2 in a layer of the same height as the mean QD. For 9As541-2, the mean dimensions of the QDs could not be measured, but as this method in any way is based on highly uncertain calculations, some guesses are made on the height and diameter of these QDs by looking at the trends of samples in the same series as 9As503-2 and 9As541-2 with QDs grown at higher temperatures found in Table I in [23, paper II]. Assuming a QD density of $\rho_{tot} = 30 \times 10^{10} \text{ cm}^{-3}$ and a mean height of 0.5 nm leads to a fraction of

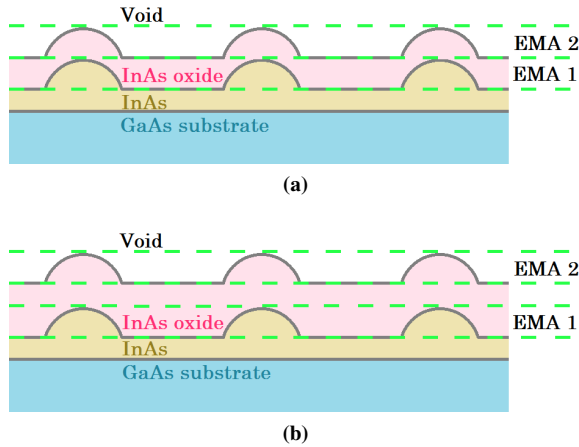


Figure 5.13: Different ways of modeling the oxide layer on top of the QDs following the approach of Steimetz *et al.* [9]. The model in (a) consists of InAs, EMA with InAs oxide and InAs followed by EMA with void and InAs oxide, and is referred to as Steimetz model 1. In (b) there is also a layer of InAs oxide between the two EMA layers, and this model is referred to as Steimetz model 2.

$f_{QD} = 7.6\%$ for a mean width of 8 nm and $f_{QD} = 4.3\%$ for a mean width of 6 nm. If instead assuming that the density is $\rho_{tot} = 18 \times 10^{10} \text{ cm}^{-3}$, the fractions would be 4.6 % and 2.6 % for 8 nm and 6 nm diameter, respectively. These estimates are of course very uncertain, but they give an idea of the order of magnitude of the volume fractions for the two samples.

As the 2QD samples in this work are measured years after they were grown, it is assumed that the oxide thickness of these cannot be neglected. Including InAs oxide in the model significantly improves the MSE, and therefore this is included in all models in this section. However, there are different ways to include the oxide. The oxide is believed to grow at equal rate on both the QDs and the WL, and as the simple models indicate an oxide layer of approximately the same thickness as the QD height for 9As503-2, and much larger than the 9As541-2 QD height, the most reasonable way to model this in a similar way as Steimetz *et al.*, is to have one EMA with InAs and InAs oxide followed by an EMA with InAs oxide and air (void), and maybe also include a bulk InAs oxide layer between the EMA layers. This is illustrated in Figure 5.13, and the model with top layers as in (a) will be referred to as Steimetz model 1, and (b) as Steimetz model 2.

The QDs inside the samples are modeled as 1 ML of InAs followed by an EMA with GaAs and InAs. When fitting the Steimetz models, the WL modeled by 1 ML of InAs was kept constant at 6.5 Å, which is the approximate thickness of 1 ML of strained InAs on GaAs [23, paper II] (although the InAs model used is for relaxed InAs). The void/InAs oxide EMA and the EMA for the QDs inside the sample were kept at 26 Å for 9As503-2. For 9As541-2, the EMA inside the sample and the void/InAs oxide EMA were kept at 5 Å for model 2, and for model 1, the thickness of the top layer EMA was allowed to vary, as model 1 with a top layer EMA thickness set to 5 Å clearly contained too little InAs oxide, even when the InAs oxide fraction was set to 100 %.

When InAs oxidizes, it is reasonable that the amount of InAs present (not in the oxide)

decreases. This is compensated for by decreasing the thickness of the InAs/InAs oxide EMA from 26 Å to 22 Å for 9As503-2 and from 5 Å to 4 Å for 9As541-2. The InAs fraction is also decreased in this layer from 6 % to 5 % in 9As503-2, and in 9As541-2, the fraction of InAs (InAs oxide in the top EMA) is set to 7 % in the top and bottom EMA, and to 6 % in the middle. As the thickness of the WL model already is set to a very low value, this is not decreased. The spacer thickness was kept constant at 41 nm for both samples, which is the value found for 9As541-2 in TEM measurements.

In Table 5.3 details on the fit of Steimetz models 1 and 2 for both samples are given. For 9As541-2 Steimetz model 1, the fitted top EMA thickness was found to be over 94 Å, which is unreasonably high considered the known details of the samples. Figure 5.14 shows the $\langle \epsilon_2 \rangle$ for the two Steimetz models, along with the simple model with InAs oxide. None of the samples provide a really good fit to the measurement, but it is clear that Steimetz model 1 is the worst fit. To see how the EMA and InAs layer for the QDs inside

Table 5.3: Comparing the MSE of Steimetz model 1 and 2 clearly shows that Steimetz 2 provides a better fit than Steimetz 1 for both 2QD samples.

	9As503-2		9As541-2	
	Steimetz 1	Steimetz 2	Steimetz 1	Steimetz 2
MSE	10.580	6.387	12.568	10.964
InAs oxide thickness [Å]	-	7.02	-	22.94

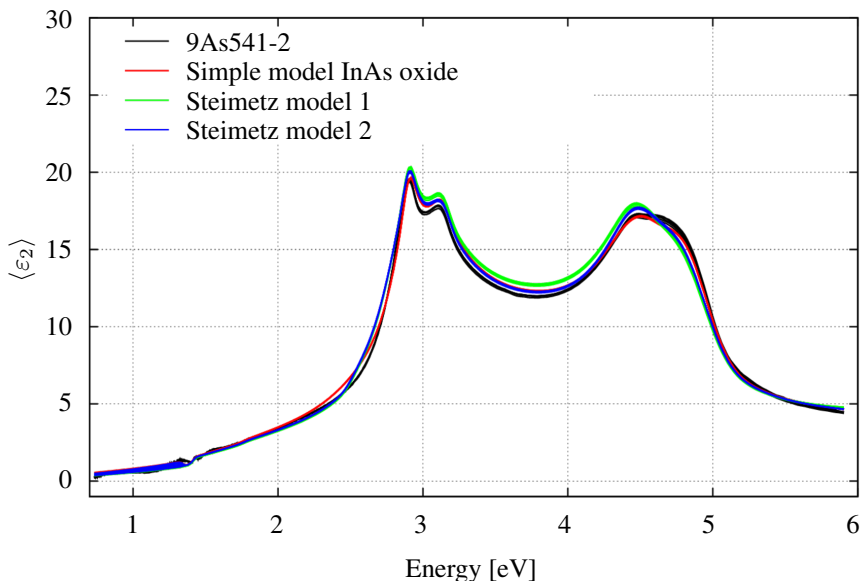


Figure 5.14: 9As541-2 together with simple model with InAs oxide and Steimetz models 1 and 2.

the sample affected the model, 9As503-2 was also modeled with the Steimetz model 2

top layer with only a GaAs substrate below. This provided a just slightly better fit than the Steimetz model 2 with the inside layers (MSE 6.342 vs 6.387), and the thickness of the InAs oxide layer was approximately the same for the two models, 6.90 Å vs 7.02 Å. In Figure 5.15, the difference between measurement and model is plotted for 9As503-2 Steimetz model 2 with and without the InAs and EMA below the spacer. The models are very similar and differ from the measurements at the same energies, and they differ from each other mostly between 2 eV and 3 eV. The fact that the model without the QD-layers inside fits the measurements as good as the more detailed model indicates that this is not a good way of modeling these QDs.

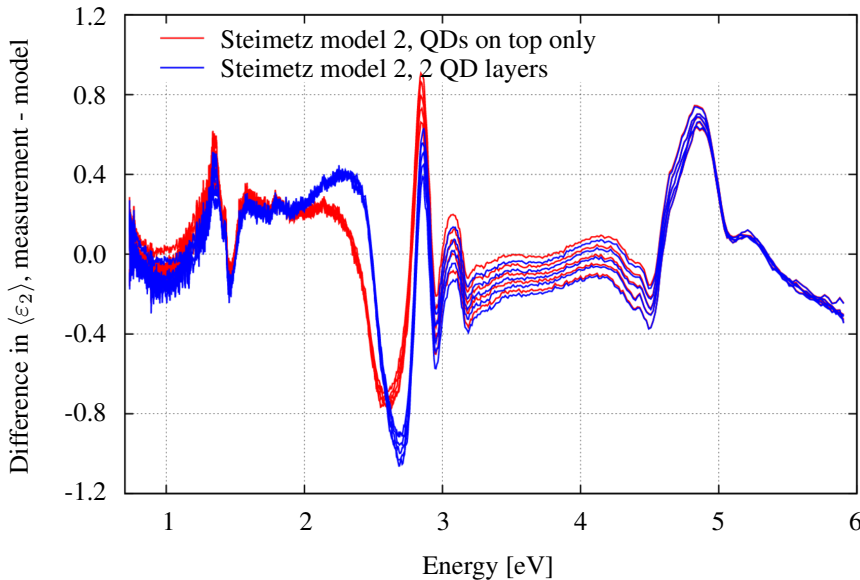


Figure 5.15: Difference in $\langle \epsilon_2 \rangle$ between 9As503-2 and Steimetz model 2 with and without the layers modeling the QDs inside the sample.

Lee model

The third model considered in this thesis is a model used by Lee *et al.* (2001) to model the InAs wetting layer at the threshold of QD formation. This is the only of the models discussed here which does not have a clear physical interpretation, but it is also the only non-macroscopic model. As seen in previous parts of this section, neither the simple nor the Steimetz model could fit any of the samples perfectly, and the explanation to this might be the quantum effects from QDs and the strained WL that cannot be modelled using a macroscopic model.

Lee *et al.* have measured single-, double- and multilayers of InAs in GaAs [10]. The thickness of the InAs layers ranged from 1 ML to 2.6 ML with a 4 nm layer of GaAs on top of the InAs. MBE was used to grow the samples, and the GaAs substrates were nominally undoped. The InAs was grown at 480 °C. To model these samples, a multilayer model

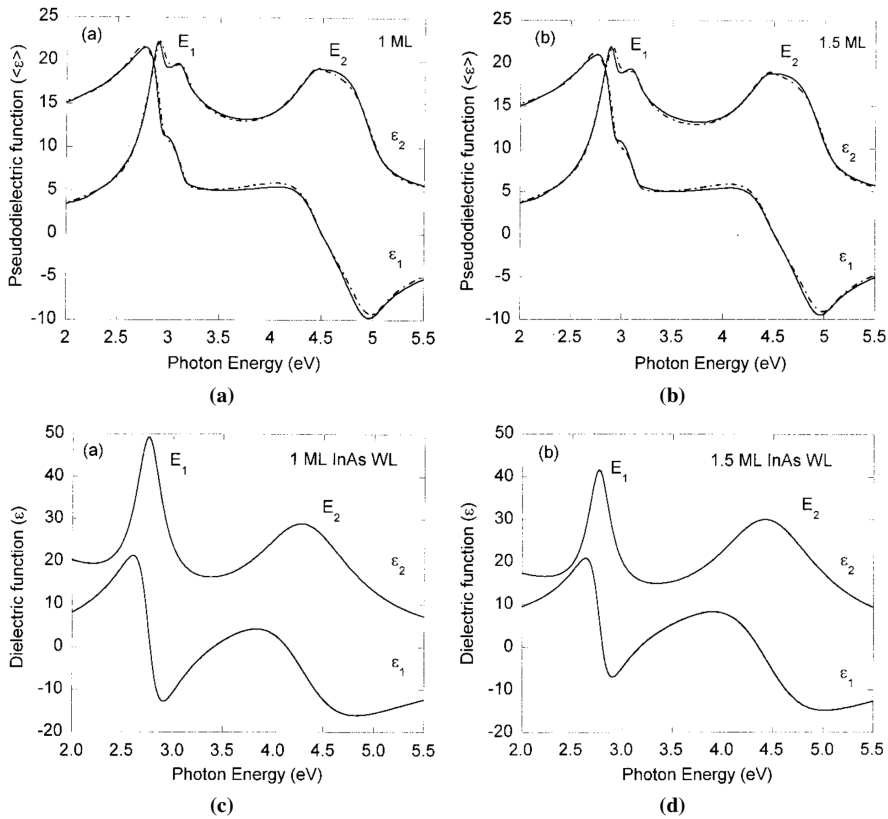


Figure 5.16: Plot of the PDF comparing measurements with model for (a) 1 ML and (b) 1.5 ML of InAs deposited. Below in (c) and (d) are the corresponding dielectric functions for the oscillator models. Figures taken from [10].

was used, with models from literature for the known layers. To fit the the WL, a damped harmonic oscillator model differing from the Lorentz oscillator (Equation 2.36) only by the constant term was applied. This model has also been used by Herzinger *et al.* (1995) in the determination of AIAs optical constants by VASE [37]. Measurements with fitted models by Lee *et al.* for samples with 1 ML and 1.5 ML InAs are found in Figure 5.16(a) and (b), and the corresponding oscillator model dielectric functions are given below, in (c) and (d). These thicknesses are below the critical thickness for QD formation, which is usually around 1.7 ML [10].

The oscillator model used by Lee *et al.* to model the WL consists of two oscillators at energies of about 2.8 eV and 4.4 eV. As seen in Figure 5.16(c) and (d), the oscillators give a positive contribution to the dielectric function. Unexpected results are seen when this model is used to fit the measurements. Oscillators with positive amplitude give a negative contribution in the PDF independent of FWHM, energy position and whether it is a Gauss, Lorentz or Tauc-Lorentz oscillator. When adding oscillators to 9As503-2, allowing them

to vary slightly around 2.8 and 4.4 eV, and letting the amplitude and FWHM vary freely, the best fit found is for a negative amplitude, which is clearly unphysical as it corresponds to negative absorption. In Figure 5.17, a model with GaAs substrate, two oscillator layers separated by a 41 nm GaAs spacer, and an InAs oxide layer on top is plotted together with the best fits of the simple and the Steimetz model. Each oscillator layer consists of the same two Lorentz oscillators, one at 2.8 eV and the other at 4.4 eV. The FWHM is set to 0.2 and the amplitude to 0.3 for both oscillators. These do not provide the best fit for this model, they are chosen to illustrate what the contribution looks like. The author has

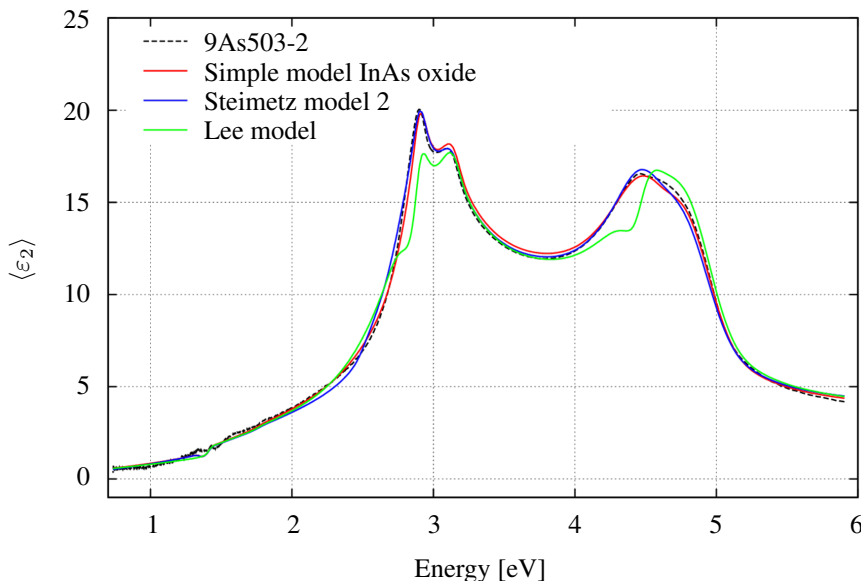


Figure 5.17: Measurement of 9As503-2 together with the best fitting versions of the simple- and Steimetz model. The Lee model only gave negative contributions to the PDF for positive amplitude, independent of strength, width or position of the oscillators, and here, oscillators with a FWHM of 0.2 and an amplitude of 0.3 are placed at 2.8 eV and 4.4 eV.

not succeeded in coming up with a physical explanation to this, and can neither deny nor confirm that this is caused by a bug in the program used for analysis and modeling.

Comparing the three models presented in this section, it is clear that for these samples, the simple models provide the best fits. This indicates that the Steimetz method of using macroscopic models to fit samples with quantum effects is not working very well. Also, increasing the complexity of a model increases the number of parameters to fit, and consequently the number of assumptions that has to be made.

Another interesting observation is that all models fit sample 9As503-2 better than 9As541-2. One reason for this could be that sample 9As541-2 is measured using focus probes, while the modeling on 9As503-2 is performed to measurement without SFP. All the models are fit to all measured wavelengths, while the samples are only aligned at 65° . For measurements using SFP, the sample should be aligned for every measured angle [25],

and this can explain the higher overall MSE for 9As541-2. Another possible explanation can be that as 9As541-2 has smaller QDs than 9As503-2. This means that the quantum confinement is higher in the QDs in 9As541-2, and this may lead to stronger quantum effects making the simple models not fit this sample as good as 9As503-2. Lastly, as the doping in the substrates ranges from $1.5 \times 10^{18} \text{ cm}^{-3}$, it is possible that 9As541-2 has a significantly higher doping concentration than 9As503-2, and differs more from the undoped GaAs library value used to model the substrates.

Comparing model-measurement difference between the 2QD samples and their best fitted simple models show that the difference follows the same trend for both samples. In Figure 5.18, a large peak in difference can be seen at approximately 2.8 eV. A positive difference means that the model has a lower value for $\langle \varepsilon_2 \rangle$ than the measurement, and a negative difference means the model has the highest $\langle \varepsilon_2 \rangle$. A small peak can also be seen at approximately 4.4 eV accompanied by a larger, but still small peak between 4.5 eV and 5.0 eV. The fact that the simple models deviate from their respective measurements following the same pattern indicates that the deviations are due to common properties of the samples, and as the Steimetz model did not improve the accuracy, this supports the theory of this being due to quantum effects from either the WL or the QDs.

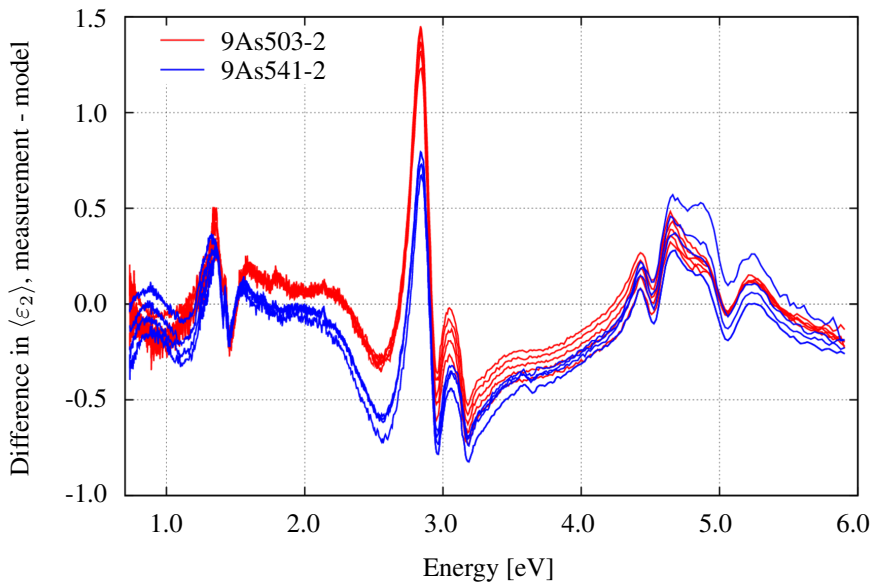


Figure 5.18: The difference in $\langle \varepsilon_2 \rangle$ between measurement and simple InAs model is very similar for the two 2QD samples. A positive difference means that the measurement has a higher $\langle \varepsilon_2 \rangle$ than the model and vice versa.

Another indication of quantum effects is found below the band-gap of 9As541-2. Here, a broad peak is observed with a maximum around 0.9 eV. A close-up between 0.7 eV and 1.2 eV of Figure 5.8 found in Figure 5.19 shows the peak clearly, and it is only present in 9As541-2. A peak attributed to QD effects at the same energy is reported by Lee *et al.* in 1999 [38, 39].

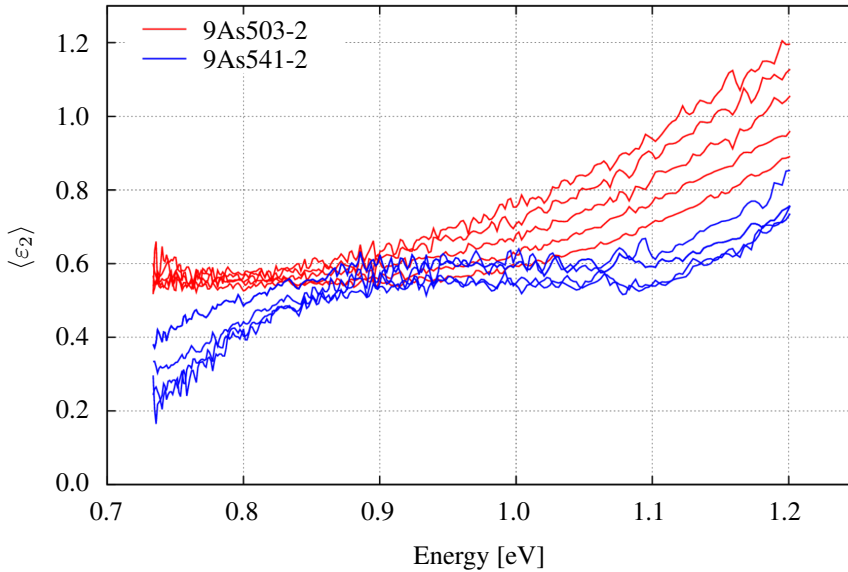


Figure 5.19: Close-up of Figure 5.8 below the band-gap.

It is natural to assume that this peak corresponds to the QD peak found in PL measurements, and that the reason that this peak is only observed in 9As541-2 is because this sample had the strongest, sharpest QD peak, and that the QD contribution in 9As503-2 is simply not sharp or strong enough to be observed in these SE measurements. However, the PL QD peak of 9As541-2 is located at 958 nm, which is approximately 1.29 eV. As the PL is performed at low temperature, one might expect the peak to be found at around 0.1 eV lower energy at room temperature, but this still means that the peak should be located at around 1.2 eV, 0.3 eV higher than the peak in the SE measurements. It is therefore hard to say if this peak is due to the QDs, or if it is caused by something else.

5.4 Samples with Ten Quantum Dot Layers

The most complex samples except the full IBSC-structures investigated in this thesis consist of ten layers of QDs. These samples differ nominally only by their spacer material, which is GaAs for 9As157 and $\text{Al}_{0.25}\text{GaAs}$ for 9As159. The samples will be referred to as the 10QD samples, and the imaginary parts of their measured PDFs are given in Figure 5.20 together with a difference plot where $\langle \varepsilon_2 \rangle$ of 9As157 is subtracted from 9As159. Comparing Figure 5.20 with Figure 5.1, the same trend with increased energy of Peak 1 and increased amplitude of Peak 2 with increasing Al-content is observed for the 10QD samples as for the simulated bulk values. Also, oscillations can be seen for higher energies in 9As159 than 9As157 due to the higher band-gap of $\text{Al}_{0.25}\text{GaAs}$.

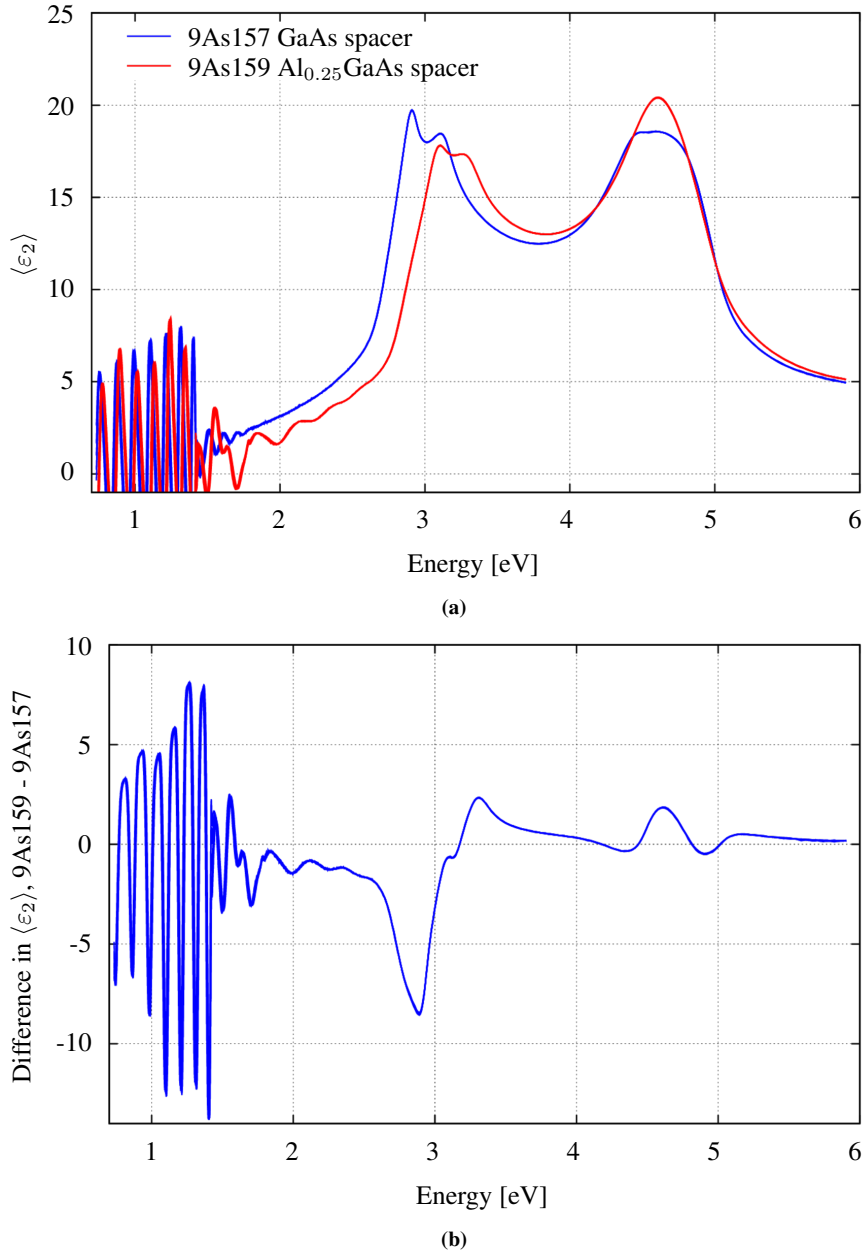


Figure 5.20: 9As157 and 9As159 compared through (a) a regular $\langle \epsilon_2 \rangle$ plot and (b) a difference plot where the $\langle \epsilon_2 \rangle$ of 9As157 is subtracted from that of 9As159.

5.4.1 Modeling the Samples with Ten QD Layers

For the 10QD samples, approximately the same approach as for the 2QD samples in modeling the PDF is used. Recalling from Section 5.3, the oscillators of the Lee model gave unexpected results and poor fit for all samples, and will therefore not be further discussed for these samples. However, combining the Steimetz and Lee models lead to an interesting model that will be presented later in this section instead of the Lee model.

Compared with the 2QD samples, the 10QD samples have much stronger oscillations below the GaAs band-gap due to the 100 nm of $\text{Al}_{0.8}\text{GaAs}$ and the 1 μm thick GaAs below the QD stack. These oscillations can be used to fit some of the layer thicknesses and parameters precisely, assuming that the models used are correct.

Simple model

As the 2QD samples, the 10QD samples were also modeled in a simple way with bulk spacer material through the whole QD stack, and InAs oxide and surface roughness on top. The $\text{Al}_{0.8}\text{GaAs}$ layer below the QDs was also included in the models. Applying the simple model with nominal values gave very poor fit for both the 10QD samples, with MSE above 100, due to a mismatch between model and measurement in the oscillations at lower energies. Adjusting the thicknesses and $\text{Al}_x\text{Ga}_{1-x}\text{As}$ compositions brought the MSE down to 6.679 for 9As157 and 6.407 for 9As159 with the values given in Table 5.4.

Table 5.4: Fitted values for the simple models applied to 9As157 and 9As159.

	9As157	9As159
MSE	6.679	6.407
Surface roughness [\AA]	0	1.90
InAs oxide thickness [\AA]	24.29	21.62
Spacer Al-content [%]	-	24.992
Spacer/QD thickness [\AA]	14573.64 in total	4889.09
1 μm GaAs thickness [\AA]		9543.43
Al-content lower layer [%]	85.128	85.792
Lower AlGaAs layer thickness [\AA]	1032.62	1009.42

Table 5.4 suggests that some of the thicknesses deviate from their nominal values. The lower AlGaAs layers are found to have approximately the nominal thickness, while the layers above appear to be thinner than expected. Also, the simple models for both samples agree that the Al-content in the $\text{Al}_{0.8}\text{GaAs}$ layer is significantly higher than the nominal value of 80 %. According to Dr. Rajpalke, the post doc who grew the samples, this is unlikely as the growth rates for Al, Ga and As were calibrated using RHEED before the growth. However, the Ga growth rate used during the growth of this layer was only extrapolated from the calibrated rate, and much lower in this layer to keep the correct Al:Ga ratio. It is therefore possible that the Ga growth rate was a bit lower than expected, which would have lead to an increase in the Al:Ga ratio. This would however not agree with the estimated thickness of these layers, as a decrease in Ga growth rate would also imply a lower total thickness than expected. [40]

The thickness and composition of the lower layers only affects the PDF at lower energies, only below the GaAs band-gap for the $\text{Al}_{0.8}\text{GaAs}$ layer and the $1\ \mu\text{m}$, while the spacer/QD layer shows slight changes in PDF with thickness up to $2.6\ \text{eV}$. The Al-content in the spacer of 9As159 affects the PDF over the whole measured spectra. When adjusting the model to fit the oscillations at lower energy, different parameters affect the oscillations in different ways. The Al-content of the lower AlGaAs layer adjusts the amplitude of the oscillations, and in Figure 5.21 a close-up of the oscillations compares the simple model with and without a fitted Al-content with the measurement of 9As157. From the figure it appears as the amplitude of the oscillations in the model with nominal Al-content is too low compared with the measurements, while the fitted value of 85 % provides a much better fit.

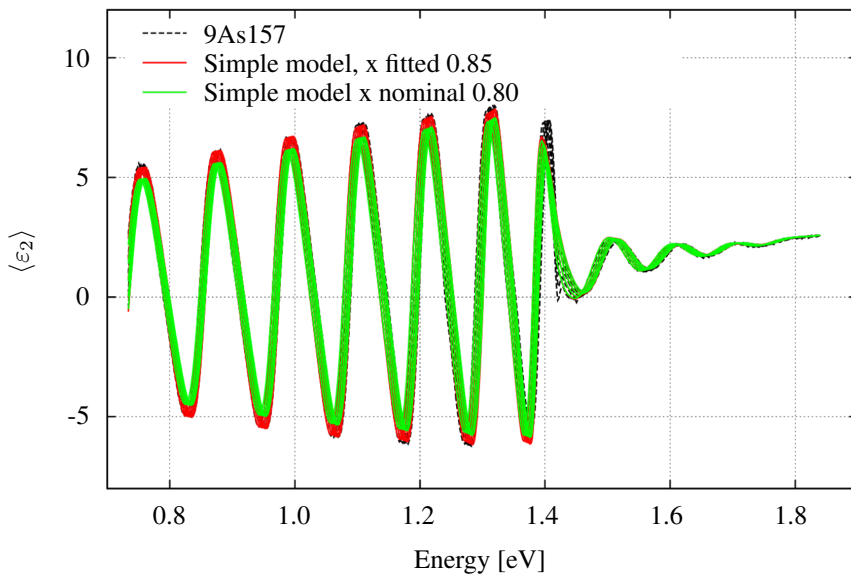


Figure 5.21: A close-up on the oscillations at low energies in 9As157 together with simple models with fitted and nominal Al-content.

The thickness of the lower AlGaAs layer affects the displacement of the oscillations and varies the amplitude as a function of energy. The thickness of the upper two layers mainly affects the displacement and frequency of the oscillations. With all of these variable parameters, there is just one solution that provides the best fit for the oscillations in the measurements. However, the values in Table 5.4 are extracted from simple models, and it is possible that a more precise model might affect the thicknesses and compositions. The substrate used in the models is obviously incorrect, and the same can be said when omitting the WL and QDs.

Table 5.4 reveal surprisingly low values of surface roughness for both samples compared to the 2QD sample 9As503-2 which has QDs grown at the same temperature. As the effects of surface roughness and oxide thickness are very similar, it is possible to adjust down the oxide thickness a little and increase the surface roughness, and still get approx-

imately the same MSE. This might be a more physically explainable composition as also the oxide layer is expected to be slightly thinner on the 10QD samples as these were measured within days after growth.

In Figure 5.22 the best fitting simple model for 9As159 is plotted together with the measurement and the models presented in the following sections. The model fits the measurement poorly, especially between 2.5 eV and 3.2 eV, and above 4.7 eV.

Steimetz model

As for the 2QD samples, the Steimetz model using 1 ML of bulk InAs for the WL and an Maxwell-Garnet EMA with InAs for the QDs was applied to the 10QD samples. As opposed to the 2QD samples, the 10QD samples Steimetz models did not improve their fit by applying a bulk InAs oxide layer between the InAs/InAs oxide EMA and the InAs oxide/void EMA. Therefore, the top layers for these samples will be modeled as in Figure 5.13(a). This might be explained by the expected difference in oxide thickness between the 2QD and the 10QD samples, as the 2QD samples have been stored much longer in air after growth. One might speculate that for the 10QD samples, the oxide layer is so thin that an EMA with three constituents, InAs, InAs oxide and void, might be more correct, but the CompleteEASE™ program used in this thesis does not work well for EMAs with three constituents, and therefore this has not been investigated further.

When building a model for the 10QD samples, it is clear that a lot of the possible fit parameters has to be kept constant as there are just too many of them to vary all. Therefore, the spacer thickness is kept at 50 nm, the InAs ML at 0.65 nm and the QD EMA height is set to 2.6 nm for all layers except the top one, which is allowed to vary. This height is chosen because it is the measured mean height of the top layer QDs in 9As503-2, which was grown with the same QD temperature as the 10QD samples. The thicknesses of the layers below the QD stacks are allowed to vary, along with Al-composition, and the thickness of the void/InAs oxide EMA.

For 9As159, this detailed model does not fit the measurement at all with an MSE of 33.775, as seen in Figure 5.22. With an MSE of 7.983, 9As157 matches its detailed model significantly better, but for both samples a model only containing details for the top QDs provides a better fit. Details on the fit parameters of this simple Steimetz model are found in Table 5.5.

Table 5.5: Fitted values for the simple Steimetz models applied to 9As157 and 9As159.

	9As157	9As159
MSE	7.112	7.473
Void/InAs oxide EMA thickness [Å]	8.09	37.28
InAs oxide/InAs EMA thickness [Å]	21.13	14.90
Spacer/QD thickness [Å]	14567.47 in total	4882.18
1 μm GaAs thickness [Å]		9544.79
Al-content lower layer [%]	85.409	86.030
Lower AlGaAs layer thickness [Å]	1031.63	1009.34

As for the 2QD samples, the simple models fit the measurements better than the

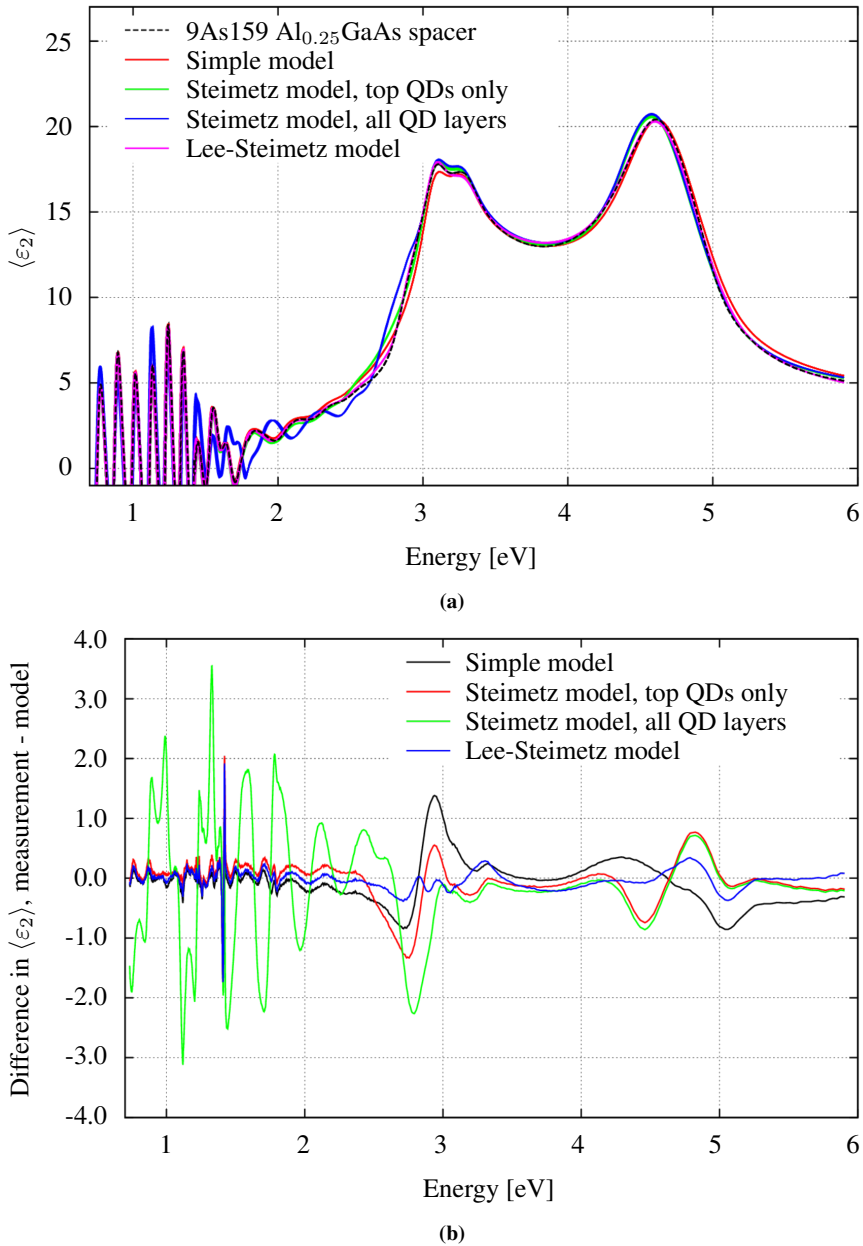


Figure 5.22: (a) $\langle \varepsilon_2 \rangle$ of the best fit versions of the different models applied to 9As159 and (b) difference plot for the same models. The reader should be aware that the colors of the different models in (b) are not the same as the colors of the corresponding plots in (a).

Steimetz models, supporting the theory that a macroscopic model does not describe the QDs and WLs of these structures well. For all of the QD samples, it is very likely that the WL and QDs does not consist of pure InAs, but rather of InGaAs with an unknown In:Ga ratio. This ratio is not known, and is expected to vary with growth temperature; for QDs grown at higher temperatures, more Ga will fuse into the InAs than at lower temperatures. An attempt to replace the InAs in the Steimetz model with $\text{In}_x\text{Ga}_{1-x}\text{As}$, letting x vary lead to best fit for $x = 0$ which is the same as the simple model, indicating that bulk InAs does not fit the measurements.

Lee-Steimetz Model

Recallign from Section 5.3, the Lee model provided unexpectedly poor fits for all samples it was applied to. However, when replacing the 1 ML bulk InAs WL ins the Steimetz model with a Bruggeman EMA consisting of bulk InAs and an oscillator model, the oscillators give contributions to the PDF as expected, which improves the MSE for both 10QD samples. As the Steimetz model, this model contains an EMA also to model the QDs, and it will be referred to as the Lee-Steimetz model. The oscillator model is put into the Steimetz WL, as Lee *et al.* seek to model the WL with this oscillator model.

The Lee-Steimetz model is only applied to the top layer QDs, ignoring the QDs inside the samples. The oscillators are, as in the Lee model, Lorentzian, and oscillator models with both one and two oscillators were tried. Figure 5.23 shows 9As157 together with the simple model and the Lee-Steimetz model with both one and two oscillators. Both Lee-Steimetz models fit the measurements better than the simple model, and the model with two oscillators has a slightly lower MSE than the one with only one oscillator.

In Figure 5.22, the best fitting Lee-Steimetz model for 9As159 with two oscillators is found. To fit the oscillators, they were given initial energy values of 2.8 eV and 4.4 eV, which are the values also reported by Lee *et al.* [10]. An overview of the fitted parameters for the Lee-Steimetz models with two oscillators is given for both 10QD samples in Table 5.6.

In Figure 5.22(b), it is seen how the oscillators of the Lee-Steimetz model dampens the deviations around the oscillators at 2.87 and 4.41 eV, providing a better overall fit to the measurement.

Comparing all the different models for the 10QD samples, there are a few similarities. They all agree that the Al-content of the $\text{Al}_{0.8}\text{GaAs}$ layer is higher than the nominal value, and that the thickness of this layer is slightly higher than expected. All models also indicate that the thickness of the nominally 1 μm thick GaAs layer is actually lower, and these trends are the same for both samples. However, as these values only affect the measurements at low energies and the models in the surface mostly affect higher energies, it is not so peculiar that the different models give approximately the same values for the parameters located deeper into the sample.

Looking at the difference between the best fitting simple model and measurement for all the four QD samples shows some clear trends. Figure 5.24 reveals a sharp, large peak in deviation at around 2.8 eV for all the samples with GaAs spacer and at around 2.9 eV for 9As159, which has $\text{Al}_{0.25}\text{GaAs}$ spacer. Other similarities include a deviation double peak at around 4.5 eV for the GaAs spacer samples, and a large deviation around the GaAs

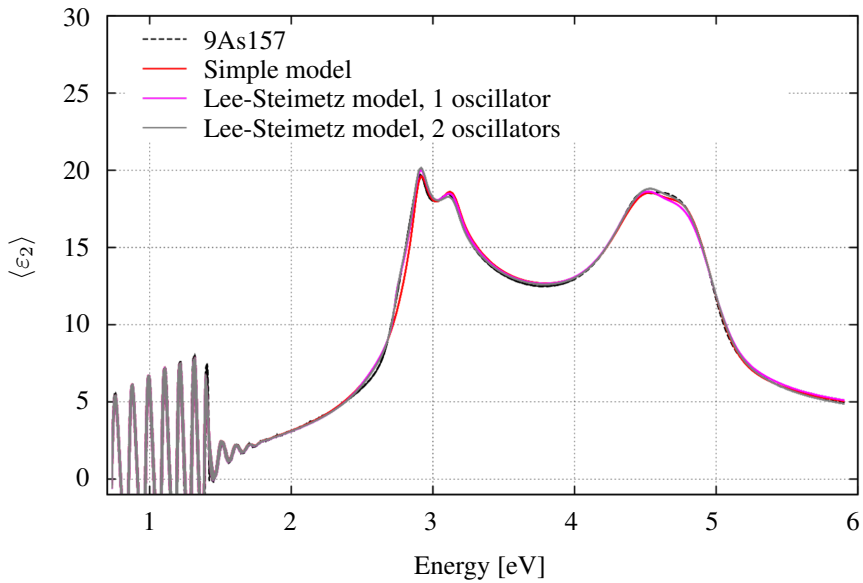


Figure 5.23: 9As157 together with best fitting simple model and Lee-Steimetz models with one and two oscillators.

Table 5.6: Fitted values for the Lee-Steimetz model with two oscillators applied to 9As157 and 9As159.

	9As157	9As159
MSE	5.981	5.428
InAs oxide/InAs EMA thickness [\AA]	15.29	11.86
Location oscillator 1 [eV]	2.737	2.865
FWHM oscillator 1	0.1000	0.1647
Amplitude oscillator 1	25.1471	21.3228
Location oscillator 2 [eV]	4.607	4.413
FWHM oscillator 2	0.6640	1.3989
Amplitude oscillator 2	4.8689	5.6447
EMA fraction, oscillators [%]	61.8	98.9
Spacer/QD thickness [\AA]		4893.46
1 μm GaAs thickness [\AA]	14572.25 in total	9541.46
Al-content lower layer [%]	85.199	85.782
Lower AlGaAs layer thickness [\AA]	1032.19	1009.97

band-gap for all samples. The deviation around the band-gap can be caused by effects from InAs QDs/WL, as reported by Rheinlinder and Gottschalch (1997) [41].

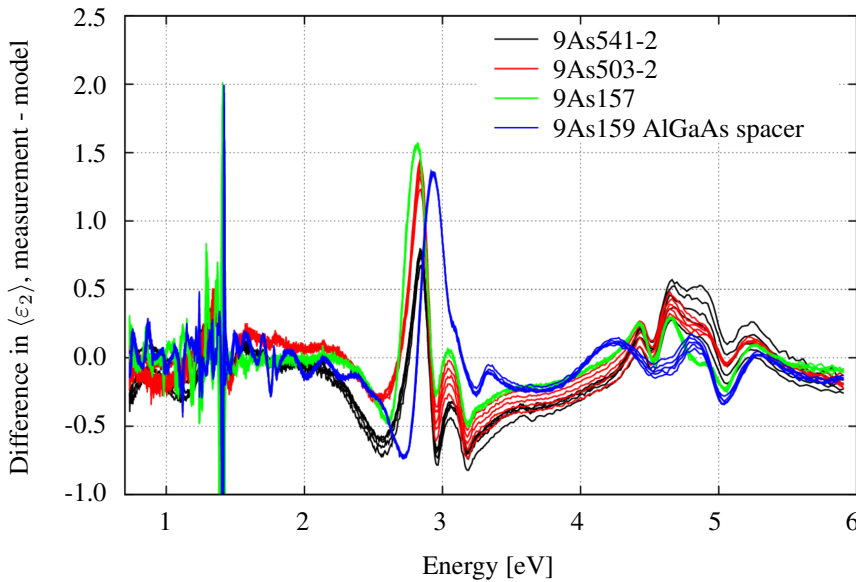


Figure 5.24: Comparing the differences between model and measurement for the best fitting simple models for all QD samples shows a clear trend in deviation.

5.5 GaAs substrates

It is reasonable to think that the trends in deviation for all the QD samples shown in Figure 5.24 are caused by something common for them, that makes them different from the simple models applied. Quantum effects from the QDs and WL is the most obvious explanation, but another element common for the samples that make them different than the simple models is the doped substrate. To investigate if this might be the reason for some of these deviations between the simple models and the measurements, one single-side polished and one double-side polished Si-doped $1 - 5 \times 10^{18} \text{ cm}^{-3}$, epi-ready substrate from the same producer are measured, shown in Figure 5.25. The single-side polished substrate is tried fitted by a model of undoped GaAs, GaAs oxide and surface roughness.

These substrates show surprisingly different PDFs. Simulations of undoped bulk GaAs with and without backside reflections in Figure 5.26 indicate that samples with identical content, where one is double-side polished and the other is single-side polished, should have identical PDFs above the band-gap. However, the exact doping of these samples is not known, and one might expect to see differences between samples with $1 \times 10^{18} \text{ cm}^{-3}$ and $5 \times 10^{18} \text{ cm}^{-3}$, but according to the observations of Snyder *et al.* shown in Figure 5.5 and the simulations comparing undoped with doped GaAs in Figure 5.6, the differences between these two substrates are so large that it is unlikely that doping difference can be the explanation alone.

Both substrates show remarkably smooth peaks compared to bulk GaAs, and also to all the QD samples, which are grown on n-type substrates. It is possible that the smooth peaks are caused by the doping, as discussed in Section 5.2, but in that case an explanation

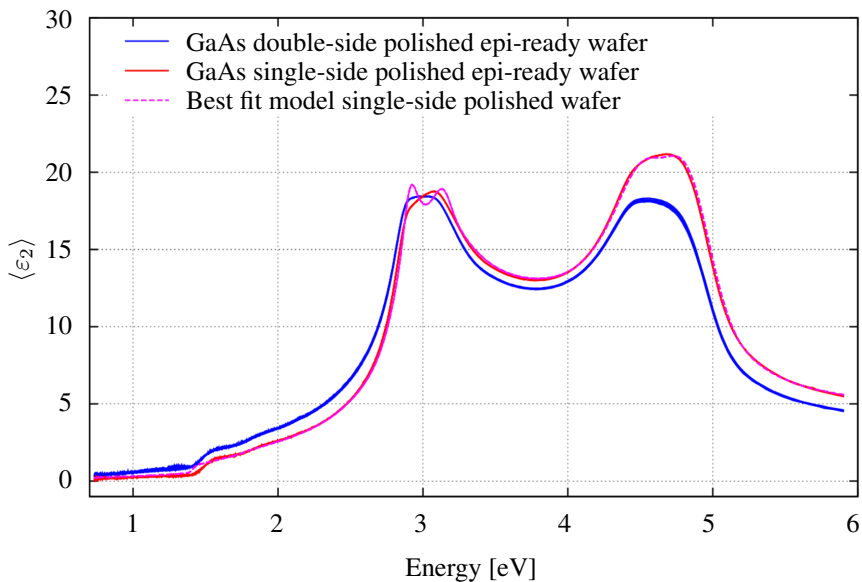


Figure 5.25: Measurements of single- and double-side polished n-doped GaAs substrates show large differences between the two samples. Using undoped GaAs to fit the single-side polished substrate works well except around Peak 1.

is needed as to why the QD samples grown on substrates with similar doping all have two distinct Peaks 1a and 1b. This could be because there are several and/or thick layers of undoped GaAs grown on top of the substrates, and as indicated by the models of the 10QD samples, layers deep down in the structure only contribute to the PDF at low energies, well below Peak 1. Another explanation can be that Peak 1a is enhanced because of contributions from the InAs in the QD layers, as InAs/InGaAs have critical points forming a Peak 1 at slightly lower energy than GaAs, as shown in Figure 5.1.

Epi-ready substrates are covered with an epi-layer applied by the producers to avoid normal oxide to form on the surfaces. The composition of this layer is a business secret, and varies between producers. When heated in a vacuum chamber, the layer is removed, and it is therefore reasonable to assume that the layer is some special kind of GaAs oxide, as it can not consist of materials that will contaminate the vacuum chamber. This assumption is supported by Allwood *et al.* (2000), who have investigated oxides on epi-ready GaAs substrates [31], and the low amplitude of Peak 2 resembles that of the simulations of GaAs with varying oxide thickness in Figure 5.3. As the exact composition of the epi-layer is not known for the samples measured in this work, it is also unknown if the epi-layer can be what causes the smooth peaks in Figure 5.25.

The remarkably different PDFs for the two measured samples and the epi-layer which composition is a business secret makes too many uncertain parameters to be able to use these substrates to model the substrates in the QD samples instead of the undoped GaAs model, as it is better to model using known values that are certainly wrong than values that are probably wrong, without knowing how and to what degree they are wrong. Instead,

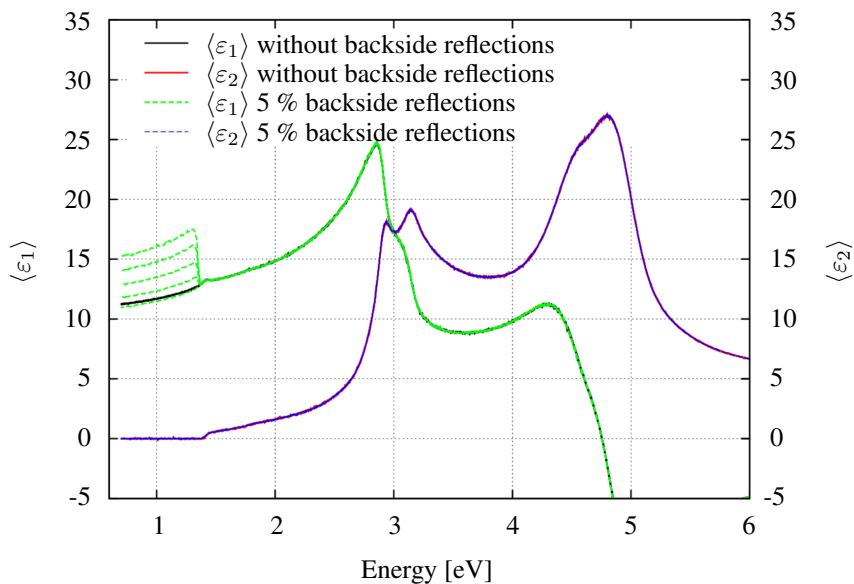


Figure 5.26: Simulations at 55-75° of bulk GaAs show that samples differing only by one being single-side polished and the other double-side polished have identical pseudo-dielectric functions above the band-gap. Data from UNL.

what can be learned from these substrates is that wafers from the same producer, which presumably have the same epi-layer oxide on them, can differ a lot in terms of their optical properties illustrated through the PDFs in Figure 5.25.

5.6 Chalmers samples

The full Chalmers solar cell structures were also measured using SE, and in this section, some simple models are presented and briefly discussed. As shown in the previous sections, there is a lot of uncertainty related to how to model the different layers, and it is clear that doping affects the optical models. The Chalmers samples have several layers of GaAs with varying dopants and doping concentration, and the QD cell investigated here, MBE2471, has 50 layers of QDs. Due to its complexity and numerous unknown variables, no effort has been put into modeling all of these.

The measured $\langle \epsilon_2 \rangle$ of MBE 2471, the QD-IBSC with GaAs spacer, and MBE2472, the reference cell, are found in Figure 5.27. The differences between the samples are small, but clear, and as these samples are nominally identical except for the active layer, it is reasonable to assume that the differences observed might be caused by quantum effects from the QD layers. The fact that there is a sheet of Si delta-doping in every spacer of MBE2471 while MBE2472 has an undoped active layer might also contribute to the differences seen in Figure 5.27, especially around Peak 2, where higher doping is believed to decrease $\langle \epsilon_2 \rangle$ [29].

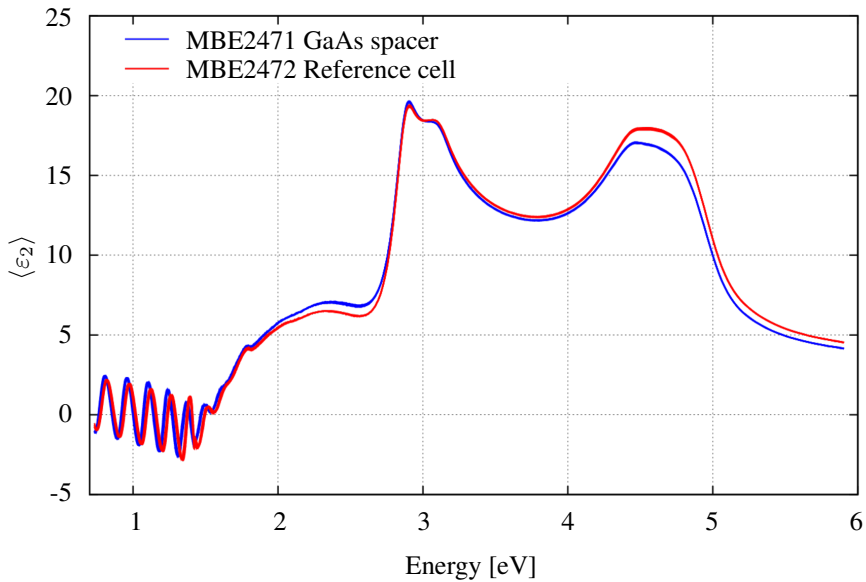


Figure 5.27: Comparison of samples MBE2471 and MBE2472 shows small but clear differences between the two samples.

Some simple models were applied to the two samples, and these are found in Figures 5.28 and 5.29 for MBE2471 and MBE2472, respectively. Most of the details of the samples are left for Appendix A.4, but some important details and observations are briefly discussed in the following.

When fitting models to both samples, the thicknesses of the different layers of MBE2471 found in TEM were used as starting points. Using these exact thicknesses lead to a poor fit of the oscillations below the GaAs band-gap, but by making some minor adjustments the fit of the samples were largely improved, and it is the adjusted fits that are shown in Figures 5.28 and 5.29. It is not possible to conclude whether the adjustments had to be made because of uncertainty in the values measured in TEM (there is approximately 10 % uncertainty of the magnification of a TEM image [27, 42], and when distances are measured without counting atomic rows, there will also be an uncertainty in the measurements), or because of the simplifications in the model such as modeling all GaAs as undoped and omitting the QD layers. The semi-detailed model for MBE2471 shown in Figure 5.28 models the active layer as an EMA of InAs and GaAs, and did not improve the fit compared to the simple model.

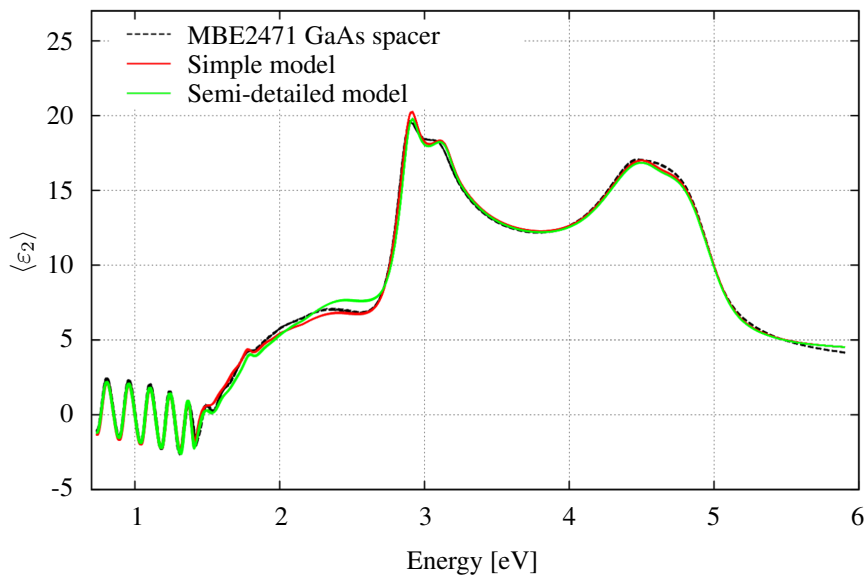


Figure 5.28: Measurement of MBE2471 together with a simple and a semi-detailed model shows that the simple model fits the measurements slightly better than the semi-detailed.

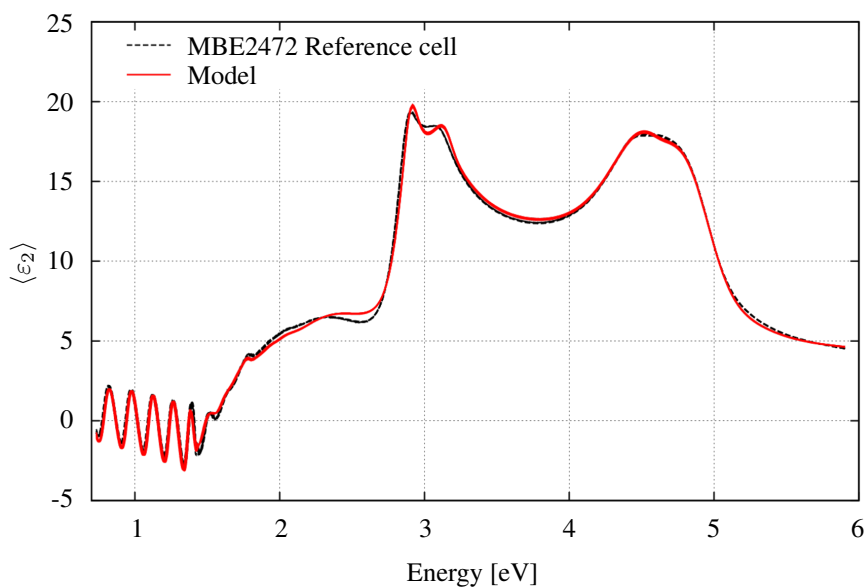


Figure 5.29: Measurement MBE2471 together with best fitting model.

Conclusions and Further Work

In this Master's Thesis, spectroscopic ellipsometry measurements has been performed on n-doped GaAs substrates, samples with varying doping, samples with two and ten layers of quantum dots (QDs) and full solar cell structures. All samples were grown in MBE and the InAs QDs were formed by Stranski-Krastanov growth. The fabrication of the samples has not been a part of this work.

The measurements of the GaAs samples with varying doping gave some surprising results. The $\langle \epsilon_2 \rangle$ of the Si-doped samples revealed a trend with doping concentration opposite of what can be found in literature, whereas the Be-doped samples did not show any trend with doping at all. No conclusion to the cause of this has been found, but it is natural to suspect that the samples does not have the doping concentrations they are assumed to have.

When analyzing the samples with two layers of QDs (2QD), three different approaches were tried. The first was very simple, not trying to model the QDs at all but simply replacing the QD stack with bulk values of the surrounding material. The second approach, Steimetz model, was macroscopic, inspired by Steimetz and co-workers, who used an EMA of bulk InAs and the material on top of the QD layer to model the QDs and 1 ML of bulk InAs to model the wetting layer (WL). The last model, Lee model, was inspired by Lee and co-workers, who tried to model the quantum effects of the WLs on the verge of QD formation using a damped harmonic oscillator model. The simple and Steimetz approaches were also applied on the samples with 10 QD layers (10QD), but instead of the Lee-model, an approach combining the Steimetz- and Lee-model by changing the WL in the Steimetz model into an EMA with InAs and an oscillator model.

For all QD samples, the Steimetz model provided a worse fit than the simple model, indicating that the effects from the QDs and WLs can not be modeled using a macroscopic approach. The oscillators in the Lee model did not behave as expected, but gave a negative contribution to $\langle \epsilon_2 \rangle$ for oscillators of positive amplitude. No explanation to this behaviour has been found. In the Lee-Steimetz model, however, the oscillators worked well, leading to better fits of the 10QD samples than the other models. The oscillators were placed at energies around 2.8 eV and 4.5 eV.

Comparing all the QD samples with their best fitting simple models showed a clear

pattern in how the models fit their measurements. For all samples, a large deviation from the measurement is seen at approximately 2.8 eV and around the GaAs band-gap. The similar deviation patterns indicate that the deviations are caused by something that are common for the samples, but not accounted for in the simple model. This might be the substrate, as it is modeled as undoped but is actually Si-doped, however, the modeling performed in this work has indicated that the layers deep in the sample have negligible effect on the measurements at higher energies. It is therefore more reasonable to assume that the main reason for the discrepancies between simple models and measurements are the effects from the QD layers. Furthermore, as the macroscopic Steimetz model did not improve the fitting, these effects are likely to be quantum effects.

Although some models fit the measurements better than others, none of them provided excellent fits. Analyzing ellipsometry measurements of such complex samples require detailed knowledge on as many parameters as possible, and the modeling in this work has suffered from the lack of such details. With too many unknowns, there is a possibility that by adjusting one parameter one might end up compensating for an error actually caused by something else. Therefore, to produce trustworthy results, much more detailed knowledge on the samples is needed.

The oscillator approach used in the Lee-model did work as expected, but oscillators in the Lee-Steimetz model performed well. It is therefore believed that using oscillators is the most promising way to model quantum effects in spectroscopic ellipsometry measurements.

This thesis has taken a few steps towards creating an optical model of InAs/(Al)GaAs intermediate band solar cells, but there is still a way to go and more research to be done before this goal is reached.

Further investigations of the samples analyzed in this thesis will be valuable to reduce the number of unknown parameters in the models. To confirm thickness of the different layers and size of the QDs inside the samples, TEM measurements of the samples not already measured can be performed. Instead of measuring distance calculated from the magnification of the TEM images, uncertainty of TEM measurements can be reduced by counting atomic rows. A quicker and non-destructive way of analyzing the layer thicknesses of the samples is by using x-ray diffraction, but this will also give higher uncertainty and can probably not be used to look at the QD size.

The QDs on top of the 2QD samples have already been measured using AFM and SEM, and the same techniques can be applied to the 10QD samples. Also, as the 2QD samples are several years old, it can be valuable to see if the QDs still can be seen through the oxide layer which presumably has increased in thickness since the last time the samples were investigated.

Hall measurements of the samples with varying doping can confirm the doping concentrations so the SE measurements performed on these samples can be interpreted by the right assumptions. Creating and measuring more samples to eventually create a more precise model of how GaAs varies with doping can be very useful in the analysis of both the substrates and the doped layers in a full solar cell structure.

To look at the composition of the epi-layer of the GaAs substrates, x-ray photoelectron spectroscopy (XPS) can be performed. Another option is to do SE of undoped GaAs substrates from the same producer as the doped ones before and after removing the epi-

layers by heating them in the MBE chamber without depositing anything on them. Then, by compensating for a known oxide grown in air at room temperature in the measurement after removing the epi-layer, a model for the GaAs substrate is found. By using this to analyze the SE measurement of the same sample, but with the epi-layer on top, a model for the epi-layer can be extracted. This way, when growing new samples, the substrates, or another piece from the same wafer, can be measured using SE, and by compensating for the epi-layer an optical model for the exact substrate used in the sample to be analyzed can be found.

In addition to performing more measurements to gain knowledge on samples already grown, it can be of interest to grow new samples similar to the ones available, but differing by one parameter. For example, growing samples differing from the already grown 10QD samples only by removing the top QD layer can be interesting in order to study how much of the quantum contributions in these samples comes from the top layer and how much comes from inside the samples.

Bibliography

- [1] U. Cubasch, D. Wuebbles, D. Chen, M. C. Facchini, D. Frame, N. Mahowald, and J.-G. Winther, "Introduction," in *Climate Change 2013: The Physical Science Basis. Contribution of Working Group I to the Fifth Assessment Report of the Intergovernmental Panel on Climate Change* (Q. D. Stocker, T.F., G.-K. Plattner, M. Tignor, S. Allen, J. Boschung, A. Nauels, Y. Xia, V. Bex, and P. Midgley, eds.), pp. 121–152, Cambridge University Press, Cambridge, United Kingdom and New York, NY, USA, 2013.
- [2] W. Shockley and H. J. Queisser, "Detailed balance limit of efficiency of p-n junction solar cells," *Journal of applied physics*, vol. 32, no. 3, pp. 510–519, 1961.
- [3] S. Rühle, "Tabulated values of the shockley–queisser limit for single junction solar cells," *Solar Energy*, vol. 130, pp. 139–147, 2016.
- [4] W. Da Silva, "Milestone in solar cell efficiency by unsw engineers," 2016.
- [5] A. Luque and A. Martí, "Increasing the efficiency of ideal solar cells by photon induced transitions at intermediate levels," *Physical Review Letters*, vol. 78, no. 26, p. 5014, 1997.
- [6] A. Sayari, M. Ezzidini, B. Azeza, S. Rekaya, E. Shalaan, S. Yaghmour, A. A. Al-Ghamdi, L. Sfaxi, R. Mghaieth, and H. Maaref, "Improvement of performance of gaas solar cells by inserting self-organized inas/ingaas quantum dot superlattices," *Solar Energy Materials and Solar Cells*, vol. 113, pp. 1–6, 2013.
- [7] W. Rouis, A. Sayari, M. Nouiri, M. Ezzdini, S. Rekaya, L. E. Mir, L. Sfaxi, and H. Maaref, "Characterisation of the gaas-based intermediate band solar cell with multi-stacked inas/ingaas quantum dots," *International Journal of Nanotechnology*, vol. 12, no. 8-9, pp. 584–596, 2015.
- [8] M. Al-Ghamdi, A. Sayari, and L. Sfaxi, "Optical study of high index substrate effect in multilayer inas/gaas quantum dot solar cells," *Journal of Alloys and Compounds*, vol. 685, pp. 202–208, 2016.

-
- [9] E. Steimetz, J.-T. Zettler, F. Schienle, T. Trepk, T. Wethkamp, W. Richter, and I. Sieber, "In situ monitoring of InAs-on-GaAs quantum dot formation in MOVPE by reflectance-anisotropy-spectroscopy and ellipsometry," *Applied Surface Science*, vol. 107, pp. 203–211, 1996.
- [10] H. Lee, S. Kim, Y. Park, and E. Kim, "Ellipsometric study of InAs wetting layer in InAs/GaAs quantum dots at the threshold of quantum dot formation," *Journal of Applied Physics*, vol. 90, no. 5, pp. 2290–2295, 2001.
- [11] H. Tompkins and E. A. Irene, *Handbook of ellipsometry*. William Andrew, 2005.
- [12] J. A. Woollam Co., Inc., "Guide to Using WVASE32®," 2010.
- [13] S. Adachi, *Optical properties of crystalline and amorphous semiconductors: Materials and fundamental principles*. Springer Science & Business Media, 1999.
- [14] H. Fujiwara, *Spectroscopic ellipsometry: principles and applications*. John Wiley & Sons, 2007.
- [15] J. A. Woollam Co., Inc., "CompleteEASE™ Data Analysis Manual," 2011.
- [16] T. Suzuki and S. Adachi, "Optical properties of amorphous Si partially crystallized by thermal annealing," *Japanese journal of applied physics*, vol. 32, no. 11R, p. 4900, 1993.
- [17] L. Piegl and W. Tiller, *The NURBS book*. Springer Science & Business Media, 2012.
- [18] B. M. Almog, I.F. and B. V., *The Lorentz Oscillator and its Applications*. Massachusetts Institute of Technology, 2011.
- [19] G. Jellison Jr and F. Modine, "Parameterization of the optical functions of amorphous materials in the interband region," *Applied Physics Letters*, vol. 69, no. 3, pp. 371–373, 1996.
- [20] J. Tauc, R. Grigorovici, and A. Vancu, "Optical properties and electronic structure of amorphous germanium," *physica status solidi (b)*, vol. 15, no. 2, pp. 627–637, 1966.
- [21] D. W. Palmer, "Properties of the III-V compound semiconductors," February 2006. Accessed: 19.06.2017.
- [22] J. R. Chelikowsky and M. L. Cohen, "Nonlocal pseudopotential calculations for the electronic structure of eleven diamond and zinc-blende semiconductors," *Physical Review B*, vol. 14, no. 2, p. 556, 1976.
- [23] S. F. Thomassen, *InAs/(Al)GaAs quantum dots for intermediate band solar cells*. PhD thesis, Norwegian University of Science and Technology, 2012.
- [24] P. C. Hemmer, *Kvantemekanikk*. Tapir, 1985. In Norwegian.
- [25] J. A. Woollam Co., Inc., "Rc2 spectroscopic ellipsometer hardware manual, vertical sample mount goniometer," October 2011.

-
- [26] J. A. Woollam Co., Inc., "Rc2 ellipsometer," 2017. Accessed: 26.06.2017.
- [27] E. Undheim, "Transmission electron microscopy characterization of quantum dot based intermediate band solar cells," Master's thesis, Norwegian University of Science and Technology, 2014.
- [28] S. Zollner, "Model dielectric functions for native oxides on compound semiconductors," *Applied physics letters*, vol. 63, no. 18, pp. 2523–2524, 1993.
- [29] P. G. Snyder and Y.-M. Xiong, "Study of concentration-dependent dielectric properties of n-type gaas using variable angle spectroscopic ellipsometry," *Surface and interface analysis*, vol. 18, no. 2, pp. 107–112, 1992.
- [30] F. Luke, "Oxidation of si and gaas in air at room temperature," *Surface Science*, vol. 30, no. 1, pp. 91 – 100, 1972.
- [31] D. Allwood, R. Carline, N. Mason, C. Pickering, B. Tanner, and P. Walker, "Characterization of oxide layers on gaas substrates," *Thin Solid Films*, vol. 364, no. 1, pp. 33–39, 2000.
- [32] G. Hollinger, R. Skheyta-Kabbani, and M. Gendry, "Oxides on gaas and inas surfaces: An x-ray-photoelectron-spectroscopy study of reference compounds and thin oxide layers," *Physical Review B*, vol. 49, no. 16, p. 11159, 1994.
- [33] C. Pickering, R. Carline, M. Emeny, N. Garawal, and L. Howard, "Dielectric functions and critical points of strained in x ga1- x as on gaas," *Applied physics letters*, vol. 60, no. 19, pp. 2412–2414, 1992.
- [34] C. Herzinger, P. G. Snyder, F. Celi, Y.-C. Kao, D. Chow, B. Johs, and J. Woollam, "Studies of thin strained inas, alas, and alsb layers by spectroscopic ellipsometry," *Journal of applied physics*, vol. 79, no. 5, pp. 2663–2674, 1996.
- [35] C. Pryor, "Eight-band calculations of strained inas/gaas quantum dots compared with one-, four-, and six-band approximations," *Physical Review B*, vol. 57, no. 12, p. 7190, 1998.
- [36] A. D. Polyinin and A. V. Manzhirov, *Handbook of mathematics for engineers and scientists*. CRC Press, 2006.
- [37] C. Herzinger, H. Yao, P. G. Snyder, F. Celi, Y.-C. Kao, B. Johs, and J. A. Woollam, "Determination of alas optical constants by variable angle spectroscopic ellipsometry and a multisample analysis," *Journal of applied physics*, vol. 77, no. 9, pp. 4677–4687, 1995.
- [38] H. Lee, E. Seong, S.-M. Kim, M.-H. Son, B.-D. Min, Y. Kim, and E.-K. Kim, "Ellipsometric study of self-assembled inas/gaas quantum dots," *Japanese journal of applied physics*, vol. 38, no. 3A, p. L245, 1999.
- [39] H. Lee, E. Seong, S. Kim, M. Son, B. Min, Y. Kim, and E. Kim, "Optical study of inas/gaas quantum dots using spectroscopic ellipsometry," *JOURNAL-KOREAN PHYSICAL SOCIETY*, vol. 34, pp. S61–S63, 1999.
-

-
- [40] M. Rajpalke. private communication by e-mail June 23rd, 2017.
- [41] B. Rheinländer, H. Schmidt, and V. Gottschalch, “Spectroscopic ellipsometric studies of inas monolayers embedded in gaas,” *Applied physics letters*, vol. 70, no. 13, pp. 1736–1738, 1997.
- [42] D. B. Williams and C. B. Carter, *The transmission electron microscope*. Springer, 2009.

Appendix

This appendix contains screenshots from CompleteEASE™ showing the details of the different models presented and discussed in this thesis.

A.1 Models of the samples with two QD layers

9As503-2

Data: As503-2 bottom 55-75deg 5deg interval 20se Model: 9As503-2 simple model (Snapshot)

Open Save Info Set Ranges

Open Save Clear

Fit: Generate Fit Fit Dynamic Reset

MSE = 7.787
Roughness = 39.38±0.081 Å
Back Reflections = 0.417±0.0031

Layer Commands: **Add Delete Save**
Include Surface Roughness = **ON** Roughness = **39.38 Å** (fit)
Substrate = **GaAs** Substrate Thickness = **0.3500 mm**
Angle Offset = **0.000**

- MODEL Options
Include Substrate Backside Correction = **ON**
Transmission SE Data = **OFF** Reverse Direction = **OFF**
Back Reflections = **0.417** (fit) % 1st Reflection = **100.00**
Model Calculation = **Ideal**

9As503-2 simple model with surface roughness only.

Data: As503-2 bottom 55-75deg 5deg interval 20se Model: 9As503-2 simple model (Snapshot)

Open Save Info Set Ranges

Open Save Clear

Fit: Generate Fit Fit Dynamic Reset

MSE = 5.371
Roughness = 20.86±0.518 Å
Thickness # 1 = 29.68±0.120 Å
Back Reflections = 0.413±0.0022

Layer Commands: **Add Delete Save**
Include Surface Roughness = **ON** Roughness = **20.86 Å** (fit)
Layer # 1 = **GaAs Oxide** Thickness # 1 = **29.68 Å** (fit)
Substrate = **GaAs** Substrate Thickness = **0.3500 mm**
Angle Offset = **0.000**

MODEL Options
Include Substrate Backside Correction = **ON**
Transmission SE Data = **OFF** Reverse Direction = **OFF**
Back Reflections = **0.413** (fit) % 1st Reflection = **100.00**
Model Calculation = **Ideal**

9As503-2 simple model with GaAs oxide and surface roughness.

Data: As503-2 bottom 55-75deg 5deg interval 20se Model: 9As503-2 simple model (Snapshot)

Open Save Info. Set Ranges Open Save C/clear

Fit: Generate Fit Fit Dynamic Reset

MSE = 5.269
 Roughness = 19.66±0.572 Å
 Thickness # 1 = 30.55±0.130 Å
 # Back Reflections = 0.413±0.0021

Layer Commands: **Add Delete Save**
 Include Surface Roughness = **ON** Roughness = **19.66 Å** (fit)
 Layer # 1 = **In_{0.53}GaAs Oxide** Thickness # 1 = **30.55 Å** (fit)
 Substrate = **GaAs** Substrate Thickness = **0.3500 mm**
 Angle Offset = **0.000**

- MODEL Options
 Include Substrate Backside Correction = **ON**
 Transmission SE Data = **OFF** Reverse Direction = **OFF**
 # Back Reflections = **0.413** (fit) % 1st Reflection = **100.00**
 Model Calculation = **Ideal**

9As503-2 simple model with In_{0.53}GaAs oxide and surface roughness.

Data: As503-2 bottom 55-75deg 5deg interval 20se Model: 9As503-2 simple model (Snapshot)

Open Save Info. Set Ranges Open Save C/clear

Fit: Generate Fit Fit Dynamic Reset

MSE = 5.267
 Roughness = 18.41±0.641 Å
 Thickness # 1 = 31.41±0.144 Å
 # Back Reflections = 0.413±0.0021

Layer Commands: **Add Delete Save**
 Include Surface Roughness = **ON** Roughness = **18.41 Å** (fit)
 Layer # 1 = **InAs Oxide** Thickness # 1 = **31.41 Å** (fit)
 Substrate = **GaAs** Substrate Thickness = **0.3500 mm**
 Angle Offset = **0.000**

- MODEL Options
 Include Substrate Backside Correction = **ON**
 Transmission SE Data = **OFF** Reverse Direction = **OFF**
 # Back Reflections = **0.413** (fit) % 1st Reflection = **100.00**
 Model Calculation = **Ideal**

9As503-2 simple model with InAs oxide and surface roughness.

Data: As503-2 bottom 55-75deg 5deg interval 20sec Model: 9As503-2 Steimetz model 1 (Snapshot)

Open Save Info Set Ranges

Open Save Clear

Fit:

Generate Fit Fit Dynamic Reset

MSE = 10.580
 Angle Offset = 0.189±0.0048
 # Back Reflections = 0.466±0.0048

Layer Commands: **Add Delete Save**
 Include Surface Roughness = OFF

- Layer # 6 = EMA Thickness # 6 = 26.00 Å
 # of Constituents = 2
 Material 1 = Void
 Material 2 = InAs Oxide
 EMA % (Mat 2) = 6.0
 depolarization = 0.000 Analysis Mode = Maxwell-Garnett
- Layer # 5 = EMA Thickness # 5 = 22.00 Å
 # of Constituents = 2
 Material 1 = InAs Oxide
 Material 2 = InAs
 EMA % (Mat 2) = 5.0
 depolarization = 0.000 Analysis Mode = Maxwell-Garnett
- Layer # 4 = InAs Thickness # 4 = 6.50 Å
- Layer # 3 = GaAs Thickness # 3 = 410.00 Å
- Layer # 2 = EMA Thickness # 2 = 26.00 Å
 # of Constituents = 2
 Material 1 = GaAs
 Material 2 = InAs
 EMA % (Mat 2) = 6.0
 depolarization = 0.000 Analysis Mode = Maxwell-Garnett
- Layer # 1 = InAs Thickness # 1 = 6.50 Å
- Substrate = GaAs Substrate Thickness = 0.3500 mm

Angle Offset = 0.189 (fit)

MODEL Options
 Include Substrate Backside Correction = ON
 Transmission SE Data = OFF Reverse Direction = OFF
 # Back Reflections = 0.466 (fit) % 1st Reflection = 100.00
 Model Calculation = Ideal

9As503-2 Steimetz model 1.

Data: As503-2 bottom 55-75deg 5deg interval 20sec Model: 9As503-2 Steimetz model 2 (Snapshot)

Open Save Info Set Ranges

Open Save Clear

Fit:

Generate Edit Fit Dynamic Reset

MSE = 6.387
 Thickness # 6 = 7.02±0.060 Å
 Angle Offset = 0.077±0.0032
 # Back Reflections = 0.428±0.0029

Layer Commands: **Add Delete Save**
 Include Surface Roughness = OFF

- Layer # 7 = EMA Thickness # 7 = 26.00 Å
 # of Constituents = 2
 Material 1 = Void
 Material 2 = InAs Oxide
 EMA % (Mat 2) = 6.0
 depolarization = 0.000 Analysis Mode = Maxwell-Garnett
- Layer # 6 = InAs Oxide Thickness # 6 = 7.02 Å (fit)
- Layer # 5 = EMA Thickness # 5 = 21.00 Å
 # of Constituents = 2
 Material 1 = InAs Oxide
 Material 2 = InAs
 EMA % (Mat 2) = 5.0
 depolarization = 0.000 Analysis Mode = Maxwell-Garnett
- Layer # 4 = InAs Thickness # 4 = 6.50 Å
- Layer # 3 = GaAs Thickness # 3 = 410.00 Å
- Layer # 2 = EMA Thickness # 2 = 26.00 Å
 # of Constituents = 2
 Material 1 = GaAs
 Material 2 = InAs
 EMA % (Mat 2) = 6.0
 depolarization = 0.000 Analysis Mode = Maxwell-Garnett
- Layer # 1 = InAs Thickness # 1 = 6.50 Å
- Substrate = GaAs Substrate Thickness = 0.3500 mm

Angle Offset = 0.077 (fit)

- **MODEL Options**
 Include Substrate Backside Correction = ON
 Transmission SE Data = OFF Reverse Direction = OFF
 # Back Reflections = 0.428 (fit) % 1st Reflection = 100.00
 Model Calculation = Ideal

9As503-2 Steimetz model 2.

Data: As503-2 bottom 55-75deg 5deg interval 20se Model: 9As503-2 Steimetz model 2 QDs only modelled on top (Snapshot)

Open Save Info. Set Ranges Open Save Clear

Fit: Generate Fit Fit Dynamic Reset

MSE = 6.342
 Thickness # 3 = 6.90±0.060 Å
 Angle Offset = 0.094±0.0031
 # Back Reflections = 0.436±0.0028

Layer Commands: **Add Delete Save**
 Include Surface Roughness = OFF

Layer # 4 = **EMA** Thickness # 4 = **26.00 Å**
 # of Constituents = 2
 Material 1 = **Void**
 Material 2 = **InAs Oxide**
 EMA % (Mat 2) = **6.0**
 depolarization = **0.000** Analysis Mode = **Maxwell-Garnett**

Layer # 3 = **InAs Oxide** Thickness # 3 = **6.90 Å** (fit)

- Layer # 2 = **EMA** Thickness # 2 = **21.00 Å**
 # of Constituents = 2
 Material 1 = **InAs Oxide**
 Material 2 = **InAs**
 EMA % (Mat 2) = **5.0**
 depolarization = **0.000** Analysis Mode = **Maxwell-Garnett**

Layer # 1 = **InAs** Thickness # 1 = **6.50 Å**

Substrate = **GaAs** Substrate Thickness = **0.3500 mm**
 Angle Offset = **0.094** (fit)

- **MODEL Options**
 Include Substrate Backside Correction = **ON**
 Transmission SE Data = **OFF** Reverse Direction = **OFF**
 # Back Reflections = **0.436** (fit) % 1st Reflection = **100.00**
 Model Calculation = **Ideal**

9As503-2 Steimetz model 2 with only top QDs modeled.

Data: As503-2 bottom 55-75deg 5deg interval 20se Model: 9As503-2 Lee model 1 (Snapshot)

Open Save Info. Set Ranges Open Save Clear

Fit: Generate Fit Fit Dynamic Reset

MSE = 10.769
 Thickness # 4 = 34.89±0.103 Å
 Angle Offset = 0.175±0.0053
 # Back Reflections = 0.283±0.0043

Layer Commands: **Add Delete Save**
 Include Surface Roughness = OFF

Layer # 4 = **InAs Oxide** Thickness # 4 = **34.89 Å** (fit)

- Layer # 3 = **Coupled** Thickness # 3 = **32.50 Å**
 Coupled to Layer # = **1** (Gen-Osc)

Layer # 2 = **GaAs** Thickness # 2 = **410.00 Å**

- Layer # 1 = **Gen-Osc** Thickness # 1 = **32.50 Å**
Add Oscillator Show Dialog Fast Gaussian Calc = **ON**
 Einf = **1.000**
 UV Pole Amp. = **0.0000** UV Pole En. = **11.000**
 IR Pole Amp. = **0.0000**
Fit All Clear All Add Amp. Add Br. Add En.
1: Type = **Lorentz** Amp1 = **0.300000** Br1 = **0.2000** En1 = **2.800**
2: Type = **Lorentz** Amp2 = **0.300000** Br2 = **0.2000** En2 = **4.400**

Substrate = **GaAs** Substrate Thickness = **0.3500 mm**
 Angle Offset = **0.175** (fit)

- **MODEL Options**
 Include Substrate Backside Correction = **ON**
 Transmission SE Data = **OFF** Reverse Direction = **OFF**
 # Back Reflections = **0.283** (fit) % 1st Reflection = **100.00**
 Model Calculation = **Ideal**

9As503-2 Lee model.

9As541-2

Data: As541-2 55-75deg 5deg interval 20sek MM (Model: 9As541-2 simple model (Snapshot))

Open Save Info. Set Ranges Open Save Clear

Fit: Generate Fit Fit Dynamic Reset

MSE = 10.376
Roughness = 34.55±0.106 Å
Back Reflections = 0.369±0.0041

Layer Commands: **Add Delete Save**
Include Surface Roughness = **ON** Roughness = **34.55 Å** (fit)
Substrate = **GaAs** Substrate Thickness = **0.3500 mm**
Angle Offset = **0.000**

MODEL Options
Include Substrate Backside Correction = **ON**
Transmission SE Data = **OFF** Reverse Direction = **OFF**
Back Reflections = **0.369** (fit) % 1st Reflection = **100.00**
Model Calculation = **Ideal**

9As541-2 simple model with surface roughness only.

Data: As541-2 55-75deg 5deg interval 20sek MM (Model: 9As541-2 simple model (Snapshot))

Open Save Info. Set Ranges Open Save Clear

Fit: Generate Fit Fit Dynamic Reset

MSE = 10.361
Roughness = 6.90±0.946 Å
Thickness # 1 = 28.36±0.218 Å
Back Reflections = 0.366±0.0041

Layer Commands: **Add Delete Save**
Include Surface Roughness = **ON** Roughness = **6.90 Å** (fit)
Layer # 1 = **GaAs Oxide** Thickness # 1 = **28.36 Å** (fit)
Substrate = **GaAs** Substrate Thickness = **0.3500 mm**
Angle Offset = **0.000**

MODEL Options
Include Substrate Backside Correction = **ON**
Transmission SE Data = **OFF** Reverse Direction = **OFF**
Back Reflections = **0.366** (fit) % 1st Reflection = **100.00**
Model Calculation = **Ideal**

9As541-2 simple model with GaAs oxide and surface roughness.

Data: As541-2 55-75deg 5deg interval 20sek MM (Model: 9As541-2 simple model (Snapshot))

Open Save Info. Set Ranges Open Save Clear

Fit: Generate Fit Fit Dynamic Reset

MSE = 10.300
Roughness = 4.00±1.046 Å
Thickness # 1 = 29.49±0.236 Å
Back Reflections = 0.366±0.0040

Layer Commands: **Add Delete Save**
Include Surface Roughness = **ON** Roughness = **4.00 Å** (fit)
Layer # 1 = **In_{0.53}GaAs Oxide** Thickness # 1 = **29.49 Å** (fit)
Substrate = **GaAs** Substrate Thickness = **0.3500 mm**
Angle Offset = **0.000**

MODEL Options
Include Substrate Backside Correction = **ON**
Transmission SE Data = **OFF** Reverse Direction = **OFF**
Back Reflections = **0.366** (fit) % 1st Reflection = **100.00**
Model Calculation = **Ideal**

9As541-2 simple model with In_{0.53}GaAs oxide and surface roughness.

Data: As541-2 55-75deg 5deg interval 20sek MM (\$ Model: 9As541-2 simple model (Snapshot)

Open Save Info Set Ranges Open Save Clear

Fit: Generate Fit Fit Dynamic Reset

MSE = 10.148
 Roughness = 5.28±1.250 Å
 Thickness # 1 = 29.30±0.290 Å
 Angle Offset = 0.064±0.0053
 # Back Reflections = 0.387±0.0044

Layer Commands: **Add Delete Save**
 Include Surface Roughness = **ON** Roughness = **5.28 Å** (fit)
 Layer # 1 = **InAs Oxide** Thickness # 1 = **29.30 Å** (fit)
 Substrate = **GaAs** Substrate Thickness = **0.3500 mm**
 Angle Offset = **0.064** (fit)
+ MODEL Options
+ FIT Options
+ OTHER Options

9As541-2 simple model with InAs oxide and surface roughness.

Data: As541-2 55-75deg 5deg interval 20sek MM (\$ Model: 9As541-2 Steimetz model 3 (Snapshot)

Open Save Info Set Ranges Open Save Clear

Fit: Generate Fit Fit Dynamic Reset

MSE = 12.568
 Thickness # 6 = 95.18±12.645 Å
 EMA % (Mat 2) = 8.0±1.26
 EMA % (Mat 2) = 8.0±4.22
 EMA % (Mat 2) = 8.0±10.61
 Angle Offset = 0.187±0.0071
 # Back Reflections = 0.408±0.0057

Layer Commands: **Add Delete Save**
 Include Surface Roughness = **OFF**
 - Layer # 6 = **EMA** Thickness # 6 = **95.18 Å** (fit)
 # of Constituents = **2**
 Material 1 = **Void**
 Material 2 = **InAs Oxide**
 EMA % (Mat 2) = **8.0** (fit)
 depolarization = **0.000** Analysis Mode = **Maxwell-Garnett**
 - Layer # 5 = **EMA** Thickness # 5 = **4.00 Å**
 # of Constituents = **2**
 Material 1 = **InAs Oxide**
 Material 2 = **InAs**
 EMA % (Mat 2) = **8.0** (fit)
 depolarization = **0.000** Analysis Mode = **Maxwell-Garnett**
 Layer # 4 = **InAs** Thickness # 4 = **6.50 Å**
 Layer # 3 = **GaAs** Thickness # 3 = **410.00 Å**
 - Layer # 2 = **EMA** Thickness # 2 = **5.00 Å**
 # of Constituents = **2**
 Material 1 = **GaAs**
 Material 2 = **InAs**
 EMA % (Mat 2) = **8.0** (fit)
 depolarization = **0.000** Analysis Mode = **Maxwell-Garnett**
 Layer # 1 = **InAs** Thickness # 1 = **6.50 Å**
 Substrate = **GaAs** Substrate Thickness = **0.3500 mm**
 Angle Offset = **0.187** (fit)
- MODEL Options
 Include Substrate Backside Correction = **ON**
 Transmission SE Data = **OFF** Reverse Direction = **OFF**
 # Back Reflections = **0.408** (fit) % 1st Reflection = **100.00**
 Model Calculation = **Ideal**

9As541-2 Steimetz model 1.

Data: As541-2 55-75deg 5deg interval 20sek MM (S Model: 9As541-2 Steimetz model 2 (Snapshot)

Open Save Info Set Ranges

Open Save Clear

Fit:

Generate Fit Fit Dynamic Reset

MSE = 10.964
 Thickness # 6 = 22.94±0.101 Å
 Angle Offset = 0.120±0.0054
 # Back Reflections = 0.390±0.0048

Layer Commands: [Add](#) [Delete](#) [Save](#)
 Include Surface Roughness = [OFF](#)

- Layer # 7 = [EMA](#) Thickness # 7 = [5.00 Å](#)
 # of Constituents = [2](#)
 Material 1 = [Void](#)
 Material 2 = [InAs Oxide](#)
 EMA % (Mat 2) = [7.0](#)
 depolarization = [0.000](#) Analysis Mode = [Maxwell-Garnett](#)
- Layer # 6 = [InAs Oxide](#) Thickness # 6 = [22.94 Å](#) (fit)
- Layer # 5 = [EMA](#) Thickness # 5 = [4.00 Å](#)
 # of Constituents = [2](#)
 Material 1 = [InAs Oxide](#)
 Material 2 = [InAs](#)
 EMA % (Mat 2) = [6.0](#)
 depolarization = [0.000](#) Analysis Mode = [Maxwell-Garnett](#)
- Layer # 4 = [InAs](#) Thickness # 4 = [6.50 Å](#)
- Layer # 3 = [GaAs](#) Thickness # 3 = [410.00 Å](#)
- Layer # 2 = [EMA](#) Thickness # 2 = [5.00 Å](#)
 # of Constituents = [2](#)
 Material 1 = [GaAs](#)
 Material 2 = [InAs](#)
 EMA % (Mat 2) = [7.0](#)
 depolarization = [0.000](#) Analysis Mode = [Maxwell-Garnett](#)
- Layer # 1 = [InAs](#) Thickness # 1 = [6.50 Å](#)
- Substrate = [GaAs](#) Substrate Thickness = [0.3500 mm](#)

Angle Offset = [0.120](#) (fit)

MODEL Options

- Include Substrate Backside Correction = [ON](#)
- Transmission SE Data = [OFF](#) Reverse Direction = [OFF](#)
- # Back Reflections = [0.390](#) (fit) % 1st Reflection = [100.00](#)
- Model Calculation = [Ideal](#)

9As541-2 Steimetz model 2.

A.2 Models of the samples with ten QD layers

9As157

Data: 9As157 55-75deg 5deg interval 20sek MM (S) Model: 9As157 simple no QDs 1 (Snapshot)

Open Save Info. Set Ranges

Open Save Clear

Fit:

Generate Fit Fit Dynamic Reset

MSE = 8.601
Thickness # 3 = 24.30±0.074 Å
Thickness # 2 = 14584.64±1.177 Å
Thickness # 1 = 995.86±2.560 Å

Layer Commands: **Add Delete Save**
Include Surface Roughness = OFF

Layer # 3 = InAs Oxide	Thickness # 3 = 24.30 Å (fit)
Layer # 2 = GaAs	Thickness # 2 = 14584.64 Å (fit)
- Layer # 1 = AlGaAs (Comp Library)	Thickness # 1 = 995.86 Å (fit)
Composition = 0.80000	
Substrate = GaAs	
Angle Offset = 0.000	

9As157 simple model with nominal Al-content.

Data: 9As157 55-75deg 5deg interval 20sek MM (S) Model: 9As157 simple no QDs 1 (Snapshot)

Open Save Info. Set Ranges

Open Save Clear

Fit:

Generate Fit Fit Dynamic Reset

MSE = 6.679
Thickness # 3 = 24.29±0.057 Å
Thickness # 2 = 14573.64±0.833 Å
Thickness # 1 = 1032.62±1.886 Å
Composition = 0.85128±0.00080259

Layer Commands: **Add Delete Save**
Include Surface Roughness = OFF

Layer # 3 = InAs Oxide	Thickness # 3 = 24.29 Å (fit)
Layer # 2 = GaAs	Thickness # 2 = 14573.64 Å (fit)
- Layer # 1 = AlGaAs (Comp Library)	Thickness # 1 = 1032.62 Å (fit)
Composition = 0.85128 (fit)	
Substrate = GaAs	
Angle Offset = 0.000	

9As157 simple model with fitted Al-content.

Data: 9As157 55-75deg 5deg interval 20sek MM (S) Model: 9As157 Steimetz simple model (Snapshot)

Open Save Info. Set Ranges

Open Save Clear

Fit:

Generate Fit Fit Dynamic Reset

MSE = 7.112
Thickness # 5 = 8.09±2.554 Å
Thickness # 4 = 21.13±0.292 Å
Thickness # 2 = 14567.47±0.892 Å
Thickness # 1 = 1031.63±2.017 Å
Composition = 0.85409±0.00085380

Layer Commands: **Add Delete Save**
Include Surface Roughness = OFF

- Layer # 5 = EMA	Thickness # 5 = 8.09 Å (fit)
# of Constituents = 2	
Material 1 = void	
Material 2 = InAs Oxide	
EMA % (Mat 2) = 6.0	
depolarization = 0.333 Analysis Mode = Bruggeman	
- Layer # 4 = EMA	Thickness # 4 = 21.13 Å (fit)
# of Constituents = 2	
Material 1 = InAs Oxide	
Material 2 = InAs	
EMA % (Mat 2) = 6.0	
depolarization = 0.333 Analysis Mode = Maxwell-Garnett	
Layer # 3 = InAs	Thickness # 3 = 6.50 Å
Layer # 2 = GaAs	Thickness # 2 = 14567.47 Å (fit)
- Layer # 1 = AlGaAs (Comp Library)	Thickness # 1 = 1031.63 Å (fit)
Composition = 0.85409 (fit)	
Substrate = GaAs	
Angle Offset = 0.000	

9As157 Steimetz model with only top QDs modeled.

Data: 9As157 55-75deg 5deg interval 20sek MM (S) Model: 9As157 Steimetz detailed model 2 (Snapshot)

Open Save Info Set Ranges Open Save Clear

Fit: Generate Fit Fit Dynamic Reset

MSE = 11.220
 Thickness # 32 = 10.00±0.854 Å
 Thickness # 2 = 9725.02±1.520 Å
 Thickness # 1 = 1004.65±3.447 Å
 Composition = 0.87702±0.001311

Layer Commands: **Add Delete Save**
 Include Surface Roughness = **OFF**

- Layer # 32 = **EMA** Thickness # 32 = **10.00 Å** (fit)
 - # of Constituents = **2**
 - Material 1 = **Void**
 - Material 2 = **InAs Oxide**
 - EMA % (Mat 2) = **6.0**
 - depolarization = **0.333** Analysis Mode = **Maxwell-Garnett**
- Layer # 31 = **EMA** Thickness # 31 = **21.00 Å**
 - # of Constituents = **2**
 - Material 1 = **InAs Oxide**
 - Material 2 = **InAs**
 - EMA % (Mat 2) = **6.0**
 - depolarization = **0.333** Analysis Mode = **Maxwell-Garnett**
- + Layer # 30 = **Coupled** Thickness # 30 = **6.50 Å**
- + Layer # 29 = **Coupled** Thickness # 29 = **500.00 Å**
- + Layer # 28 = **Coupled** Thickness # 28 = **26.00 Å**
- + Layer # 27 = **Coupled** Thickness # 27 = **6.50 Å**
- + Layer # 26 = **Coupled** Thickness # 26 = **500.00 Å**
- + Layer # 25 = **Coupled** Thickness # 25 = **26.00 Å**
- + Layer # 24 = **Coupled** Thickness # 24 = **6.50 Å**
- + Layer # 23 = **Coupled** Thickness # 23 = **500.00 Å**
- + Layer # 22 = **Coupled** Thickness # 22 = **26.00 Å**
- + Layer # 21 = **Coupled** Thickness # 21 = **6.50 Å**
- + Layer # 20 = **Coupled** Thickness # 20 = **500.00 Å**
- + Layer # 19 = **Coupled** Thickness # 19 = **26.00 Å**
- + Layer # 18 = **Coupled** Thickness # 18 = **6.50 Å**
- + Layer # 17 = **Coupled** Thickness # 17 = **500.00 Å**
- + Layer # 16 = **Coupled** Thickness # 16 = **26.00 Å**
- + Layer # 15 = **Coupled** Thickness # 15 = **6.50 Å**
- + Layer # 14 = **Coupled** Thickness # 14 = **500.00 Å**
- + Layer # 13 = **Coupled** Thickness # 13 = **26.00 Å**
- + Layer # 12 = **Coupled** Thickness # 12 = **6.50 Å**
- + Layer # 11 = **Coupled** Thickness # 11 = **500.00 Å**
- + Layer # 10 = **Coupled** Thickness # 10 = **26.00 Å**
- + Layer # 9 = **Coupled** Thickness # 9 = **65.00 Å**
- + Layer # 8 = **Coupled** Thickness # 8 = **500.00 Å**
- + Layer # 7 = **Coupled** Thickness # 7 = **26.00 Å**
- + Layer # 6 = **Coupled** Thickness # 6 = **6.50 Å**
- Layer # 5 = **GaAs** Thickness # 5 = **500.00 Å**
- Layer # 4 = **EMA** Thickness # 4 = **26.00 Å**
 - # of Constituents = **2**
 - Material 1 = **GaAs**
 - Material 2 = **InAs**
 - EMA % (Mat 2) = **6.0**
 - depolarization = **0.333** Analysis Mode = **Maxwell-Garnett**
- Layer # 3 = **InAs** Thickness # 3 = **6.50 Å**
- Layer # 2 = **GaAs** Thickness # 2 = **9725.02 Å** (fit)
- Layer # 1 = **AlGaAs (Comp Library)** Thickness # 1 = **1004.65 Å** (fit)
 - Composition = **0.87702** (fit)
- Substrate = **GaAs**

Angle Offset = **0.000**

9As157 Steimetz model with all QD layers modeled. Layers #6, 9, 12 etc. are coupled to layer #3, layers #7, 10, 13 etc. are coupled to layer #4, layers #8, 11, 14 etc. are coupled to layer #5.

Data: 9As157 55-75deg 5deg interval 20sek MM (S) Model: 9As157 Lee-Steimetz simple model 1 osc (Snapshot)

Open Save Info Set Ranges Open Save Clear

Fit: Generate Fit Fit Dynamic Reset

MSE = 6.266
 Thickness # 4 = 15.04±0.083 Å
 Amp1 = 32.146059±3.5242743
 Br1 = 0.0489±0.00621
 En1 = 2.731±0.0026
 EMA % (Mat 2) = 42.9±0.84
 Thickness # 2 = 14571.81±0.786 Å
 Thickness # 1 = 1032.06±1.773 Å
 Composition = 0.85244±0.00075366

Layer Commands: [Add](#) [Delete](#) [Save](#)
 Include Surface Roughness = [OFF](#)

- Layer # 5 = [EMA](#) Thickness # 5 = [26.00 Å](#)
 # of Constituents = 2
 Material 1 = [Void](#)
 Material 2 = [InAs Oxide](#)
 EMA % (Mat 2) = [6.0](#)
 depolarization = [0.333](#) Analysis Mode = [Bruggeman](#)
- Layer # 4 = [EMA](#) Thickness # 4 = [15.04 Å](#) (fit)
 # of Constituents = 2
 Material 1 = [InAs Oxide](#)
 Material 2 = [InAs](#)
 EMA % (Mat 2) = [6.0](#)
 depolarization = [0.333](#) Analysis Mode = [Maxwell-Garnett](#)
- Layer # 3 = [EMA](#) Thickness # 3 = [5.60 Å](#)
 # of Constituents = 2
 Material 1 = [InAs](#)
 - Material 2 = [Gen-Osc](#)
[Add Oscillator](#) [Show Dialog](#) Fast Gaussian Calc = [ON](#)
 Einf = [1.000](#)
 UV Pole Amp. = [0.0000](#) UV Pole En. = [11.000](#)
 IR Pole Amp. = [0.0000](#)
[Fit All](#) [Clear All](#) [Add Amp.](#) [Add Br.](#) [Add En.](#)
 1. Type = [Lorentz](#) Amp1 = [32.146059](#) (fit) Br1 = [0.0489](#) (fit) En1 = [2.731](#) (fit)
 EMA % (Mat 2) = [42.9](#) (fit)
 depolarization = [0.333](#) Analysis Mode = [Bruggeman](#)
- Layer # 2 = [GaAs](#) Thickness # 2 = [14571.81 Å](#) (fit)
- Layer # 1 = [AlGaAs \(Comp Library\)](#) Thickness # 1 = [1032.06 Å](#) (fit)
 Composition = [0.85244](#) (fit)
- Substrate = [GaAs](#)
- Angle Offset = [0.000](#)

9As157 Lee-Steimetz model with one oscillator.

Data: 9As157 55-75deg 5deg interval 20sek MM (S) Model: 9As157 Lee-Steimetz simple model 2 osc (Snapshot)

Open Save Info Set Ranges Ogen Save Clear

Fit: Generate Fit Dynamic Reset

MSE = 5.981
 Thickness # 4 = 15.29±0.086 Å
 Amp1 = 25.147119±1.5967539
 Br1 = 0.1000±0.00803
 En1 = 2.737±0.0029
 Amp2 = 4.868786±0.3016827
 Br2 = 0.6640±0.05566
 En2 = 4.607±0.0228
 EMA % (Mat 2) = 61.8±1.56
 Thickness # 2 = 14572.25±0.750 Å
 Thickness # 1 = 1032.19±1.691 Å
 Composition = 0.85199±0.00072027

Layer Commands: **Add Delete Save**
 Include Surface Roughness = OFF

- Layer # 5 = EMA Thickness # 5 = 26.00 Å
 # of Constituents = 2
 Material 1 = Void
 Material 2 = InAs Oxide
 EMA % (Mat 2) = 5.0
 depolarization = 0.333 Analysis Mode = Bruggeman
- Layer # 4 = EMA Thickness # 4 = 15.29 Å (fit)
 # of Constituents = 2
 Material 1 = InAs Oxide
 Material 2 = InAs
 EMA % (Mat 2) = 6.0
 depolarization = 0.333 Analysis Mode = Maxwell-Garnett
- Layer # 3 = EMA Thickness # 3 = 6.50 Å
 # of Constituents = 2
 Material 1 = InAs
 - Material 2 = Gen-Osc
 Add Oscillator Show Dialog Fast Gaussian Calc = ON
 Einf = 1.000
 UV Pole Amp. = 0.0000 UV Pole En. = 11.000
 IR Pole Amp. = 0.0000
Fit All Clear All Add Amp. Add Br. Add En.
 1. Type = Lorentz Amp1 = 25.147119 (fit) Br1 = 0.1000 (fit) En1 = 2.737 (fit)
 2. Type = Lorentz Amp2 = 4.868786 (fit) Br2 = 0.6640 (fit) En2 = 4.607 (fit)
 EMA % (Mat 2) = 61.8 (fit)
 depolarization = 0.333 Analysis Mode = Bruggeman
- Layer # 2 = GaAs Thickness # 2 = 14572.25 Å (fit)
- Layer # 1 = AlGaAs (Comp Library) Thickness # 1 = 1032.19 Å (fit)
 Composition = 0.85199 (fit)
 Substrate = GaAs
 Angle Offset = 0.000

9As157 Lee-Steimetz model with two oscillators.

9As159

Data: 9As159 55-75deg 5deg interval 20sek MM (S) Model: 9As159 simple no QDs 1 (Snapshot)

Open Save Info Set Ranges

Open Save Clear

Fit: Generate Fit Fit Dynamic Reset

MSE = 6.407
Roughness = 1.90±0.790 Å
Thickness # 4 = 21.62±0.180 Å
Thickness # 3 = 4889.09±1.143 Å
Composition = 0.24992±0.00053359
Thickness # 2 = 9543.42±1.130 Å
Thickness # 1 = 1009.42±1.631 Å
Composition = 0.85792±0.00073052

Layer Commands: **Add Delete Save**
Include Surface Roughness = **ON** Roughness = **1.90 Å** (fit)
Layer # 4 = **InAs Oxide** Thickness # 4 = **21.62 Å** (fit)
- Layer # 3 = **AlGaAs (Comp Library)** Thickness # 3 = **4889.09 Å** (fit)
Composition = **0.24992** (fit)
Layer # 2 = **GaAs** Thickness # 2 = **9543.42 Å** (fit)
- Layer # 1 = **AlGaAs (Comp Library)** Thickness # 1 = **1009.42 Å** (fit)
Composition = **0.85792** (fit)
Substrate = **GaAs**
Angle Offset = **0.000**
+ MODEL Options

9As159 simple model with fitted Al-content.

Data: 9As159 55-75deg 5deg interval 20sek MM (S) Model: 9As159 Steimetz simple model (Snapshot)

Open Save Info Set Ranges

Open Save Clear

Fit: Generate Fit Fit Dynamic Reset

MSE = 7.473
Thickness # 6 = 37.28±2.780 Å
Thickness # 5 = 14.90±0.324 Å
Thickness # 3 = 4882.18±1.011 Å
Thickness # 2 = 9544.79±1.290 Å
Thickness # 1 = 1009.34±1.907 Å
Composition = 0.86030±0.00084838
Angle Offset = 0.133±0.0036

Layer Commands: **Add Delete Save**
Include Surface Roughness = **OFF**
- Layer # 6 = **EMA** Thickness # 6 = **37.28 Å** (fit)
of Constituents = **2**
Material 1 = **Void**
Material 2 = **InAs Oxide**
EMA % (Mat 2) = **6.0**
depolarization = **0.333** Analysis Mode = **Bruggeman**
- Layer # 5 = **EMA** Thickness # 5 = **14.90 Å** (fit)
of Constituents = **2**
Material 1 = **InAs Oxide**
Material 2 = **InAs**
EMA % (Mat 2) = **6.0**
depolarization = **0.333** Analysis Mode = **Maxwell-Garnett**
Layer # 4 = **InAs** Thickness # 4 = **6.50 Å**
- Layer # 3 = **AlGaAs (Comp Library)** Thickness # 3 = **4882.18 Å** (fit)
Composition = **0.25000**
Layer # 2 = **GaAs** Thickness # 2 = **9544.79 Å** (fit)
- Layer # 1 = **AlGaAs (Comp Library)** Thickness # 1 = **1009.34 Å** (fit)
Composition = **0.86030** (fit)
Substrate = **GaAs**
Angle Offset = **0.133** (fit)

9As159 Steimetz model with only top QDs modeled.

Data: 9As159 55-75deg 5deg interval 20sek MM (S) Model: 9As159 Steimetz detailed model (Snapshot)

Open Save Info. Set Ranges Open Save Clear

Fit: Generate Fit Fit Dynamic Reset

MSE = 33.775
 Thickness # 33 = 25.51±12.059 Å
 Thickness # 32 = 16.89±1.351 Å
 Thickness # 2 = 9149.32±4.235 Å
 Thickness # 1 = 969.42±9.564 Å
 Composition = 0.86681±0.003746

Include Surface Roughness = OFF

+ Layer # 33 = EMA Thickness # 33 = 25.51 Å (fit)
+ Layer # 32 = EMA Thickness # 32 = 16.89 Å (fit)
+ Layer # 31 = Coupled Thickness # 31 = 6.50 Å
+ Layer # 30 = Coupled Thickness # 30 = 500.00 Å
+ Layer # 29 = Coupled Thickness # 29 = 26.00 Å
+ Layer # 28 = Coupled Thickness # 28 = 6.50 Å
+ Layer # 27 = Coupled Thickness # 27 = 500.00 Å
+ Layer # 26 = Coupled Thickness # 26 = 26.00 Å
+ Layer # 25 = Coupled Thickness # 25 = 6.50 Å
+ Layer # 24 = Coupled Thickness # 24 = 500.00 Å
+ Layer # 23 = Coupled Thickness # 23 = 26.00 Å
+ Layer # 22 = Coupled Thickness # 22 = 6.50 Å
+ Layer # 21 = Coupled Thickness # 21 = 500.00 Å
+ Layer # 20 = Coupled Thickness # 20 = 26.00 Å
+ Layer # 19 = Coupled Thickness # 19 = 6.50 Å
+ Layer # 18 = Coupled Thickness # 18 = 500.00 Å
+ Layer # 17 = Coupled Thickness # 17 = 26.00 Å
+ Layer # 16 = Coupled Thickness # 16 = 6.50 Å
+ Layer # 15 = Coupled Thickness # 15 = 500.00 Å
+ Layer # 14 = Coupled Thickness # 14 = 26.00 Å
+ Layer # 13 = Coupled Thickness # 13 = 6.50 Å
+ Layer # 12 = Coupled Thickness # 12 = 500.00 Å
+ Layer # 11 = Coupled Thickness # 11 = 26.00 Å
+ Layer # 10 = Coupled Thickness # 10 = 6.50 Å
+ Layer # 9 = Coupled Thickness # 9 = 500.00 Å
+ Layer # 8 = Coupled Thickness # 8 = 26.00 Å
+ Layer # 7 = Coupled Thickness # 7 = 6.50 Å
+ Layer # 6 = Coupled Thickness # 6 = 500.00 Å
+ Layer # 5 = EMA Thickness # 5 = 26.00 Å
Layer # 4 = InAs Thickness # 4 = 6.50 Å
- Layer # 3 = AlGaAs (Comp Library) Thickness # 3 = 500.00 Å Composition = 0.25000
Layer # 2 = GaAs Thickness # 2 = 9149.32 Å (fit)
- Layer # 1 = AlGaAs (Comp Library) Thickness # 1 = 969.42 Å (fit) Composition = 0.86681 (fit)
Substrate = GaAs
Angle Offset = 0.000

9As159 Steimetz model with all QD layers modeled. Layers #6, 9, 12 etc. are coupled to layer #3, layers #7, 10, 13 etc. are coupled to layer #4, layers #8, 11, 14 etc. are coupled to layer #5.

Data: 9As159 55-75deg 5deg interval 20sek MM Model: 9As159 Lee-Steimetz simple model 2 osc (Snapshot)

Open Save Info Set Ranges Open Save Clear

Fit: Generate Edit Fit Dynamic Reset

MSE = 5.428
 Thickness # 6 = 11.86±0.098 Å
 Amp1 = 21.322771±0.8143336
 Br1 = 0.1647±0.00973
 En1 = 2.865±0.0022
 Amp2 = 5.644707±0.2108646
 Br2 = 1.3989±0.04742
 En2 = 4.413±0.0171
 EMA % (Mat 2) = 98.9±3.66
 Thickness # 3 = 4893.46±1.103 Å
 Composition = 0.25388±0.00059826
 Thickness # 2 = 9541.97±0.967 Å
 Thickness # 1 = 1009.97±1.380 Å
 Composition = 0.85782±0.00061958
 Angle Offset = 0.036±0.0034

Layer Commands: **Add Delete Save**
 Include Surface Roughness = OFF

- Layer # 6 = [EMA](#) Thickness # 6 = [26.00 Å](#)
 # of Constituents = 2
 Material 1 = [Void](#)
 Material 2 = [InAs Oxide](#)
 EMA % (Mat 2) = [6.0](#)
 depolarization = [0.333](#) Analysis Mode = [Bruggeman](#)
- Layer # 5 = [EMA](#) Thickness # 5 = [11.86 Å](#) (fit)
 # of Constituents = 2
 Material 1 = [InAs Oxide](#)
 Material 2 = [InAs](#)
 EMA % (Mat 2) = [6.0](#)
 depolarization = [0.333](#) Analysis Mode = [Maxwell-Garnett](#)
- Layer # 4 = [EMA](#) Thickness # 4 = [6.50 Å](#)
 # of Constituents = 2
 Material 1 = [InAs](#)
 - Material 2 = [Gen-Osc](#)
[Add Oscillator](#) [Show Dialog](#) Fast Gaussian Calc = [ON](#)
 Einf = [1.000](#)
 UV Pole Amp. = [0.0000](#) UV Pole En. = [11.000](#)
 IR Pole Amp. = [0.0000](#)
Fit All Clear All Add Amp. Add Br. Add En.
 1. Type = [Lorentz](#) Amp1 = [21.322771](#) (fit) Br1 = [0.1647](#) (fit) En1 = [2.865](#) (fit)
 2. Type = [Lorentz](#) Amp2 = [5.644707](#) (fit) Br2 = [1.3989](#) (fit) En2 = [4.413](#) (fit)
 EMA % (Mat 2) = [98.9](#) (fit)
 depolarization = [0.333](#) Analysis Mode = [Bruggeman](#)
- Layer # 3 = [AlGaAs \(Comp Library\)](#) Thickness # 3 = [4893.46 Å](#) (fit)
 Composition = [0.25388](#) (fit)
- Layer # 2 = [GaAs](#) Thickness # 2 = [9541.97 Å](#) (fit)
- Layer # 1 = [AlGaAs \(Comp Library\)](#) Thickness # 1 = [1009.97 Å](#) (fit)
 Composition = [0.85782](#) (fit)
- Substrate = [GaAs](#)
 Angle Offset = [0.036](#) (fit)

9As159 Lee-Steimetz model with two oscillators.

A.3 Models of the GaAs substrates

Data: GaAs 350 um undoped substrate SS polishec Model: GaAs SS polished 350 um (Snapshot)

Open Save Info. Set Ranges Open Save Clear

Fit: Generate Fit Fit Dynamic Reset

MSE = 3.841
 Roughness = 2.88±0.392 Å
 Interface Thickness = 13.82±0.092 Å
 Substrate Thickness = 3750000.00±9999.000

Layer Commands: **Add Delete Save**
 Include Surface Roughness = **ON** Roughness = **2.88 Å** (fit)
 Layer # 1 = **GaAs Oxide** Interface Thickness = **13.82 Å** (fit)
 Substrate = **GaAs**
 Angle Offset = **0.000**
+MODEL Options
+FIT Options

Single-side polished n-type GaAs substrate model.

A.4 Models of the Chalmers samples

Data: MBE2471 L piece, L container 55-75deg 5dex Model: MBE2471 simple model 2 (Snapshot)

Open Save Info. Set Ranges Open Save Clear

Fit: Generate Fit Fit Dynamic Reset

MSE = 36.438
 Roughness = 39.75±4.329 Å
 Thickness # 5 = 22.48±1.064 Å
 Angle Offset = 0.075±0.0178

Layer Commands: **Add Delete Save**
 Include Surface Roughness = **ON** Roughness = **39.75 Å** (fit)
 Layer # 5 = **GaAs Oxide** Thickness # 5 = **22.48 Å** (fit)
 Layer # 4 = **GaAs** Thickness # 4 = **484.00 Å**
+ Layer # 3 = Coupled Thickness # 3 = **298.00 Å**
 Layer # 2 = **GaAs** Thickness # 2 = **10841.00 Å**
- Layer # 1 = AlGaAs (Comp Library) Thickness # 1 = **1077.00 Å**
 Composition = **0.25000**
 Substrate = **GaAs**
 Angle Offset = **0.075** (fit)

MBE2471 simple model with thicknesses from TEM measurements.

Data: MBE2471 L piece, L container 55-75deg 5dex Model: MBE2471 simple model 2 (Snapshot)

Open Save Info. Set Ranges Open Save Clear

Fit: Generate Fit Fit Dynamic Reset

MSE = 7.908
 Thickness # 5 = 30.42±0.066 Å

Layer Commands: **Add Delete Save**
 Include Surface Roughness = **ON** Roughness = **5.00 Å**
 Layer # 5 = **GaAs Oxide** Thickness # 5 = **30.42 Å** (fit)
 Layer # 4 = **GaAs** Thickness # 4 = **524.00 Å**
■ Layer # 3 = Coupled Thickness # 3 = **298.00 Å**
 Coupled to Layer # = **1** (AlGaAs (Comp Library))
 Layer # 2 = **GaAs** Thickness # 2 = **10376.00 Å**
- Layer # 1 = AlGaAs (Comp Library) Thickness # 1 = **1147.00 Å**
 Composition = **0.25939**
 Substrate = **GaAs**
 Angle Offset = **0.000**

MBE2471 simple model with best fitting thicknesses and compositions.

Data: MBE2471 L piece, L container 55-75deg 5deg Model: MBE2471 semi-simple model 1 (Snapshot)

Open Save Info Set Ranges Open Save Clear

Fit: Generate Fit Fit Dynamic Reset

MSE = 8.631
 Thickness # 5 = 31.95±0.072 Å
 EMA % (Mat 2) = 2.5±0.10
 Composition = 0.26638±0.00079837

Layer Commands: **Add Delete Save**
 Include Surface Roughness = OFF

Layer # 5 = GaAs Oxide	Thickness # 5 = 31.95 Å (fit)
Layer # 4 = GaAs	Thickness # 4 = 484.00 Å
- Layer # 3 = Coupled	Thickness # 3 = 298.00 Å Coupled to Layer # = 1 (AlGaAs (Comp Library))
- Layer # 2 = EMA	Thickness # 2 = 10440.00 Å # of Constituents = 2 Material 1 = GaAs Material 2 = InAs EMA % (Mat 2) = 2.5 (fit) depolarization = 0.333 Analysis Mode = Maxwell-Garnett
Layer # 1 = AlGaAs (Comp Library)	Thickness # 1 = 1077.00 Å Composition = 0.26638 (fit)
Substrate = GaAs	
Angle Offset = 0.000	

MBE2471 semi-detailed model with best fitting thicknesses and compositions.

Data: MBE2472 55-75deg 5deg interval 20 sek MM Model: MBE2472 model 2 (Snapshot)

Open Save Info Set Ranges Open Save Clear

Fit: Generate Fit Fit Dynamic Reset

MSE = 7.337
 Roughness = 25.83±0.825 Å
 Thickness # 5 = 20.58±0.201 Å
 Composition = 0.25111±0.00059499
 Angle Offset = 0.118±0.0036

Layer Commands: **Add Delete Save**
 Include Surface Roughness = ON Roughness = 25.83 Å (fit)

Layer # 5 = GaAs Oxide	Thickness # 5 = 20.58 Å (fit)
Layer # 4 = GaAs	Thickness # 4 = 488.82 Å
+ Layer # 3 = Coupled	Thickness # 3 = 350.81 Å
Layer # 2 = GaAs	Thickness # 2 = 10160.00 Å
- Layer # 1 = AlGaAs (Comp Library)	Thickness # 1 = 1070.00 Å Composition = 0.25111 (fit)
Substrate = GaAs	
Angle Offset = 0.118 (fit)	

MBE2472 model with best fitting thicknesses and compositions.